6-30-2017

In Situ Arsenic Speciation using Surface-enhanced Raman Spectroscopy

Mingwei Yang
Florida International University, minyang@fiu.edu

DOI: 10.25148/etd.FIDC001951

FLORIDA INTERNATIONAL UNIVERSITY

Miami, Florida

IN SITU ARSENIC SPECIATION USING SURFACE-ENHANCED RAMAN SPECTROSCOPY

A dissertation submitted in partial fulfillment of

the requirements for the degree of

DOCTOR OF PHILOSOPHY

in

CHEMISTRY

by

Mingwei Yang

2017

To: Dean Michael R. Heithaus
College of Arts, Sciences and Education

This dissertation, written by Mingwei Yang, and entitled In situ Arsenic Speciation using Surface-enhanced Raman Spectroscopy, having been approved in respect to style and intellectual content, is referred to you for judgment.

We have read this dissertation and recommend that it be approved.

_____
Yi Xiao

_____
Rudolf Jaffe

_____
Bruce McCord

_____
Anthony McGoron

_____
Yong Cai, Major Professor

Date of Defense: June 30 2017

The dissertation of Mingwei Yang is approved.

_____
Dean Michael R. Heithaus
College of Arts, Sciences and Education

_____
Andrés G. Gil
Vice President for Research and Economic Development
and Dean of the University Graduate School

Florida International University, 2017

ACKNOWLEDGMENTS

I would like to express my sincere appreciation to Dr Cai−my major Professor, for providing the opportunity to work in his research group and leading me into the right pathway when I was on the wrong tracks many times. Without his patient guidance, financial support and insightful understanding of chemistry, I would not have completed this work. I am also grateful to the rest of my committee members, Dr Yi Xiao, Dr Rudolf Jaffe, Dr Bruce McCord, and Dr Anthony McGoron for their support, critical comments, and suggestions during all these meetings. Special thanks to Dr Anthony McGoron, Dr Wei-chiang Lin and Dr Yun Qian in Biomedical Engineering Department for allowing me to work on the Raman instrument and for financial support to maintain the equipment. This work would have been impossible without Raman spectroscopy.

Special thanks to Dr Guangliang Liu (our lab manager and assistant director), Dr Yuzhen Sun (Jianghan University, China) and Dr Changjun Fan (a current postdoc in our research group) for their numerous time input and critical comments and beneficial suggestions.

I am grateful to Dr Shannon Matulis and Dr Lawrence Boise from Emory University for their generous providing cell pellets, my research will be less significant without these important samples.

I also would like to thank the following persons, Dr Mebel Alexander for beneficial suggestions in theoretical computation, Dr Abuzer Kabir for the discussion of silver nanofilm fabrication, REU student Kelli Sylvers for the help with coffee ring experiments, Dr Vinay Bhardwaj for his help in the use of Raman spectroscopy, Dr

Daniel Belisario-Lara for his help in Gaussian density functional theory training, Ya-Li Hsu for his help in NMR analysis, Dr Cassian D'Cunha from FIU HPC faculty for the technical support and FIU mass facility for their help in MS analysis.

Also I like to thank all members in Dr Cai's lab for offering a nice academic and pleasant working atmosphere from past to the present, including, Dr Shujuan Sun, Dr Cheng Zhang, Dr Na Zhu, Szabina Stice, Dionne Dickson, Ping Jiang, Wenbin Cui, Yuping Xiang, et al.

Lastly, I would like to express my deepest appreciation and gratefulness to all my family members and my fiancée Miss Yan Zhang in China, without their constant and unconditional supports, encouragements and love; this work will be pale and less meaningful.

ABSTRACT OF THE DISSERTATION

IN SITU ARSENIC SPECIATION USING SURFACE-ENHANCED RAMAN SPECTROSCOPY

by

Mingwei Yang

Florida International University, 2017

Miami, Florida

Professor Yong Cai, Major Professor

Arsenic (As) undergoes extensive metabolism in biological systems involving numerous metabolites with varying toxicities. It is important to obtain reliable information on arsenic speciation for understanding toxicity and relevant modes of action. Currently, popular arsenic speciation techniques, such as chromatographic/electrophoretic separation following extraction of biological samples, may induce the alternation of arsenic species during sample preparation. The present study was aimed to develop novel arsenic speciation methods for biological matrices using surface-enhanced Raman spectroscopy (SERS), which, as a rapid and non-destructive photon scattering technique. The use of silver nanoparticles with different surface coating molecules as SERS substrates permits the measurement of four common arsenicals, including arsenite (As^{III}), arsenate (As^{V}), monomethylarsonic acid (MMA^{V}) and dimethylarsinic acid (DMA^{V}). This speciation was successfully carried out using positively charged nanoparticles, and simultaneous detection of arsenicals was achieved. Secondly, arsenic speciation using coffee ring effect-based separation and SERS detection was explored on a silver nanofilm (AgNF), which was prepared by close packing of silver nanoparticles (AgNPs) on a glass

substrate surface. Although arsenic separation using the conventional coffee ring effect is difficult because of the limited migration distance, a halo coffee ring was successfully developed through addition of surfactants, and was shown to be capable of arsenicals separation. The surfactants introduced in the sample solution reduce the surface tension of the droplet and generate strong capillary action. Consequently, solvent in the droplet migrated into the peripheral regions and the solvated arsenicals to migrated varying distances due to their differential affinity to AgNF, resulting in a separation of arsenicals in the peripheral region of the coffee ring. Finaly, a method combining experimental Raman spectra measurements and theoretical Raman spectra simulations was developed and employed to obtain Raman spectra of important and emerging arsenic metabolites. These arsenicals include monomethylarsonous acid (MMA^{III}), dimethylarsinous acid (DMA^{III}), dimethylmonothioarinic acid ($DMMTA^{V}$), dimethyldithioarsinic acid ($DMDTA^{V}$), S-(Dimethylarsenic) cysteine ($DMA^{III}Cys$) and dimethylarsinous glutathione ($DMA^{III}GS$). The fingerprint vibrational frequencies obtained here for various arsenicals, some of which have not reported previously, provide valuable information for future SERS detection of arsenicals.

TABLE OF CONTENTS

CHAPTER PAGE

Chapter 1 Introduction, Problem Statement, Objectives and Hypotheses 1
1.1 Relationship between arsenic and human health 2
1.2 Cellular stress from arsenic metabolism in human 8
1.3 Current analytical techniques for arsenic speciation 11
1.4 Surface-enhanced Raman spectroscopy for arsenic detection 14
1.5 Problem Statement 18
1.6 Hypotheses 19
1.7 Objectives 21

Chapter 2 Potential Application of SERS for Arsenic Speciation in Biological Matrices 23
2.1 Abstract 24
2.2 Introduction 25
2.3 Material and Methods 30
2.4 Experimental Procedures 32
2.5 Results and Discussions 37
2.6 Conclusions 51

Chapter 3 Employing Coffee Ring Effect on Silver Nanofilm for Arsenic Speciation Study 53
3.1 Abstract 54
3.2 Introduction 55
3.3 Material and Methods 59
3.4 Results and Discussions 65
3.5 Conclusion 87

Chapter 4 Raman Spectra of Thiolated Arsenicals with Biological Importance 89
4.1 Abstract 90
4.2 Introduction 91
4.3 Materials and Chemicals 95
4.4 Experimental procedures 95
4.5 Results 103
4.6 Discussion 127
4.7 Conclusion 137

Chapter 5 Summary, Significance, and Future Research Directions 138
5.1 Summary 139
5.2 Significance of this study 141
5.3 Future research directions 144

Reference 146

VITA 170

LIST OF TABLES

TABLE		PAGE
Table 2.1	Changes in deprotonation of arsenicals in different AgNPs colloidal suspensions	41
Table 4.1	Comparison of experimental and calculated Raman frequencies for DMA^{V} using all basis set	105
Table 4.2	Comparisons of computational performance of all basis sets	109
Table 4.3	Comparison of all As─O bonds Raman frequencies between experimental and calculated Raman spectra	113
Table 4.4	Vibrational frequencies assignment for MMA^{III} and DMA^{III}	117
Table 4.5	Vibrational frequencies assignment for $DMMTA^{V}$ and $DMDTA^{V}$	122
Table 4.6	Vibrational frequencies assignment for $DMA^{III}GS$ and $DMA^{III}Cys$	127
Table 4.7	Summary of As─O Raman frequencies	131
Table 4.8	Summary of As─C Raman frequencies	134
Table 4.9	Summary of As─S Raman frequencies	136

LIST OF FIGURES

FIGURE		PAGE
Figure 2.1	The distribution of individual arsenic species in aqueous solution with different pH	37
Figure 2.2	Typical zeta potential and size distribution of AgNPs-Citrate (A) and AgNPs-Spermine (B).	38
Figure 2.3	SERS spectra of individual arsenic species obtained in colloidal suspensions of AgNPs-Citrate (A) and AgNPs-Spermine (B).	39
Figure 2.4	Adsorption of arsenic in colloidal suspensions of AgNPs-Citrate (A) and AgNPs-Spermine (B).	44
Figure 2.5	Arsenic concentration in the sample reservoir vs. in the filtrate receiver (%)	46
Figure 2.6	SERS spectra of arsenic species in the cell lysate.	47
Figure 2.7	Changes in size (A) and zeta potential (B) of AgNPs upon interaction with cell lysate.	50
Figure 3.1	Optimization the usage of APTMS.	66
Figure 3.2	Properties of the AgNF.	67
Figure 3.3	Individual arsenic SERS signals on the AgNF as droplet (as black curves) and at the edge of dry film (as red curves).	69
Figure 3.4	Typical SERS background signals from different buffer system with or without SDS including.	70
Figure 3.5	The typical coffee ring signal profile of aresnicals on the AgNF	74
Figure 3.6	Arsenic speciation based on regular coffee ring phenomenon in different buffer solutions	76
Figure 3.7	Typical halo coffee ring phenomenon as droplet and as dry film using the phosphate buffer system containing 0.05% SDS.	80
Figure 3.8	SERS signals along the radius of the sessile droplet containing 0.05% CTAB.	81
Figure 3.9	Halo coffee ring SERS signal profile of 4 arsenic species in acetic acid.	82

Figure 3.10 Halo coffee ring SERS signal profile of 4 arsenic species in phosphate buffer. 83

Figure 3.11 Halo coffee ring SERS signal profile of 4 arsenic species in ammonium formate. 85

Figure 4.1 3D structures of arsenicals optimized by DFT 104

Figure 4.2 Theoretical DMA^{V} Raman spectra calculated from different basis sets..... 112

Figure 4.3 Raman spectra of DMA^{V} obtained via experimental measurement and calculation 113

Figure 4.4 Experimental and calculated Raman spectra of MMA^{III} (A) and DMA^{III} (B) 116

Figure 4.5 HPLC-ICP-MS chromatograms of arsenic standards and MMA^{III} synthesized in the laboratory showing the identity and purity 117

Figure 4.6 Proton NMR spectra for the confirmation of DMA^{III} synthesized in the laboratory 118

Figure 4.7 Molecular ion peaks confirmation of $DMMTA^{V}$ (A) and $DMDTA^{V}$ (B) 120

Figure 4.8 Experimental and calculated Raman spectra of $DMMTA^{V}$ (A) and $DMDTA^{V}$ (B)..... 121

Figure 4.9 Mass spectrum fragmentations of DMA^{III}Cys by ESI-MS 124

Figure 4.10 Experimental and calculated Raman spectra of DMA^{III}GS (A) and DMA^{III}Cys (B) 125

ABBREVIATIONS

AFM	Atomic force microscopy
AgNF	Silver nanofilm
AgNPs	Silver nanoparticles
AgNPs-C	Citrate coating silver nanoparticles
AgNPs-Citrate	Citrate coating silver nanoparticles
AgNPs-S	Spermine coating silver nanoparticles
AgNPs-Spermine	Spermine coating silver nanoparticles
APTMS	3-Aminopropyl)trimethoxysilane
As	Arsenic
As^{III}	Arsenite
As^{V}	Arsenate
B3LYP	Becke, 3-parameter, Lee-Yang-Parr
CE	Capillary electrophoresis
CTAB	Cetrimonium bromide
DFT	Density functional theory
DI water	Deionized water
DMA^{III}	Dimethylarsinous acid
$DMA^{III}Cys$	S-(Dimethylarsenic) cysteine
$DMA^{III}GS$	Dimethylarsinous glutathione
DMA^{V}	Dimethylarsinic acid
DMA^{V}-Salt	Sodium cacodylic
$DMDTA^{V}$	Dimethyldithioarsinic acid
$DMMTA^{V}$	Dimethylmonothioarinic acid

$DMMTA^{V}$(GS)	Dimethylarsinothioyl glutathione complex
ESI-MS	Electrospray mass spectrometer
EXAFS	X-ray absorption fine structure
FT-ICR-MS	Fourier transform ion cyclotron resonance mass spectrometry
HPLC	High performance liquid chromatography
IC	Ion chromatography
ICP-MS	Inductively coupled plasma mass spectrometer
LDA	Linear discriminant analysis
LOD	Limit of detection
MMA^{III}	Monomethylarsonous acid
MMA^{V}	Monomethylarsonic acid
$MMMTA^{V}$	Monomethylmonothioarsonic acid
PCA	Principle components analysis
RMS	Root mean square error
ROS	Reactive oxygen species
SDD	Stuttgart/Dresden double-ζ
SDS	Sodium dodecyl sulfate
SERS	Surface-enhanced Raman spectroscopy
Sodium-DMDTA	Sodium dimethyldithioarsinate
TOF-MS	Time-of-flight mass spectrometer
XANES	X-ray absorption near edge structure

Chapter 1

Introduction, Problem Statement, Objectives and Hypotheses

1.1 Relationship between arsenic and human health

1.1.1 Arsenic source and distribution

Arsenic can be introduced into the environment through both natural and anthropogenic sources. Arsenic is the 20th most abundant element in crustal rock, with an average concentration of 2−3 mg/kg. Inorganic arsenic compounds are the major naturally existing arsenicals, including arsenite (As^{III}) and arsenate (As^{V}). Arsenic-containing minerals were widely found in the rocks presenting as orpiment (As_2S_3), realgar (AsS), arsenopyrite (FeAsS), arsenolite (As_2O_3), olivenite (Cu_2OHAsO_4), cobaltite (CoAsS) and proustite (Ag_3AsS_3) [1, 2]. Two significant natural environmental processes, including weathering ractions and volcanic emmissions, are responsible for the universal introduction and distribution of arsenicals into ecosystem cycling (e.g., groundwater, sediment, soil etc [3, 4]). Globally, naturally existing arsenicals do not pose substantial health hazard and risk towards human beings, because of the generally low arsenic concentration in the environment. However, in some particular areas of world, geological arsenic sources have caused severe public health issues. In Bangladesh and West Bengal, alluvial Ganges aquifers used for public water supply are polluted with naturally occurring arsenic. This has endangered the health of millions of people; arsenic concentrations up to 1000 μg/l have been detected [5]. In Taiwan a condition known as blackfoot disease is common due to well drinking water contamined by arsenic. In the southwest regions of this island, high arsenic concentrations have been found in groundwater originating from deep artesian wells in sediments which include fine sands, muds and black shale [4].

Human activities introduce an extreme amount of arsenic into the ecosystem in modern society. Mining [6, 7], application of pesticides and herbicides in agriculture [8, 9], burning of fossil fuels [10], and the poultry industry [11] contribute major arsenic contamination to air, water and soil. Arsenic is released into the environment primarily via mining, smelting and ore beneficiation processes, since arsenic is a natural component of lead, zinc, copper and gold-bearing ores [12]. Coal burning usually does not pose any health risks towards human beings, because the arsenic content in coals is less than 5 mg kg^{-1} [13]. However certain sources of coal contain an extremely high concentration of arsenic (up to 9600 mg kg^{-1}). This material can cause serious arsenic pollution issues if used improperly. For example, when power plants have to use coal containing a high concentration of arsenic in the developing countries, polluted water and air are common [14]. Arsenic-containing pesticides were been widely used by American farmers before 1900, including lead arsenate, calcium arsenate. During this time there was no regulation for the usage of arsenic pesticides, and they were applied widely in the U.S. agriculture. White arsenic was extensively used for agricultural purposes in the US with 10,800 tons of arsenic-containing insecticides consumed in 1995 [15]. During the early 2000s, organic arsenicals were being added to animal feeds [16]. Recently the US FDA rescinded approval for three arsenic drugs, which have been used as food additives for chickens, turkeys and pigs to prevent disease, increase feed efficiency and promote growth [17]. The use of arsenic in the preservation of timber has also led to contamination of the environment. Chromated copper arsenate (CCA) is a wood preservative that protects wood products from the decaying effects of fungi and insects [18]. Large quantities of these timbers have been used in outdoor playground facilities.

With a long-term exposure to outdoor weathering conditions, arsenic compounds present in the wood will leach out [19], and has great potential hazard towards human, especially children who play in the playground because young children have a high frequency of hand-to-mouth behavior which is a major pathway for arsenic ingestion [18].

1.1.2 Arsenic human exposure pathways

Drinking water is a significant source for human exposure to arsenic in many areas in the world, because drinking water is consumed on a daily base. There are about 30 million of people in Bangladesh, 6 million in West Bengal, India and over 1 million in Vietnam suffering from the poisoning due to arsenic contaminated groundwater [20]. The majority of arsenic species found in groundwater are mainly inorganic arsenic forms, including arsenite (As^{III}) and arsenate (As^{V}) [21, 22].

Arsenic exposure from food sources has attracted much attention in the past decade. Since humans are at the top of the food chain, human exposure to arsenic depends on the surrounding environment. Many food contamination events may be attributed to the arsenic, including, surface water and soil contaminated by arsenic, using arsenic polluted water to irrigate crops, organic arsenicals used in food additives in poultry industry, seafood dietary preference, etc. Major sources of arsenic contaminated food include rice and rice related food products [23, 24] and seafood [25, 26]. Because of daily consumption, these food products can pose a chronic health hazard to the human body. Usually, rice grain contamination by arsenic occurs in areas close to mining fields [27] or due to irrigation with contaminated underground water [28]. Contaminated seafood often results from the food chain bioaccumulation [25, 29].

Inhalation of arsenic contaminated soil, dust and air can be a major pathway for arsenic exposure for some groups in the population. Workers in the mining industry, smelting industry and silicon factory tend to inhale a large quantity of inorganic arsenic during their long-term working history [30-33]. Depending on the workplace, the blood arsenic speciation and concentration varies. Workers in the glass industry and arsenic manufacturing tend to have the highest concentration of arsenic in their blood [32].

Arsenic occupational exposure in copper factories has been reported to have a positive relationship with the lung cancer cases. Furthermore, it was also revealed that smoking has a significant contribution to arsenic exposure [34]. Burning coal with a high concentration of arsenic could cause the exposure through coal fly ash [35]. Arsenicals have been used as medication/poison for a very long time. For example, arsenic trioxide obtained from smelting copper was used as a drug and as a poison as early as 2000 BC; Fowler's solution (1% potassium arsenite, $KAsO_2$) was used as a tonic for anaemia and rheumatism in the 1800s [36] and arsenic trioxide was used to treat granulocytic leukemia in China [37].

1.1.3 Arsenic uptake in human body

Arsenicals are introduced into the human body via ingestion and inhalation, with subsequent uptake by the gastrointestinal tract and lung. Once adsorbed by human gastrointestinal tract and lung, it is eventually metabolized in certain human cells, such as liver cells [38, 39]. The uptake of toxic inorganic arsenicals, such as arsenite and arsenate, is well studied. These two arsenicals have significant difference in protonation ability in the cellular matrix. Therefore, they have different mechanisms of transportation into cells. Arsenite has a very high pKa value and thus it is usually neutralized in the cellular matrix,

on the other hand, arsenate has a very low pKa value and it is negatively-charged in the cellular matrix. It is believed that arsenite transfers into cells via diffusion [38, 40], because there is a linear relationship between arsenite cellular level and the arsenite concentration in the extracellular matrix, This relationship was not affected by a membrane sulfhydryl modifiers or energy poisons [38, 40]. The energy poisons stops cellular energy supply and disrupts carrier-mediated uptake systems. The arsenate uptake is inhibited by high concentration of phosphate in the cells, which indicates that the uptake of arsenate is assisted by a phosphate carrier protein [40].

1.1.4 Arsenic induced diseases/cancers

Arsenic has been recognized as a group 1 carcinogen to humans by the International Agency for Research on Cancer. The adverse health effects of arsenic strongly depend on dose, duration of exposure, and the nutrition status of the exposed population. Generally, human exposure to arsenic can be categorized into two processes, chronic exposure and acute/lethal exposure. Taking drinking water as an example, in long-term chronic arsenic exposure, the arsenic concentration range may range from 136~1000 μg/l, which is significantly higher than the minimum recommended concentration of 10 ppb proposed by the US Environmental Protection Agency. A lethal dose for human beings was estimated to be 1 mg/kg/day [41], and it is less than 100 mg for a adulate weigh less than 200 lb. While another study claimed the acute poisoning ranges from 100 mg to 300 mg [42]. Exposures to arsenic at a low dose over a long term can cause multisystem diseases, including cancer. Because of the high affinity between arsenic and keratin, arsenic accumulates in scleroproteins such as the hair and nails [43]. The study of arsenic speciation in hair/nails has been employed as an effective biomarker

of arsenic intake in exposed populations [44, 45]. The initial symptom of arsenic poisoning is hyperpigmentation palmar and solar keratosis, induced by the deposition of arsenic on the skin [42]. With arsenic exposure over a long term, the human body can suffer from a number of diseases, including respiratory/pulmonary system diseases, cardiovascular failure, the hematological problems including anemia, leucopenia, and thrombocytopenia, and hepatic system damage, causing cancer [46]. It is well known that chronic arsenic exposure of highs concentration in drinking water has been associated with a series of cardiovascular diseases, including hypertension, ischaemic heart disease and carotidatherosclerosis. Epidemiological studies also have shown that chronic arsenic exposure is associated with increased morbidity and mortality from cardiovascular disease [47, 48]. The occurrence of diabetes mellitus was also found to be associated with the inorganic arsenic exposure. For example, a survey of 163 subjects having keratosis revealed that diabetes was prevalent among those subjects in western Bangladesh [49]. In United States, urine arsenic determination in a cross-sectional study of 788 adults indicated that type 2 diabetes has a positive correlation with the total urinal arsenic concentration. In this study it was found that chronic, low to moderate concentrations of arsenic may cause type 2 diabetes [50]. Acute arsenic exposure can cause early symptoms such as abdominal pain, dysphagia, nausea, vomiting, diarrhea, headache, restlessness to patients. As the poisoning progresses, patients may develop gastrointestinal irritation and bleeding, which can lead to massive fluid and electrolyte losses potentially causing the the death of patients [51, 52]. For the treatment of acute arsenic poisoning, dimercaprol has been used used to chelate arsenic in the body fluids [51, 52].

1.2 Cellular stress from arsenic metabolism in human

1.2.1 Cellular redox system

Cells are the fundamental units of human beings; the health status of cells is directly related to human health. A human cell consists of many organelles, including the nucleus, Golgi body, ribosomes, mitochondria, and cytoplasm. These are enclosed by a cellular membrane. The mitochondria plays a imperative role in cells, involving the oxidation of glucose from the cytoplasm to produce adenosine triphosphate (ATP), which is the carrier of energy for most cellular metabolism. During the mitochondrial oxidization of organic compounds, a superoxide anion is generated by electron leakage [53], which induces the generation of other reactive oxygen species (ROS), including hydroxyl, peroxyl and alkoxyl radicals. Reactive oxygen species play important roles in the regulation of cell survival [53]. In healthy cells, the redox balance is controlled through generation and elimination of ROS/RNS in the physiologic environment. Usually, the generation of ROS happens within the mitochondria in cells [54], and cells have an antioxidant defense system to eliminate ROS stress. This includes the following enzymatic scavengers such s superoxide dismutase (SOD), catalase, and glutathione peroxidase [55]. Glutathione is the substrate of glutathione peroxidase which is active during the elimination of ROS. The concentration of glutathione in the cellular environment is usually maintained at millimolar concentration levels [56]. Thus it is obvious that glutathione is critical for the proper concentration of ROS maintenance.

1.2.2 Arsenic inhibits glycolytic energy metabolism

The human body requires energy to meet its metabolic requirements, and glucose is one of the major energy supplies for human beings. In human cells, the glycolytic reaction breaks down glucose step by step and energy is generated during these processes as ATP is formed in the cells. A glucose molecule chelates with a phosphate molecule at the beginning reaction of the glucose oxidization in the cells. Owing to the structural similarity between arsenate and phosphate, the presence of arsenate will greatly affect the cellular glycolytic reaction by substituting phosphate in the oxidation of glucose molecules [57]. Free phosphate ions are constantly required during glycolysis for the generation of ATP; arsenic disturbs this biological reaction by complexation with ADP into ADP-As, the reactant of the ATP. However, ADP-As is easier to hydrolyze when compared to ATP, a disturbance occurs in cellular processes.

1.2.3 Arsenic deplete cellular glutathione

Inorganic arsenic has a very high affinity towards thiol-containing small molecules in the cytoplasm, including glutathione, cysteine, and proteins. Once arsenic enters the human bloodstream and is delivered to cells, it binds to thoil-containing proteins, especially enzymes, and will depress enzymatic activities leading to cell malfunction.It can form chelating complexes with glutathione and cysteine, which are the antioxidants in the cellular plasma, thus imposing oxidative stress on targeted cells. Under chronic arsenic exposure, the cellular glutathione will be depleted and thus cause oxidative damage to various cell components. Studies of patients suffering from chronic arsenic exposure indicate that long-term exposure causes significant oxidative stress on

cells, including protein oxidation, cellular membrane damage, and an increase in lipid peroxides in blood serum [58, 59].

1.2.4 Arsenic suppress cellular enzymatic activities

The normal functioning of cells depends on enzymatic activities in the cellular plasma. Enzymes play a critical role in cells, being the catalysts that increase the rate of all biochemical reactions within cells [60]. Arsenic toxicity is believed to be related to the binding of arsenite to enzyme thiols, because of its high affinity towards these compounds. Consequentially, inorganic arsenic can induce enzymes malfunction once it enters the cell. Pyruvate dehydrogenase (PDH), a mitochondrial multi enzyme complex containing many sulfhydryl groups, catalyzes the oxidative decarboxylation of the end product of glycolysis. It has been demonstrated that the presence of arsenic trioxide can cause the inactivation of PDH, due to the generation of ROS [61]. Inorganic arsenic also inhibits deoxyribonucleic acid (DNA) repair process, however, a detailed mechanism is not yet available [62].

Arsenic metabolism causes DNA damage and disturbs DNA repair. Certain types of damage to DNA result in structural changes that create issues when the DNA is replicated [63]. Damage to DNA frequently happens in cells and can occur due to ROS generation during cellular metabolism. In order to maintain accurate genetic information, cells have enzymatic mechanisms to repair broken DNA sequences, involving a collection of processes by which DNA damages are identified and later corrected. As mentioned in the previous section, arsenic metabolism will escalate the ROS concentration in the cellular environment and can worsen DNA damage [64-66]. As a consequence of the high affinity of arsenic towards thiol-containing biomolecules,

arsenic can inhibit enzymes during DNA repair, such as the bacterial Fpg protein and the mammalian XPA protein [67]. In addition direct damage can occur through DNA nicking by MMA^{III} and DMA^{III} [68-70].

1.3 Current analytical techniques for arsenic speciation

1.3.1 Chromatography-based methods

Arsenic speciation in biological matrices has been routinely conducted using techniques coupling chromatography/electrophoresis separations and sensitive detectors. The separation methods that have been explored in arsenic speciation include high performance liquid chromatography (HPLC) [71-74], capillary electrophoresis (CE) [75-77], and ion chromatography (IC) [78, 79]. Among these separation techniques, HPLC is the most popular technique used in the arsenic speciation because of its ability to perform separations in a wide range of research areas, using various sample matrixes. Depending on the need to emphasize analytical sensitivity or structure determination of the arsenic species, one could select different detection methods, such as inductively coupled plasma mass spectrometer (ICP-MS) [80], electrospray mass spectrometry (ESI-MS) [72], or time-of-flight mass spectrometry (TOF-MS) [81]. Sample preparation in all these speciation methods involves the release of arsenicals from the biological matrix, followed by clean-up of the sample matrix. Extraction using an organic solvent or strong acid/base has the potential to change the integrity of many arsenic species. For instance, MMA^{III} or DMA^{III}, two important arsenic metabolites, are unstable and readily oxidized during extraction [5]. Arsenate could be reduced to arsenite and form $As(GS)_3$ in the cellular environment because of the presence of high concentrations of glutathione [56]. The $As(GS)_3$ complex is not stable in the mice bile and it is only stable in the presence of 5

mM of glutathione. It is understandable that $As(GS)_3$ could be decomposed and oxidized during the solvent extraction procedure. Additionally, recently observed thiolated arsenicals, such as dimethylmonothioarsinic acid ($DMMTA^V$), dimethyldithioarsinic acid ($DMDTA^V$) and trivalent arsenicals conjugate with thiol-containing molecules in biological samples, and are sensitive to acidic/basic chemical environment and temperature changes [82]. It has become clear that problems in sample preparation can cause misleading results, consequently hindering the arsenic speciation studies in biological matrices. Therefore, it is necessary to develop an arsenic speciation method in biological matrices that can remain as much as possible the integrity of arsenic species or to eliminate extraction steps during the sample preparation and analysis completely. Beside potential degradation of the sample in chromatographic studies, identical retention during chromatographic separation could also undermine our understanding of arsenic metabolism. For example, recently dimethylarsinothioic acid was mistakenly determined in wool extract as DMA^{III} [83], which brought lots of research attention towards thiol-containing arsenicals and some sulfur-involved metabolic pathways were proposed[84, 85]. The case of wrong / inconclusive results owing to overlapped HPLC retention times has not only happened in arsenic speciation, but also has occurred in certain protein identification studies [86, 87].

1.3.2 X-ray absorption spectroscopy related methods

The technique of X-ray absorption spectroscopy (XAS) has also been employed in arsenic speciation, including X-ray absorption near edge structure (XANES) and extended X-ray absorption fine structure (EXAFS). The XANES method involves the near edge absorption structure which is the K-absorption edge (K-edge), which is defined

as the energy required to remove an electron in the innermost orbit and eject it into the continuum [88], while EXAFS deals with a relatively higher range of energy absorption. Both near edge structure and fine structure are determined by the following factors, interatomic distances, chemical valence, local coordination environmental, coordination number, and oxidation state [89-93]. Both techniques were employed for arsenic speciation in environmental samples, including arsenic species in samples collected from mining field [94] and arsenic in plants (e.g., rice samples) [95, 96]. Application of these techniques has also been used for arsenic speciation in *in-situ* environments [97, 98]. Bacquart et al. [98] employed a micro-XANES to study the arsenic speciation inside of frozen hydrated cells. The successful application of these methods for arsenic speciation in many environmental and biological samples provides opportunities that the chromatography-based techniques cannot offer, because X-ray based methods are non-destructive to the sample and also simplify sample preparation. However the satisfactory application of these techniques is highly dependent on the availability of arsenic standards. As described by Foster et al. [94], data analysis was accomplished using the EXAFSPAK programs. In this study, the XANES spectra of model compounds and samples were background subtracted and normalized to the edge jump, and then the second derivative of each XANES spectrum was then calculated using a 2eV smoothing interval. Another data processing method employed in XANES involved a linear combination fitting of the spectra, in which the XANES spectra of the samples were fitted to these standards to further calculate the relative percentage of each species. In these studies, the application of XAS was mostly restricted to environmental samples, and samples in solid form were required during sample measurement. Although the non-

destructive sample preparation would be promising for its application in arsenic speciation in a biological matrix, the application in the biological matrix is rarely reported, which could be the result of a requirement for solid or powder samples. Also, the availability of the synchrotron radiation X-ray absorption is limited, generating a real problem for routine analytical needs

1.4 Surface-enhanced Raman spectroscopy for arsenic detection

1.4.1 Surface-enhanced Raman spectroscopy for bioanalytical application

In comparison with other analytical techniques for analysis of biological samples, SERS is a rapid and non-destructive photon scattering technique, which provides fingerprint information regarding molecular vibrational energy levels [99]. With a significant enhancement in the Raman signal via the interaction between the incident light and the well-designed metallic surface of a substrate, SERS has emerged as a novel technique for the analysis of a broad range of chemical substances in complex biological matrices. Compared to infrared spectroscopy, Raman spectroscopy has minimal interference from water molecules, which exists in most biological samples. Thus this unique advantage allows Raman spectra to be obtained directly from biological matrices [100]. Different strategies for SERS studies in biological matrices have been found in the current literature. Firstly, biofluids, including saliva, urine, tear, blood, blood serum, were directly placed on SERS-active substrates or mixed with metallic colloidal suspensions [101-108]. The SERS signals were generated owing to the evaporation of solution evaporation or the creation of hot spots from the aggregation of nanoparticles caused by introducing aggregation agents. Overall, SERS signals obtained using this method was not of high quality, and the possible reason for poor signal response could be the

following: the SERS-active substrates were not optimized in the size and material and the aggregation process is difficult to control. Secondly, statistical methods like the chemometrics was employed for biofluids Raman spectra data analysis. Through employing principal components analysis (PCA) and linear discriminant analysis (LDA) in most cases, this methodology was successfully applied for cancer detection and disease diagnosis with a high percentage of diagnosis accuracy [109-115]. Chemometrics might not be applicable in arsenical's speciation study due to a limited number of diagnostic Raman vibrational bands. Thirdly, SERS metallic substrates of well-organized surface morphology were employed for biomolecules measurement, such as nanofilm fabricated by a self-assembled membrane, closely packed nanorods [116-119]. The well-organized substrate surface ensured strong SERS signals upon the sample introduction. Fourthly, the methodology of immunoassay, taking advantage of the binding reaction between antigens and antibodies, was carried out by using SERS tags and surface modification of antibodies [120-123]. Usually, magnetic materials were capsulated into nanoparticles for further magnetic separation nanoparticles from matrices as soon as the equilibrium is established between the interactions between nanoparticles with biological matrices using this method. Furthermore, derivatization of targeted molecules was employed when the molecule's Raman activity was poor. Taking the glucose determination for example [124, 125], boric acid was employed in order to capture glucose in the sample matrix. Very few molecules have a universal binding reaction or specific derivatization reaction with arsenicals, thus the application of SERS tags and derivatization methods may be limited.

1.4.2 Surface-enhanced Raman spectroscopy for arsenic detection

The very first application of SERS in arsenic analysis can be dated back to 1988, when Greaves and Griffith obtained arsenate SERS signal response around 780 cm^{-1} by directly mixing arsenate with silver nanoparticles [126]. In the past several decades, many studies have been carried out for the applications of SERS in arsenic analysis and speciation with an emphasis on improvement of the substrates for strong SERS signal production. Metallic colloidal suspensions [127-130] and metallic nanofilms [131-138] are two common substrates for SERS measurement while some indirect SERS methods employing nanoparticles for arsenite analysis [127, 129, 130] has also been reported. Upon the introduction of arsenite into modified nanoparticle solutions, these aptamers could release from the nanoparticles and bind with arsenite. The release of aptamers on the nanoparticles causes a significant drop in the surface charge and thus the nanoparticles aggregate and Raman report molecules' signals are greatly enhanced. As a consequence of its simplicity, metallic colloidal suspensions as SERS substrates are most widely used. Modification in the shape of the nanoparticles has often been performed in order to enhance the SERS signal, structures such as nanostar, nanorods, etc have been used [139-141]. Metallic nanofilm is the other popular SERS substrate for arsenic speciation, and it is easy to obtain arsenic SERS signals from nanofilms because of evaporation of droplets or diffusion of arsenicals on the nanofilm. Currently, different strategies are employed for nanofilm fabrication to study arsenic species, such as the modified mirror reaction for silver nanofilm deposition [137, 138, 142], coffee-ring evaporation [131], through the Langmuir-Blodgett assembly [132], electrothermal deposition [134, 135]. Overall the surface morphology of the nanofilm is critical for the

sensitivity and reproducibility of arsenic analysis. Until now, SERS application for arsenic analysis has been mainly limited to inorganic arsenic species, such as As^{III} or As^{V} and environmental samples, such as well water or underground water. Comparing to inorganic arsenic compounds, analysis of organic arsenicals using SERS was much less reported [134, 135, 143]. Furthermore, the SERS application of arsenic speciation in biological matrices has not been explored to the best of our knowledge. Performing SERS for arsenic speciation in biological media is challenging because the presence of complicated electrolytes and biomolecules. Previous studies have shown that nanoparticles aggregate immediately upon mixing with a physiological buffer solution [144, 145]. The uncontrolled aggregation of nanoparticles can hinder the SERS signal response in the physiological matrix. Furthermore, nanoparticles can be coated with a film of biological molecules in some biological matrices, such as proteins in blood and cellular extracts. This is known as a protein corona and has been studied in drug delivery systems using nanomaterials [146]. However, coating nanoparticle surfaces with proteins can reduce the SERS active area on the surface and thus quench the SERS signal. Therefore, minimal coating of biomolecules on nanoparticles surface with particle aggregation is necessary for successful SERS applications in cellular matrices.

1.4.3 Current issues in surface-enhanced Raman spectroscopy for arsenic detection

The development of SERS application in arsenic speciation is still in its infancy, and currently reports are mostly focused on environmental samples [126, 128, 132, 133, 136-138, 142, 147-149]. Studies of arsenic SERS responses in the presence of cellular matrices or physiologic samples have scarcely been explored. Arsenic speciation studies in cellular matrices are more important than the determination of total arsenic

concentration, as these studies will yield the arsenical bioavailability and provide necessary information for toxicological evaluation. Furthermore, most previous reports were focused on inorganic arsenicals, such as As^{III} and As^{V}. Arsenic metabolism in cellular environments will convert inorganic arsenicals into various organoarsenicals. However, Raman spectra of many potential arsenical metabolites were not available in the literature or never studied, therefore, it is urgent to obtain this firsthand SERS information prior to arsenic speciation for cellular or physiological samples.

Current arsenic speciation methods may not be capable of depicting correct arsenical profiles in cellular matrices, since chromatographic-based methods require sample preparation using strong acids or oxidative reagents, which may cause changes in the integrity of arsenic species. XAS-based methods may be able to preserve the arsenic species in the sample, however, the ideal sample state is solid, and cellular samples are rarely reported in the XAS studies. Here, SERS is proposed for arsenic speciation in the cellular matrix, because it has the following advantages high sensitivity because of the great signal enhancement from the interaction of arsenicals with nano size metallic surface and non-destructive sample preparation.

There are two SERS substrates employed mostly in current reports, metallic colloidal suspension and metallic nanofilms. Both of these have high potential in the SERS application of arsenic speciation. My dissertation studies are mostly related to employment of these two SERS substrates to explore their potential in arsenic speciation.

1.5 Problem Statement

The application of SERS in arsenic speciation is still at the early research stage. Currently, arsenic speciation using SERS is mainly restricted to inorganic arsenic species,

such as As^{III} and As^{V}. Two common existing organarsenicals, e.g., monomethylarsonic acid (MMA^{V}) and dimethylarsinic acid (DMA^{V}) found in human body were not studied by SERS. Furthermore, arsenic speciation studies were mostly conducted for environmental samples, while arsenic speciation in biological or physiological samples was rarely reported in the literature. It is unknown if SERS is capable of simultaneous detection of arsenic species in the presence of biological matrices.

Application of SERS in biological matrices holds promise because it is a non-destructive analytical approach and it could have high sensitivity detection capabilities because of the great enhancement factor which originates from surface plasmon resonance (SPR) on the nanosize metal surface. However, to the best of our knowledge, Raman spectra of some important arsenic metabolites have been rarely recorded and reported. These important arsenic metabolites are mostly unstable, including the following, monomethylarsonous acid (MMA^{III}), and dimethylarsinous acid (DMA^{III}), dimethylmonothioarinic acid ($DMMTA^{V}$), dimethyldithioarsinic acid ($DMDTA^{V}$), S-(Dimethylarsenic) cysteine (DMA^{III}(Cys)) and dimethylarsinous glutathione (DMA^{III}GS). It is therefore important to characterize these arsenicals' Raman spectra or fingerprint Raman frequencies prior to applying SERS analysis of arsenic speciation under the influence of biological matrices. The availability of Raman spectra is the prerequisite requirement for SERS studies and the Raman spectra will be helpful for the assignment of SERS spectra.

1.6 Hypotheses

The established objectives were guided by the following hypotheses:

1. Electrostatic interactions between arsenicals and the nanoparticle surface in the colloidal suspension are critical for an optimal SERS response. To be more specific, the adsorption of arsenic compounds onto the nanoparticles surface in the aqueous solution will mostly be controlled by the electrostatic interactions. These adsorptive effects will determine whether SERS signals are generated or not. Selected arsenicals have different molecular structures and they should have specific fingerprint signal responses, which will makes the simultaneous detection possible. Different molecular surface coatings of these nanoparticles will be used in order to obtain nanoparticles with variations in surface charge, permitting the impact of surface charge to be monitored.

2. Compared to hot spots generated by the aggregation of gold/silver nanoparticles in the solution, hot spots on nanofilm is relatively easy to control, since nanofilms are usually consisted of closely parking nanoparticles on solid surface. The surface morphology is relatively controllable to obtain an organized surface with nanoparticles during the fabrication procedure. This closely parking nanofilm should be able to yield strong SERS signal for arsenic compounds SERS simultaneous detection.

3. Density functional theory (DFT) is capable of predicting molecular properties, including vibrational profiles. The discrepancy between calculated and experimental Raman frequencies of a standard molecule will determine whether the DFT calculation is reliable or not and comparison methods will be adapted from previous work [162-165]. Different empirical scaling factors will be employed to reduce the difference. After optimization of this method, the DFT calculation will be employed to generate theoretical Raman spectra of unknown arsenicals and detect specific vibrational modes of

arsenicals. Using this data, the experimental Raman spectra of unknown arsenicals can be identified by a combination of calculated and experimental Raman spectra.

1.7 Objectives

The present work involves a study of the applications of SERS in arsenic speciation and the identification of Raman spectra of major potential arsenic metabolites.

1. Employing silver nanoparticles as the SERS substrate to explore the possibility of arsenic speciation.

Silver nanoparticles of different surface charges will be used to study arsenic speciation under the influence of a cellular matrix. The response of individual arsenic species will be obtained in nanoparticles of different surface charge first and then arsenic speciation in the presence of a cellular matrix will be carried out using the same nanoparticles. To have a better understanding of the differences in SERS signal response, adsorption of arsenicals on the silver nanoparticles colloidal suspensions and arsenicals in the cellular matrice will be studied. Size and charge effects of nanoparticles in the cellular matrice will be monitored to obtain an in-depth understanding of the SERS signal response.

2. Study of arsenic speciation employing silver nanofilm

Arsenic speciation of four common existing arsenicals will be carried out on the silver nanofilm (AgNF). Different approaches will be carried out to fabrication nanofilm with relatively organized surface morphology, including a modified mirror reaction [142] and a self-assembled metal colloid monolayers method [166]. Individual arsenic fingerprint signals will be obtained first to see whether these signals are different from signals in the colloidal suspensions. Furthermore, arsenic speciation uses nanofilm will

be studied. The mixture will be prepared in different solution with different pH to modulate the deprotonation states of these arsenicals. If this approach is not able to fulfill the purpose of the simultaneous detection, the coffee ring effect will be employed. Arsenic SERS signals from the center to the edge of the dry coffee ring will be measured.

3. Identification of sulfur-containing arsenicals' Raman spectra

Raman spectra of potential arsenical metabolites will be studied to assign and identify arsenicals' fingerprint Raman frequencies. The combination of theoretical calculation with experimental studies will be carried out in order to determine the fingerprint Raman vibrations of different arsenicals, including, MMA^{III}, DMA^{III}, $DMDTA^{V}$, $DMMTA^{V}$, $DMA^{III}Cys$ and $DMA^{III}GS$. Most of these arsenicals will be synthesized in the laboratory and their molecular structures will be identified with a molecular mass spectrometer. Density functional theory will be employed for theoretical Raman spectra simulation in order to assign experimental Raman spectra.

Chapter 2

Potential Application of SERS for Arsenic Speciation in Biological Matrices

Part of this chapter was accepted for publication in the journal of Analytical and Bioanalytical Chemistry. Adapted with permission from Yang, M., Matulis, S., Boise, L. H., McGoron, A. J., & Cai, Y. (2017). Potential application of SERS for arsenic speciation in biological matrices. Analytical and Bioanalytical Chemistry. doi:10.1007/s00216-017-0434-3. Copyright (2017) Springer and Copyright Clearance Center.

2.1 Abstract

Speciation of arsenic is usually carried out using chromatography-based methods coupled with spectroscopic determination; however, the inevitable procedures involving sample preparation and separation could potentially alter the integrity of the arsenic metabolites present in biological samples. Surface-enhanced Raman spectroscopy (SERS) could be a promising alternative for providing a reliable arsenic analysis under the influence of a cellular matrix. A method for arsenic speciation using SERS in cellular matrix was developed in this study and four arsenicals were selected, including arsenite (As^{III}), arsenate (As^{V}), monomethylarsonic acid (MMA^{V}) and dimethylarsinic acid (DMA^{V}). Silver nanoparticles in the form of colliodal suspension with different surface charges, i.e. coated with citrate (AgNPs-Citrate) and spermine (AgNPs-Spermine) were employed as SERS substrates. Adsorption of arsenicals on nanoparticles in colloidal suspensions and the cellular matrix along with the pH, size and zeta potential of the colloidal suspensions were investigated for better understanding of SERS signals response of arsenicals in the colloidal suspensions or under the influence of cellular matrix. Arsenicals showed substantially different SERS responses in the two colloidal suspensions, mainly due to the distinct difference in the interaction between the arsenicals and the nanoparticles. Arsenic speciation in cell lysate could be successfully carried out in AgNPs-Spermine suspension, while AgNPs-Citrate could not yield significant SERS signals under the experimental conditions. This study proved that AgNPs-Spermine colloidal suspension could be a promising SERS substrate for studying arsenic metabolism in a biological matrix, reducing the bias caused by traditional techniques that involve sample extraction and pretreatment.

Keywords: Arsenic • SERS • Speciation • Nanoparticles • Cell lysate

2.2 Introduction

Millions of people around the world are suffering from arsenic-induced diseases, including various types of cancers [132, 167-169]. Generally, human beings are exposed to arsenicals via ingestion and inhalation. The metabolism of arsenicals in the human body involves a multistep transformation in the arsenic species, including reduction/oxidation, methylation, and thiolation reactions [170, 171], ending up with methylated arsenic compounds such as monomethylarsonic acid (MMA^V) and dimethylarsinic acid (DMA^V) in urine and blood. Methylation of inorganic arsenic is traditionally considered to be a detoxification process for harmful inorganic arsenicals, since the toxicity of MMA^V or DMA^V is much lower than that of inorganic arsenicals [84, 172]. However, this view has been challenged because of the studies on monomethylarsonous acid (MMA^{III}) and dimethylarsinous acid (DMA^{III}), two recently found organic arsenicals from urine samples of patients chronically exposed to inorganic arsenicals in drinking water [173, 174]. MMA^{III} and DMA^{III} are possible metabolic products of arsenic in humans and their toxicity was found to be higher than the inorganic As^{III} [175, 176]. The toxicity of arsenic is greatly related to its chemical forms, hence a full investigation of arsenic speciation in biological samples, such as cell, tissue and blood, becomes critical for a better understanding of arsenic toxicity and mode of action.

Arsenic speciation in biological matrices has been routinely conducted using techniques coupling chromatographic/electrophoretic separation and sensitive detectors. The separation methods that have been explored in arsenic speciation include high performance liquid chromatography (HPLC) [33, 72, 73, 177], capillary electrophoresis

(CE) [75-77], and ion chromatography (IC) [78, 79]. Based on either the analytical sensitivity needed or the molecular information of the arsenic species desired, one could select different detection methods, such as inductively coupled plasma mass spectrometer (ICP-MS) [80], electrospray mass spectrometer (ESI-MS) [72], and time-of-flight mass spectrometer (TOF-MS) [81]. Sample preparation in all these speciation methods is an essential step for successful detection and involves the release of arsenicals from the biological matrix and the cleanup of the matrix. Extraction using organic solvents or strong acid/base has a great potential to alter the integrity of many arsenic species. For instance, MMA^{III} or DMA^{III}, two important arsenic metabolites are unstable and readily oxidized during the course of extraction [178]. Arsenate could be reduced to arsenite and form $As(GS)_3$ in the cellular environment due to the presence of a high concentration of glutathione (GSH) [56]. $As(GS)_3$ could be decomposed and oxidized during the solvent extraction process since the $As(GS)_3$ complex is only stable in the present of certain levels of GSH. Additionally, the recently observed thiolated arsenicals, such as dimethylmonothioarsinic acid ($DMMTA^{V}$) and dimethyldithioarsinic acid ($DMDTA^{V}$) or trivalent arsenicals conjugated with thiol-containing molecules in biological samples, are only stable under a narrow range of pH and are sensitive to temperature changes [82]. It becomes clear that sample preparation can cause misleading results, consequently hindering the study of arsenic speciation in biological matrices. Therefore, it is necessary to develop an arsenic speciation method in biological matrices that can retain as much as possible the integrity of the arsenic species profile, or ideally to eliminate the extraction steps during sample preparation and analysis completely.

Surface-enhanced Raman spectroscopy (SERS) is a promising technique that can be potentially used in arsenic speciation in biological samples. SERS is a rapid and non-destructive photon scattering technique, providing fingerprint information regarding molecular vibrational energy levels [99]. SERS has emerged as an important technique for the analysis of a broad range of chemical substances in complex biological matrices. For instance, metallic nanoparticles were employed to determine some chemical substances present in various biological samples including saliva, urine, tear, blood, blood serum, by directly introducing nanoparticles into these biological matrices [101-108, 179]. However, SERS signals are usually not strong enough or suffer from interference from components in biological matrices. In some cases, derivatization was employed to enhance the SERS response if the Raman cross section of the molecule of interest was poor [124, 125]. A useful derivatization reaction or binding agent has not been reported for the arsenic species with biological interest, thus limiting the application of SERS in arsenic speciation. In other cases, complicated SERS signals are interpreted using the methods of chemometrics, such as principal components analysis and linear discriminant analysis. This method was successfully applied for cancer detection and the diagnosis of other diseases with a fairly high accuracy [109-115]. However, since principal component analysis (PCA) and linear discriminant analysis (LDA) usually need a lot of vibrational frequencies to perform the data analysis, this approach is not suitable for studying arsenic owing to the limited number of Raman vibrational bands.

The very first application of SERS for arsenic analysis can be dated back to 1988 when Greaves and Griffith obtained an arsenate SERS signal response around 780 cm^{-1} by directly mixing arsenate with silver nanoparticles [126]. In the past several decades,

SERS has been applied in arsenic analysis and speciation in water with an emphasis on improvement of the substrates for strong SERS signal production. Metallic colloidal suspension [127-130] and metallic nanofilm [131-138] are two common substrates used for SERS measurement while some indirect SERS methods employing nanoparticles for arsenite analysis [127, 129, 130] have also been reported. Due to simplicity, metallic colloidal suspensions are most widely used as SERS substrates. Modification of the shape of the nanoparticles, such as nanostar and nanorods, has often been performed in order to enhance the SERS signal [139-141]. Another popular SERS substrate is metallic nanofilm since SERS signals can be readily obtained due to the evaporation of the droplet sample which brings the analytes close to the nanofilm surface. Up to now, the application of SERS for arsenic analysis has been mainly limited to inorganic arsenic species, such as As^{III} or As^{V} in water samples, such as from wells or other underground water sources [126, 128, 132, 133, 136-138, 147]. Comparing to inorganic arsenic compounds, the analysis of organic arsenicals using SERS has been much less reported [134, 135, 143]. Furthermore, the study of arsenic speciation in biological matrices using SERS has not been explored to the best of our knowledge. Performing SERS for arsenic speciation in biological media is challenging because of the presence of complicated electrolytes and biomolecules [144, 145]. The uncontrolled aggregation of nanoparticles could hinder SERS signal response in a physiological matrix. Nanoparticles could become coated with a film of biological molecules in some biological matrices, such as proteins present in blood and cellular extract. This phenomenon is named protein corona and has been studied in drug delivery using nanomaterials [146]. The nanoparticle surface coated with proteins could reduce the SERS active area on its surface and thus

quench the SERS signal. Therefore, lessening the coating of biomolecules on the nanoparticle's surface and uncontrolled aggregation is necessary for the successful application of SERS on arsenic speciation in biological matrices. In addition, SERS technique as a promising analytical tool for detection of inorganic arsenic species in water media is well discussed recently [180].

In this study, a method for arsenic speciation using SERS, based on silver colloidal suspensions in the presence of cellular matrix, was explored. As the first step for our research on arsenic speciation in biological samples using SERS, we decided to provide a proof-of-concept study focusing mainly on the fundamentals that determine the SERS measurement of selected arsenicals. We studied the electrostatic interactions between arsenicals and nanoparticles in colloidal suspension and the controlling factors, alterations of the nanoparticle surface through coating, and interferences of cell lysates to arsenic measurement by SERS. Four arsenic species that are widely studied in biological matrices, namely As^{III}, As^{V}, MMA^{V} and DMA^{V} were included in this study. To the best of our knowledge, this is the first study attempting to perform SERS arsenic speciation under the influence of a biological matrix. The 8226/S multiple myeloma cell line was selected to provide a cell lysate and arsenicals were added to the cell lysate for the simulation of cellular environment. Special attention was given to controlling and improving the electrostatic interactions between particles and arsenic in the colloidal suspension as it is critical for successful SERS measurements in solution. Two silver nanoparticles (AgNPs) with different surface charge were employed. The size, zeta potential and pH of AgNPs colloidal suspensions under the influence of cell lysate were

monitored to understand the impact of the cellular matrix on the arsenic SERS signal response.

2.3 Material and Methods

2.3.1 Material and Chemicals

Sodium metaarsenite, 98% (As^{III}), sodium arsenate dibasic, 99% (As^{V}), cacodylic acid sodium salt, 98% (DMA^{V}) were purchased from Sigma-Aldrich, USA. Monosodium acid methane arsonate sesquihydrate, 99.5% (MMA^{V}) was purchased from Chem Service, USA. Silver nitrate (99.99%) was purchased from STREM Chemicals, USA. Spermine tetrahydrochloride (99%, powder) was purchased from Alfa Aesar, USA. Sodium citrate dehydrate (Granular certified), NaOH, HCl, $MgCl_2$, Na_2SO_4, NaCl, KNO_3 were purchased from Fisher Scientific Inc as certified A.C.S grade. The phosphate-buffered saline (PBS), 1×PBS was prepared in the laboratory. All solutions were prepared in deionized water (DI water, 18.2 MΩ, Barnstead Nanopure Diamond).

The selected cell line was 8226/S multiple myeloma, which was purchased from the American Type Culture collection (ATCC, Manassas, VA), maintained at 37 °C in a humidified atmosphere with 5% CO_2 in RPMI-1640 media, supplemented with 100 U ml^{-1} of penicillin, 100 μg ml^{-1} of streptomycin, 10% heat inactivated fetal bovine serum, and 2 mM L-glutamine (all culture reagents from Cellgro, MediaTech, Herndon, VA). The cells were cultured at a concentration of 2×10^5 cells/ml and then harvested by centrifugation at 1000 rpm for 5 minutes, washed with PBS once, and spun down again, and then the pellets were frozen in liquid nitrogen and stored at −20°C for future usage.

2.3.2 Instrumentation

An Elan DRC-e (Perkin-Elmer) ICP-MS was employed for arsenic analysis. The ICP-MS was equipped with an auto sampler, a cyclonic spray chamber, and a Meinhard nebulizer. All arsenic samples were diluted in 2% nitric acid and spiked with 20 ppb yttrium prior to ICP-MS quantification analysis. The following signals were monitored: 75 for arsenic, 89 for yttrium (as internal standard). A standard calibration curve was obtained on a daily base.

The Raman spectrometer used was a Perkin-Elmer RamanStation 400F Raman spectroscopy, employing a 785 nm diode laser with average power of 100 mW at the sample and 100-micron spot size. This Raman station was equipped with a x-y-z sample stage accepting standard 96-well plate with a glass bottom. The 96-well plates were purchased from PerkinElmer (Waltham, MA) and were reused by cleaning with cotton swabs and drying under a stream of nitrogen gas. Raman spectra were acquired by transferring 200 µl of solution into wells of the 96-well plate. Typical sample measurement was carried out for 1 second of exposure and 4 times of accumulation for each measurement. This Perkin-Elmer Ramanstation was also equipped with a Perkin-Elmer RamanMicro 300 system, which had three optical objectives 5×, 20× and 50×. Usually, the 20× optical objective was used for better sample focus and lower background signal. For SERS measurements using an optical objective, 40 µl of solution was dropped onto a glass microscope slide and SERS signals were obtained under the same conditions as using 96 well plates.

The size and zeta potential of nanoparticles were measured with a Malvern Zetasizer Nano-ZS (Westborough, MA). The hydrodynamic diameters reported in this

study represent the average particle diameter "z-average" intensity peak as a function of size. UV-vis absorption spectra of silver nanoparticles were obtained using a Cary 300 UV-vis spectrometer. The pH measurements were normally carried out on a Fisher Scientific Accumet Research AR15 pH/mV/°C Meter, while for pH measurement of low volume solutions (<50 µl), pH testing paper with multiple pH ranges was used.

A Pall Microsep centrifugal device (centrifuge filters) (PALL Corporation, USA) with 1K Da molecular weight cutoff was employed for the centrifugal filtration experiments. This centrifugal device consisted of a sample reservoir and a filtrate receiver separated by a semi-permeable membrane (Omega membrane), which has low protein-binding. The filtration was carried out at room temperature using a Marathon 21000R benchtop centrifuge (Fisher Scientific, USA) for 25 minutes at a speed of 8000 rpm (over 5000 g).

2.4 Experimental Procedures

2.4.1 Synthesis and characterization of silver nanoparticles

AgNPs of different surface coating were synthesized in the laboratory. The procedures for synthesizing citrate coated silver nanoparticles (AgNPs-Citrate) were adopted from Lee & Meisel [181] with a minor modification. Briefly, all glassware were cleaned by emerging in Aqua Regia solution (HCl/HNO_3 = 3:1, v/v) overnight and rinsing with a large amount of tap water and DI water and finally dried in an oven at 80 ºC prior to use. Fifty ml of 1×10^{-3} mol/l of $AgNO_3$ was added to a 250 ml round bottom flask and then heated to boil in an oil bath under vigorous stirring with a condenser equipped to reflux. Sodium citrate dihydrate (1%, 2 ml) was introduced drop by drop and then kept heating for one hour. Characteristics of the AgNPs-Citrate, such as

hydrodynamic size, zeta potential (surface charge), pH and UV-vis absorption were recorded soon after the colloids were synthesized.

The synthesis of spermine coated silver nanoparticles (AgNPs-Spermine) was performed following Faulds & Graham [182] with a minor modification. Prior to reaction, the glass flask was filled with 30 ml of 0.001 mol/l spermine stirring for 30 minutes to form a positively charged glass surface to prevent the adhering of positively charged nanoparticles, and then rinsed with a large amount of DI water multiple times and dried under nitrogen gas. The glass flask was wrapped with aluminum foil to avoid exposure to light. In brief, 20 ml of 1×10^{-3} mol/l of $AgNO_3$ was mixed with 10 µl of 0.1 mol/l spermine in a round bottom flask and then degassed with a flow of nitrogen for 30 minutes under vigorous stirring. Fresh prepared $NaBH_4$ (0.1 mol/l, 50 µl) was then added and kept stirring for one hour. Upon introduction of $NaBH_4$, the solution turned yellow in seconds and the solution was stored in the refrigerator overnight prior to use in order to let excess $NaBH_4$ degrade. Characteristics of AgNPs-Spermine were obtained in the same way as AgNPs-Citrate.

2.4.2 SERS measurement of arsenic species in different silver nanoparticle suspensions

AgNPs-Citrate or AgNPs-Spermine colloidal suspension (480 µl) was mixed with 20 µl of 100 ppm arsenic standards individually. Different amounts of Na_2SO_4 solutions (0.5 M) were introduced to initiate the aggregation of AgNPs-Citrate and the solution was vortexed for 30 seconds, while no salt-initiated aggregation was carried out for the AgNPs-Spermine suspension. Within 3 minutes, 200 µl of the resulted AgNPs colloidal suspension was transferred to the 96-well plate. Raman signals were obtained as described in the Instrumental section.

Experiments assessing the adsorption of arsenic species on nanoparticles were conducted to provide a better understanding of arsenic SERS signal response from different AgNPs colloidal suspensions. Adsorption experiments were carried out by adding 60 µl of a 1000 ppm individual arsenic standard into 1440 µl of an AgNPs colloidal suspension in a 1.5 ml centrifuge tube. The centrifuge tube was shaken for one hour at a speed of 80 rpm on an orbital shaker. After shaking, the solution was split into two parts, one of which was aggregated by introducing 30 µl of 0.5 mol/l Na_2SO_4 and the other was used as control (no Na_2SO_4 added). Afterward, both solutions were centrifuged at 8000 rpm (over 5000g) for 10 minutes and the supernatants were analyzed for arsenic using ICP-MS. To calculate the mass balance during adsorption, experiments were also carried out by substituting the AgNPs solution with deionized water. All experiments were performed in triplicate. Results of arsenic concentrations in the supernatant were expressed as the mean ± standard deviation (SD) (n=3). Statistical analysis was performed and one-way ANOVA was employed with a $P < 0.05$ being considered to be significant.

2.4.3 Interactions between arsenic and cellular matrix

Interactions between arsenicals and biomolecules in the cell lysate, through binding/adsorption, during the SERS measurement of arsenic were inevitable. Thiol-containing molecules present in the cell lysate could complex directly with trivalent arsenicals. Arsenicals might also interact with proteins in the cell lysate via electrostatic forces. Centrifugal filtration was used to study the adsorption of arsenic in the cellular matrix. The centrifugal filtration was able to let small arsenic compounds/complexes pass through the molecular cutoff membrane (1K Da) and to retain arsenicals binding to

proteins or biomolecules. A pellet of 2×10^5 cells was thawed and 900 µl DI water was added. A sonication probe (Fisher Scientific Sonic Dismembrator Model 100, Waltham, MA) was employed to break up the cells following a previously reported procedure [183]. The cell lysate (45 µl) was mixed with 25 µl of 100 ppm individual arsenic standard solution and then 430 µl of 1× PBS buffer were added. Control experiments were carried out by substituting the cell lysate with an equal volume of DI water in order to study the distribution of arsenic in the sample reservoir and the filtrate receiver of the centrifugal device. The PBS buffer and cell lysate were analyzed separately for arsenic background. All solutions were incubated at 37 °C for 30 minutes and transferred into the centrifugal device equipped with a membrane of molecular weight cut-off of 1K Da. Centrifugation was carried out at 8000 rpm (over 5000 g) for 25 minutes. The volume of solutions in the sample reservoir (upper) and the filtrate receiver (lower) were recorded approximately according to the weight assuming the density of the solution is equal to water. Arsenic concentrations in the sample reservoir and the filtrate receiver were measured by ICP-MS. All adsorption experiments were performed in triplicate.

2.4.4 Effect of cell media on SERS measurement of arsenic species

The cell lysate solution (2×10^5 cells in 900 µl of DI water) was diluted with DI water ten times in sequence in order to prepare cell lysate in 900 µl solutions with different concentrations of 2×10^4, 2×10^3, and 2×10^2 cells, respectively. Individual arsenic standard solutions (100 ppm, 2 µl of each standard) were added to 90 µl of the diluted cell lysate solutions, followed by adding 2 µl of DI water. This procedure generated diluted lysate solutions containing 2 ppm of each arsenic species. These solutions were vortexed for 30 seconds and then placed on an orbital shaker at 80 rpm for 30 minutes

prior to use. For measurement of arsenic using SERS, 90 µl of AgNPs was mixed with 10 µl of the diluted cell lysate containing 2 ppm of arsenic. For AgNPs-Citrate, 5 µl of 0.5 mol/l Na_2SO_4 was introduced in order to aggregate the nanoparticles. Finally, 40 µl of the mixed solution was transferred onto a glass slide and SERS signals were obtained by using the 20× optical objective.

In order to better understand the SERS signal from arsenic under the influence of cell lysate, the colloidal suspensions properties including, particles size, surface charge and pH value were measured upon interaction with different concentrations of cell lysate. The AgNPs colloidal solution containing 2×10^4 cell/ml was prepared by adding 90 µl of 2×10^5 cell lysate solution (prepared in 900 µl DI water) into 910 µl of AgNPs colloidal suspension and the solution was vortexed prior to properties measurements. The final concentrations of cell lysate in the AgNPs colloidal suspension were 2×10^4, 2×10^3, 2×10^2 and 2×10 cell/ml by using different concentrations of cell lysate solution. The pH of colloidal suspensions was measured using different pH test papers because of the small volume of the samples. The size and zeta potential of the AgNPs were measured using the Malvern Zetasizer Nano-ZS. All experiments were carried out in triplicate. Sizes and zeta potentials for all samples were summarized as mean ± SD (n = 3) and analyzed using one-way ANOVA and the $P < 0.05$ was considered to be significant.

2.5 Results and Discussions

2.5.1 SERS Measurement of Arsenic Species in Silver Nanoparticle Suspensions

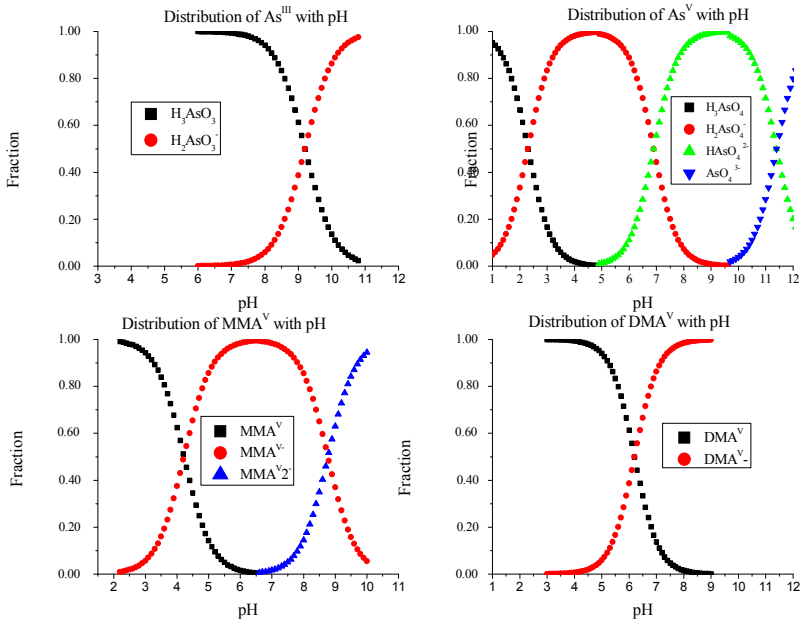

Figure 2.1 The distribution of individual arsenic species in aqueous solution with different pH

The four selected arsenic species have different pKa values and therefore show different charges at a certain pH (Fig. 2.1). The characteristics of the synthesized AgNPs-Citrate and AgNPs-Spermine are shown in Fig. 2.2. The sizes of the nanoparticles were 60 and 53 nm for AgNPs-Citrate and AgNPs-Spermine, respectively and the polydispersity index (PDI) values were less than 0.2, indicating that their hydrodynamic sizes were likely homogeneously distributed in the colloidal suspension. These two AgNPs suspensions had significantly different solution pH, due to the different surface capping agents. AgNPs-Citrate suspension was usually at approximately pH 9 as prepared, while AgNPs-Spermine was about pH 4. The surface charges of the

nanoparticles, described in zeta potential, were -50.1 and +50 mV in AgNPs-Citrate and AgNPs-Spermine suspensions respectively.

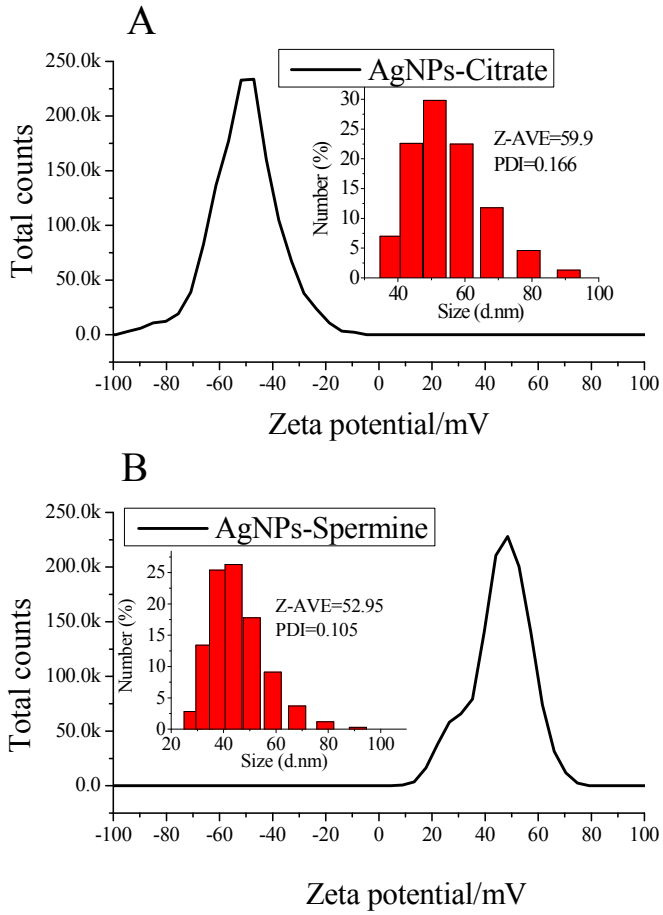

Figure 2.2 Typical zeta potential and size distribution of AgNPs-Citrate (A) and AgNPs-Spermine (B). Both nanoparticles had PDI (polydispersity index) values less than 0.2, indicating that their hydrodynamic sizes were considered as homogeneous distribution in the colloidal suspension. AgNPs-Citrate suspension was usually at pH 9 as prepared. AgNPs-Spermine suspension was at pH 4. In AgNPs-Citrate suspension, nanoparticles were coated by negatively charged citrate ions and the zeta potential is negative, while in AgNPs-Spermine suspension, nanoparticles were coated by positively charged spermine ions and the zeta potential is positive.

Raman spectra of the four arsenicals in AgNPs-Citrate and AgNPs-Spermine colloidal suspension are shown in Fig. 2.3A and B, respectively, and background SERS signals from the colloidal suspensions are in red.

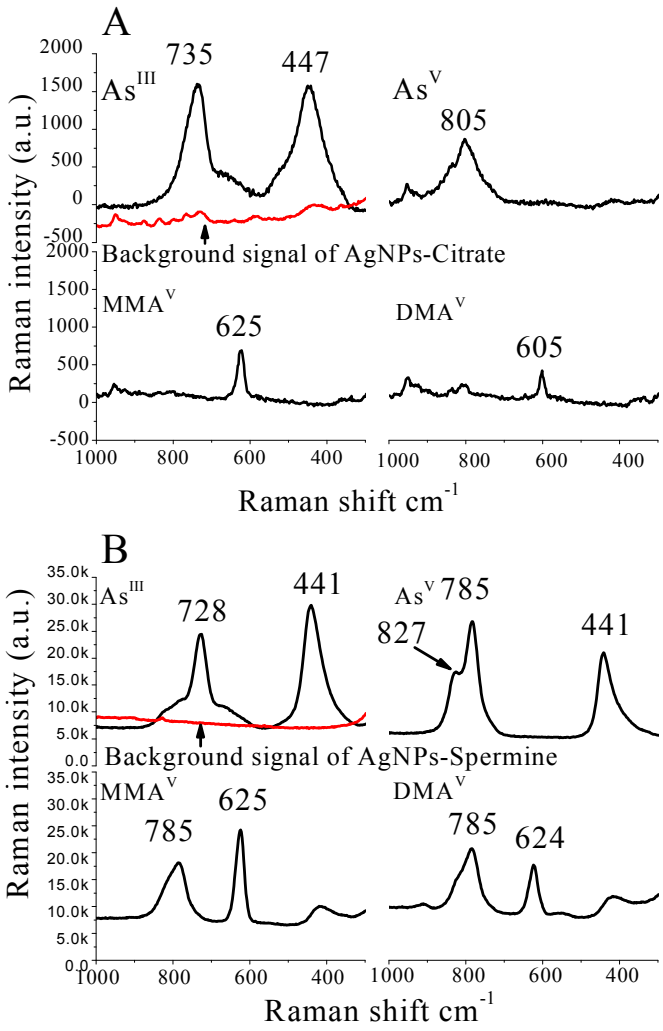

Figure 2.3 SERS spectra of individual arsenic species obtained in colloidal suspensions of AgNPs-Citrate (A) and AgNPs-Spermine (B). Colloidal suspension of 4 ppm of arsenic was prepared by mixing 480 µl of AgNPs-Citrate or AgNPs-Spermine with 20 µl of 100 ppm individual arsenic solution. The AgNPs-Citrate suspension was then aggregated with 20 µl of 0.5M Na_2SO_4, while no such aggregation was performed for AgNPs-Spermine.

In the AgNPs-Citrate colloidal suspension, there were two characteristic vibrational bands for As^{III} with 735 cm^{-1} resulting from the As─O stretch mode [128, 142, 184]. The peak at 447 cm^{-1} was not reported previously and could not be assigned in this study. For As^{V}, one peak at 805 cm^{-1}, corresponding to the As─O symmetric vibration [185, 186] was observed. For these two organoarsenicals, characteristic As─C stretching vibrations, due to different numbers of methyl group, were identified at 625 and 605 cm^{-1} as the fingerprint vibration for MMA^{V} and DMA^{V}, respectively [135, 187-189]. The SERS signals of organoarsenicals were much weaker, especially for DMA^{V} in comparison to the inorganic arsenic species. For SERS measurement in AgNPs-Spermine suspension, similar results were observed for As^{III} with a slight shift in wavenumber for both bands in comparison to that in AgNPs-Citrate, being likely attributed to the difference in chemical environments (Fig. 2.3B). SERS spectra of As^{V} showed two vibrational bands, 785 cm^{-1} being attributed to the As─O symmetric stretch mode [128, 142] (including the shoulder at 827 cm^{-1}, which belonged to the As─O asymmetric stretch mode [149, 189]) and 441 cm^{-1} being the superposition stretch of ν_2 and ν_5 of the arsenate molecule [132, 136]. The two organoarsenicals, MMA^{V} and DMA^{V} had very similar vibrational profiles with a slight difference in the As─C vibrational frequency. The As─O stretch mode at 785 cm^{-1} was observed for both compounds and the As─C vibration at 625 cm^{-1} and 624 cm^{-1} were found in MMA^{V} and DMA^{V}, respectively. Obviously, clear differences in SERS signal of arsenicals were observed between the two AgNPs colloidal suspensions. Arsenicals had much stronger SERS responses in AgNPs-Spermine than in AgNPs-Citrate. The superposition vibration of As─O in As^{V} was found in AgNPs-Spermine but not in AgNPs-Citrate. The As─O vibration at 785 cm^{-1} was

found for both organoarsenicals [135, 187, 188] in AgNPs-Spermine colloidals suspension, which was based on the fact that both organoarsenicals have the As─O bond and the SERS vibrational frequency of As─O of organoarsenicals was around 780 cm^{-1} [135], while not in AgNPs-Citrate. Furthermore, the As─C vibrations of the two organoarsenicals at approximately 625 cm^{-1} were almost the same in AgNPs-Spermine, however, a shift of 20 cm^{-1} between the two compounds appeared in AgNPs-Citrate (Fig 2.3A and 2.3B).

The electrostatic interactions between arsenicals and nanoparticles in the colloidal suspension plays an important role in arsenicals SERS sensing, making individual arsenicals manifest SERS signals differently in these two colloidal suspensions. Silver nanoparticles employed in this study were coated with different surface capping agents, thus they had different surface charges. Upon introducing arsenic standards, there was no significant pH change in the AgNPs colloidal suspensions. Arsenicals were in different protonation states in these two suspensions, for instance, As^{III} being neutralized (H_3AsO_3) in the AgNPs-Spermine colloidal suspension, however it was about 50 % negatively charged ($H_2AsO_3^{-1}$) and about 50 % neutralized (H_3AsO_3) in AgNPs-Citrate (Table 2.1).

Table 2.1 Changes in deprotonation of arsenicals in different AgNPs colloidal suspensions

	AgNPs-Citrate, pH 9, negatively charged	AgNPs-Spermine, pH 4, positively charged
As^{III}	50 % H_3AsO_3, 50% $H_2AsO_3^{-1}$	100% H_3AsO_3
As^{V}	Almost 100% $HAsO_4^{-2}$	Almost 100% $H_2AsO_4^{-1}$
MMA^{V}	100% $CH_3As(OH)O_2^{-1}$	50% $CH_3As(OH)_2$, 50% $CH_3As(OH)O_2^{-1}$
DMA^{V}	100% $(CH_3)_2AsOH^{-1}$	100% $(CH_3)_2AsOH_2$

The electrostatic attraction between arsenicals and nanoparticles promotes the adsorption of arsenicals onto nanoparticles, thus greatly enhancing the SERS signals. Individual arsenicals have different protonation status in these two colloidal suspensions. For instance, As^{V} and MMA^{V} were negatively charged ions in both the positively charged AgNPs-Spermine and in the negatively charged AgNPs-Citrate colloidal suspensions. In the AgNps-Spermine suspension, As^{V} and MMA^{V} are attached onto the nanoparticle's surface via electrostatic interaction, however, in the AgNPs-Citrate suspension, they are repelled by the negatively charged nanoparticle's surface. This could explain why SERS signals in AgNPs-Spermine were stronger than in AgNPs-Citrate. As^{III} and DMA^{V} were neutralized in AgNPs-Spermine and negatively charged in AgNPs-Citrate. As^{III} and DMA^{V} had poorer SERS signals in AgNPs-Citrate than in AgNPs-Spermine, owing to a repulsive interaction between these two arsenicals and the negatively charged AgNPs-Citrate nanoparticles. However, the strong SERS signal for As^{III} and DMA^{V} in AgNPs-Spermine indicates that these arsenicals were brought to the surface close enough for efficient SERS to occur.

In order to better understand the factors controlling the SERS signals of the four arsenicals in AgNPs-Citrate and AgNPs-Spermine colloidal suspensions, the interactions between arsenicals and nanoparticle were investigated using adsorption experiments (Fig. 2.4). For AgNPs-Citrate (Fig. 2.4A), adding salt (i.e. aggregation of nanoparticles) seems to enhance the adsorption of arsenicals on nanoparticles. This is particularly true for As^{III}. Overall, the adsorption of arsenicals on the AgNPs-Citrate nanoparticles was less than 10%. A different pattern was observed in AgNPs-Spermine (Fig. 2.4B). The adsorption of As^{III} and As^{V} on the nanoparticles was about 23 and 15%, respectively in AgNPs-

Spermine suspension without addition of salt. Additing salt to the suspension either inhibited the adsorption of inorganic arsenicals or caused the release of adorbed arsenicals from the surface of the nanoparticles. The adsorption of the two organoarsenicals in the AgNPs-Spermine suspension was less than 5%. The adsorption of arsenicals onto the nanoparticles surface is critical for SERS response because adsorption is an efficient way to bring these arsenicals in the solution close to the surface of AgNPs, ideally with a distance of less than 10 nm [190]. Adsorption of As^{III} and As^{V} onto nanoparticles in the AgNPs-Spermine suspension was larger than that in the AgNPs-Citrate, being consistent with the fact that stronger SERS signals of As^{III} and As^{V} in AgNPs-Spermine than in AgNPs-Citrate. However, the adsorption of MMA^{V} and DMA^{V} on the AgNPs-Spermine was poor even though the SERS signals observed for MMA^{V} and DMA^{V} were stronger compared to AgNPs-Citrate, suggesting that other factors, in addition to adsorption of arsenicals on the surface of nanoparticles, contributed significantly to the SERS measurement of organoarsenicals [135, 191].

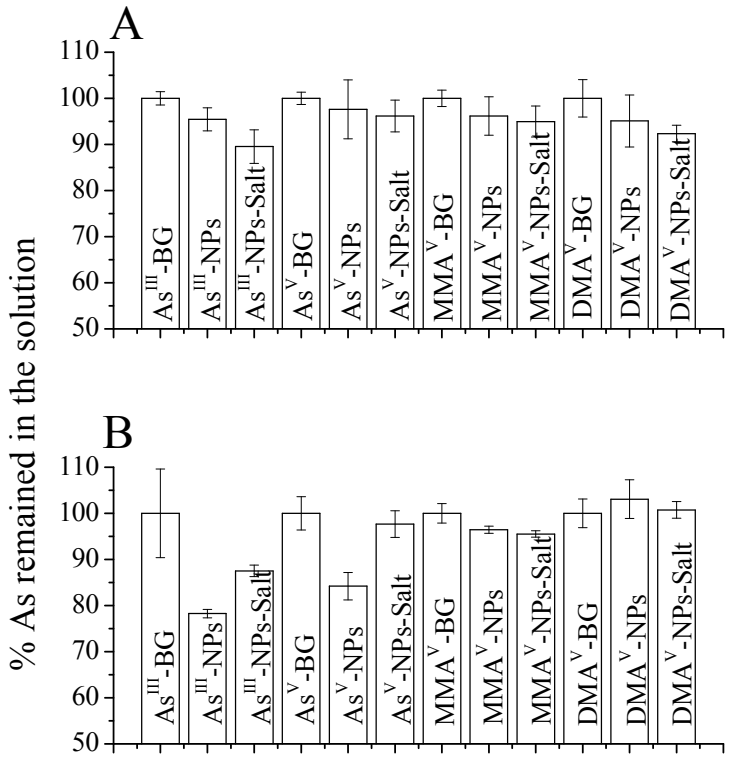

Figure 2.4 Adsorption of arsenic in colloidal suspensions of AgNPs-Citrate (A) and AgNPs-Spermine (B). BG and NPs indicate that the arsenic remained in the solution for controls (prepared in DI water only) and samples with nanoparticle, respectively. Salt represents the results for trials with the addition of nanoparticles and salt. All arsenic concentrations in the BG, NPs and NPs-Salt were significantly different according to One-way ANOVA at $P < 0.05$ level.

Major vibrational frequencies of As^{III} and As^{V} were reduced 7 and 20 cm^{-1} when changing from AgNPs-Citrate to AgNPs-Spermine suspensions, respectively, representing a red-shift in wavelength. A possible reason for this difference could be a charge transfer effect [135, 192] induced by the stronger adsorption of these two arsenicals onto nanoparticle's surface in the AgNPs-Spermine, as shown in the aforementioned adsorption experiments. Charge transfer excitations could significantly reduce the intrinsic intramolecular excitation of the adsorbate, thus resulting in a red-shift

[193]. For the two organoarsenicals, SERS signals were feeble in the AgNPs-Citrate suspension, but their characteristic vibrational frequencies of the As─C were distinguishable between MMA^V (625 cm^{-1}) and DMA^V (605 cm^{-1}). In the AgNPs-Spermine suspension, the SERS signals of MMA^V and DMA^V were similar to each other. Both organoarsenicals had a 785 cm^{-1} vibrational band, which was attributed to the symmetric As─O stretch [187, 188], and the stretch frequencies of As─C in MMA^V and DMA^V were 625 and 624 cm^{-1}, respectively. The vibrational band at 785 cm^{-1} was present in As^V, MMA^V and DMA^V. These three pentavalent arsenicals had As─O single bonds in their molecules despite their different deprotonation status in the AgNPs-Spermine suspension (Table 3.1). Since there were two methyl groups in DMA^V, the Raman spectra should have two vibrational modes of As─C [187], including symmetric and asymmetric vibrations. The symmetric and asymmetric vibrational frequencies for As─C in DMA^V were reported to be different, being 651 and 605 cm^{-1} respectively [187]. However, there was only one vibrational band found for the As─C vibration in the AgNPs-Spermine for DMA^V. This 624 cm^{-1} vibrational band was not reported previosuly and it might belong to the symmetric vibrational of As─C in DMA^V [70].

2.5.2 Measurement of Arsenicals using SERS in Cell Lysate

The potential interactions between arsenicals and cell lysate could inhibit the adsorption of arsenicals onto the nanoparticles, and hence reduce the SERS signal. Experiments were therefore conducted to investigate the interactions of arsenicals and cell lysate using a centrifugal filtration technique. Arsenic concentrations in the sample reservoir and filtrate receiver were monitored individually and arsenic concentration ratios in the sample reservoir vs filtrate receivers are shown in Fig. 2.5. Significant

differences in arsenic concentrations between the two reservoirs were not observed for both control and samples with cell lysate for all arsenicals, indicating the lack of significant adsorption of arsenicals on biomolecules larger than 1K Da. However, the effect of biomolecules less than 1K Da could not be evaluated by this experiment.

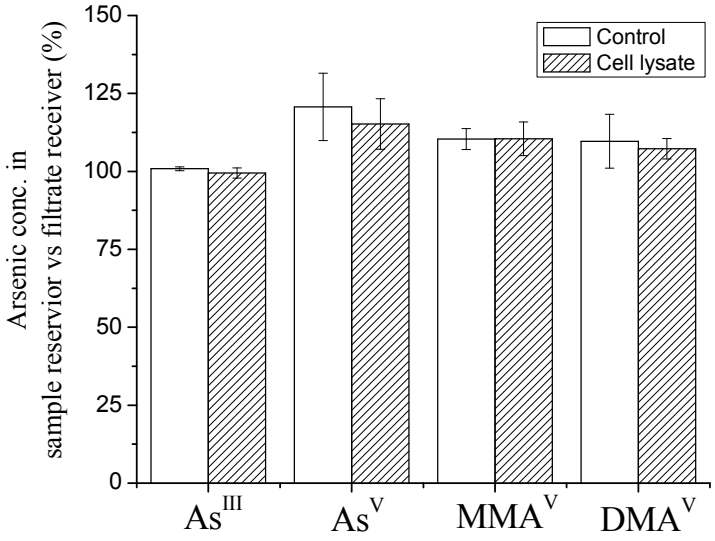

Figure 2.5 Arsenic concentration in the sample reservoir vs. in the filtrate receiver (%)

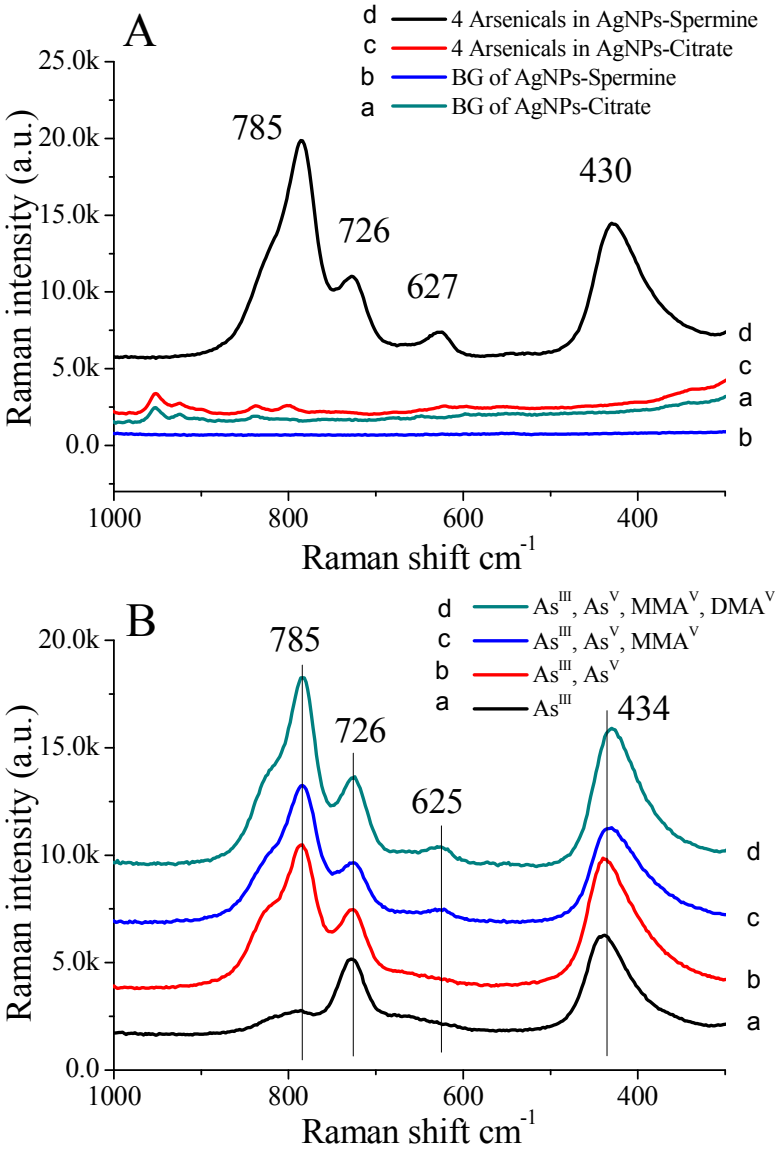

Figure 2.6 SERS spectra of arsenic species in the cell lysate.The SERS signals of arsenic mixture obtained in AgNPs-Citrate (A) and AgNPs-Spermine colloidal suspensions (B). The final concentration of individual arsenic in the AgNPs colloidal suspension was 200 ppb. The background signals from AgNPs-Citrate and AgNPs-Spermine colloidal suspensions were included for comparison. Figure B illustrates SERS spectra obtained in AgNPs-Spermine suspension with sequential addition of 20 µl of 100 ppm individual arsenic species into 180 µl of AgNPs-Spermine.

Substantial differences in SERS measurement of the four arsenicals were observed between AgNPs-Citrate and AgNPs-Spermine suspensions (Fig. 2.6A). The cell lysate at 2×10^4 cells/ml in both AgNPs-Citrate and AgNPs-Spermine suspensions did not generate significant background signal in the range of 1000~300 cm^{-1}, making the SERS measurement of arsenic possible. Intense SERS signals of arsenic were found in AgNPs-Spermine in comparison with AgNPs-Citrate. Arsenic fingerprint vibrational bands under the influence of cell lysate were confirmed by the method of sequential addition of individual arsenic standards where charactristic bands associated with each arsenic species appeared with the addition of As^{III}, As^{V}, and MMA^{V}/DMA^{V} (Fig. 2.6B). The vibrational bands 785, 726, and 627 cm^{-1} that appeared in the AgNPs-Spermine suspension were the characteristic vibrations of As^{V}, As^{III}, and MMA^{V}/DMA^{V}, respectively. The vibrational band at 430 cm^{-1} was from both As^{III} and As^{V}, as the sequential addition of As^{V} into the solution increased its intensity. Among these vibrational signals, the As^{V} signal was the strongest, followed by As^{III} and MMA^{V}/DMA^{V}. The relative standard deviations (RSD) for the intensities of these three vibrational band were 11.4, 9.8, and 10.3 % (n=3), respectively. The RSD values were less than 20 %, indicating a relatively reliable SERS measurement [194]. The limit of detections (LOD) calculated based on three times of standard deviation of the blank samples were 1.0, 2.8, and 9.9 ppb for As^{V}, As^{III}, and MMA^{V}/DMA^{V}, respectively.

For a better understanding of the SERS response under the influence of cell lysate, pH, size and zeta potential of the AgNPs were monitored under different concentrations of cell lysate (Fig. 2.7). No obvious changes in pH were observed in the cell lysate at different concentrations in both AgNPs suspensions (data not shown). The size of the

nanoparticles increased with the amount of cell lysate introduced, especially in the AgNPs-Spermine suspension (Fig. 2.7A), where the size increased from approximately 50 to 90 nm. The zeta potential of the nanoparticles in AgNPs-Spermine maintained a positively charge, while that in AgNPs-Citrate was still negative at different concentrations of cell lysate (Fig. 2.7B). In the AgNPs-Citrate suspension, no significant change in zeta potential was observed with the increase in the concentrations of cell lysate. Considering the fact that under the highest concentration of cell lysate used, the size of AgNPs-Spermine increased sharply, while less of a change appeared for AgNPs-Citrate, it was postulated that there were more negatively charged biomolecules than positively charged ones in the cell lysate. The zeta potential of the 2×10^4 cell/ml cellular matrix was about -18 mV, indiciating the presence of negatively charged biomolecules in the cell lysate. The size of AgNPs-Spermine increased likely due to the electrostatic attraction in AgNPs-Spermine and as opposed to a repulsive effect in AgNPs-Citrate. This could also explain the changes in zeta potential in the AgNPs suspension, where the zeta potential of AgNPs-Spermine dropped upon introduction of cell lysate due to neutralization of positive charges on the AgNPs surface. The zeta potential remained almost unchanged in the AgNPs-Citrate suspension owing to electrostatic repulsion preventing biomolecules from getting close to the surface of nanoparticles.

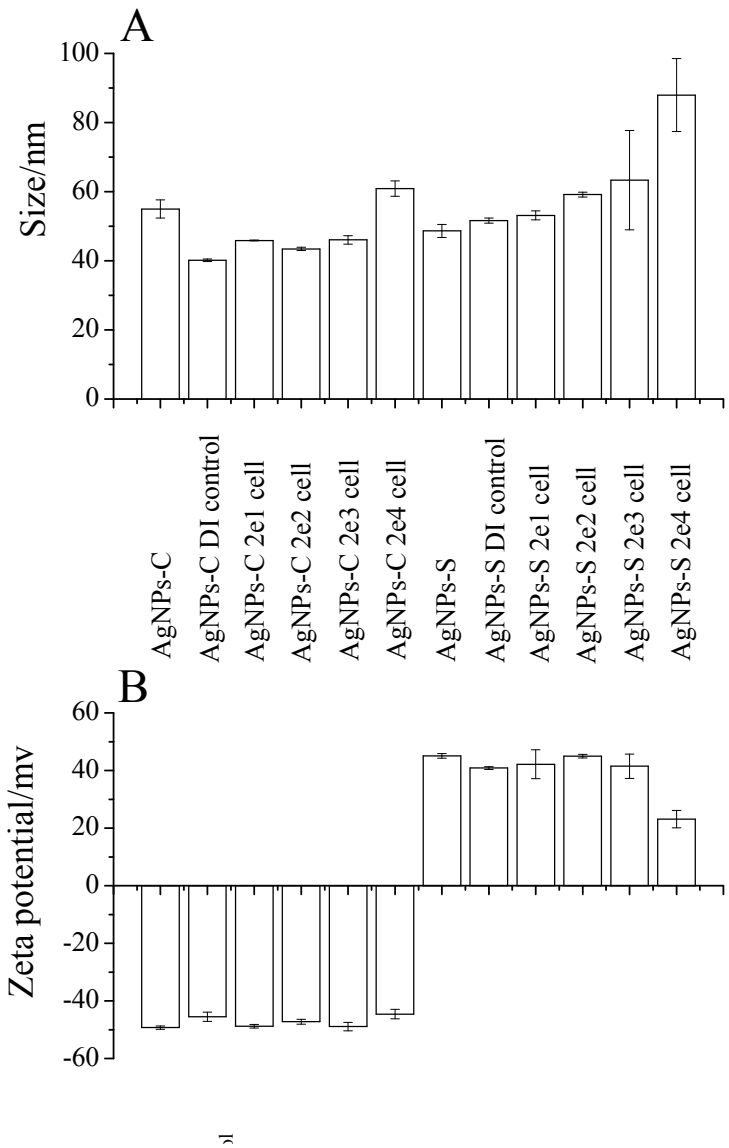

Figure 2.7 Changes in size (A) and zeta potential (B) of AgNPs upon interaction with cell lysate. AgNPs-C and AgNPs-S stand for AgNPs-Citrate and AgNPs-Spermine colloidal suspensions, respectively. For both DI controls, 910 µl of AgNPs colloidal suspension was mixed with 90 µl of DI water. The AgNPs containing different concentrations of cell lysate were prepared by mixing 910 µl of AgNPs colloidal suspension and 90 µl of different concentrations of cell lysate. At $P = 0.05$ level, changes in size and zeta potential were significant among different cell lysate introduced.

The size and zeta potential of AgNPs-Spermine changed upon exposure to cell lysate, however these changes did not significantly alter the stability of AgNPs in the

suspension, making the measurement of arsenic using SERS possible. The stability of AgNPs upon interaction with cell lysate was mostly evaluated by the zeta potential, being beyond the range of -30 to +30mV under most concentrations of cell lysate introduced. The AgNPs-Spermine positive charge was the key to producing an intense SERS response. In the presence of cell lysate, the AgNPs-Spermine surface could be coated through the formation of a protein corona [144-146, 195], as indicated by the hydrodynamic size of AgNPs-Spermine that increased from 50 to 90 nm. Arsenicals were able to get close to the positively charged surface of AgNPs, despite the formation of a protein corona on the AgNps surface. As^{V} was the only 100% negatively charged among all arsenic species studied using AgNPs-Spermine in the presence of cell lysate (Table S1), it therefore yielded the strongest SERS signal. Another possibility was the aggregation of AgNPs-Spermine upon introduction of the cellular matrix, as the size of AgNPs-Spermine in the presence of 2×10^{4} cell/ml cellular matrix increased. The aggregation could induce the generation of SERS hot spots, hence increasing the SERS signals. The aggregation could be attributed to surface charge of AgNPs-Spermine being neutralized during the process as evidenced by the dramatically drop in the zeta potential.

2.6 Conclusions

Arsenic speciation in a cellular matrix by SERS was studied by employing AgNPs colloidal suspensions. Nanoparticle surface was manipulated by citrate and spermine to form negatively or positively charged AgNPs. Arsenicals showed substantially different SERS responses in the two colloidal suspensions, mainly due to the distinct difference in the interaction between arsenicals and the nanoparticles. This study revealed that salt-induced aggregation is not required for SERS measurement of arsenic in an AgNPs-

Spermine suspension. However, AgNPs-Citrate required aggregation in order to generate SERS signals. Arsenic speciation in cell lysate could be successfully carried out in an AgNPs-Spermine suspension, while AgNPs-Citrate could not yield significant SERS signals under the experimental conditions used. Both AgNPs colloidal suspensions maintained their original surface charges in the presence of cell lysate. However, a significant drawback of this method was that it was unable to distinguish MMA^V from DMA^V. This study proved that AgNPs-Spermine colloidal suspension could be a promising SERS substrate for studying arsenic metabolism in a biological matrix, reducing the bias caused by traditional techniques that involve sample extraction and pretreatment.

Chapter 3

Employing Coffee Ring Effect on Silver Nanofilm for Arsenic Speciation Study

3.1 Abstract

In this study, an analytical method using a new coffee ring phenomenon was developed and used for arsenic speciation. The coffee ring effect was created via reducing the surface tension of the sessile droplet and enhancing the capillary action generated by closed packing nanoparticles at the three-phase (air, solid and liquid) contact line. For easy discussion, it was named halo coffee ring phenomenon since two concentric circles of coffee ring stain were formed on the surface. The outwards flow caused by the capillary action provides an alternative driving force for separation and the separation mostly depends on the interaction between analyte and the nanofilm surface. Arsenic speciation based on this halo coffee ring phenomenon was demonstrated on a silver nanofilm, which was formed by coating with silver nanoparticles on the glass substrate. Four arsenic species commonly occurred in biological and environmental samples including arsenite, arsenate, monomethylarsonic acid and dimethylarsinic acid, were selected for arsenic speciation analysis using this halo coffee ring effect coupled with surface enhanced Raman Scattering (SERS) technique. Typically, 2 μL of arsenic solution was dropped onto the silver nanofilm surface and SERS signals were obtained from the center to edge after complete evaporation. Surfactants were employed to reduce the surface tension and different buffer solutions were used to achieve separation. The separation of arsenic species from the center to edge of halo coffee ring was promising, although peak overlapping for some arsenicals were observed. The method using this new halo coffee ring effect has a great potential to become an alternative and unique technique for separation of arsenic in biological and environmental samples.

Key words: Coffee ring effect • Halo coffee ring • Arsenic speciation • SERS • Silver nanofilm

3.2 Introduction

The coffee ring phenomenon is the ring-shaped coffee stain left on the solid surface when one coffee drop is dried on a solid surface [150]. Deegan and colleagues unveiled the mystery of coffee ring phenomenon and pointed out that when the contact line was pinned everything in the solution will move to the edge with the process of evaporation [150]. With the evaporation of liquid over the liquid drop surface, liquid from the center region would move towards the edge to replenish to lose of liquid since the evaporation rate is higher at the edge than the center. The movement of liquid from the center to the edge is named capillary flow and Deegan pointed out that this capillary flow is not stoppable since surface-tension gradients, solute diffusion, electrostatic and gravity effects—are negligible in ring formation [150]. Currently, a majority of studies involving the coffee ring effect in analytical chemical applications take advantage of the procedure for signal enhancement. For example a drop coating deposition method was employed to concentrate analytes on the coffee ring region and improve detection sensitivity via Raman spectroscopy [151, 152]. Furthermore, the coffee ring effect can be effectively coupled with surface-enhanced Raman spectroscopy (SERS), only requiring introduction of metallic nanostructure, nanoparticles [131, 153-155] or nanofilms [156]. Because the capillary flow will push everything in the liquid drop towards the edge of the droplet, the accumulated nanoparticles will create hotspots and facilitate SERS signal enhancement [131, 154, 157]. Meanwhile, there are many other techniques developed to enhance SERS signals, e.g., the coffee ring effect and improve the uniformity of

deposition after the liquid is dried on the surface, including introduction of ellipsoids particles [158] or introduction of hydrosoluble polymer additives into the solution [159].

Although Deegan's paper demonstrated the mechanism of the coffee ring phenomenon, there was a critical matter missing in the paper. The paper did not explain how a liquid drop was pinned on the surface and only stated that it was a geometrical constraint [150]. Later on Ball noted that Thomas Young's famous condition for surface wetting was the key for the coffee ring mechanism [196]. Thomas Young's equation defined the force balance when a liquid droplet forms a hemisphere shape on a solid surface, as the following:

$$\gamma sv = \gamma sl + \gamma \cos \theta_{eq}$$

Where γsv, γsl and γ stand for the solid/air, solid/liquid and liquid/air interfacial tensions and θ_{eq} is the contact angle at equilibrium. Typically, when $\gamma sv < \gamma sl + \gamma \cos \theta_{eq}$, the liquid drop will form a spherical cap on the solid surface and when $\gamma sv > \gamma sl + \gamma \cos \theta_{eq}$, the surface will be complete wetted and the liquid will form a thin film on the surface known as a Van der Waals pancake [197]. In Deegan's experiments, the coffee ring phenomenon was observed by placing drops of deionized water (DI) water containing polystyrene microspheres on a surface. These microspheres head towards the contact line during the evaporation [150]. Due to the strong surface tension of water and no surfactant existing in the solution, the liquid drop was held on the surface as a hemisphere cap (pinned on the surface.) This kind of liquid drop on a surface is termed a sessile droplet, which is characterized with a defined wetted area and a contact line [198].

The dynamics of a sessile drop have been extensively studied in order to understand different solute deposition patterns, particle self-assemble during evaporation,

inkjet printing applications, internal flow directionality, etc [199-202]. Until now it is still considered as a complicated process, and it is suggested that more universal models should be considered for the better understanding of droplet evaporation [203]. However, due to the simplicity, one of the potential applications of sessile drop is the separation capability, which is intriguing. The coffee ring effect has been employed for the successful separation of different sized particles. Owing to geometrical constraints, particles were arranged according to their size at the coffee ring edge [160, 161]. However, these particles were extremely close to each other along a narrow strip less than 100 μm at the edge of the coffee ring as capillary flow drove all solution toward the edge [160]. This study was exciting because it demonstrated the separation capability of coffee ring effect (albeit for particles only) and the sizes of droplets were very small (ranging 0.5~2.0 μL). By dropping such a small volume of liquid onto the surface, the simplicity of coffee ring-based separation was demonstrated as the separation was merely driven by the capillary flow under the evaporation of the droplet. Again, the strong capillary flow is capable of driving all solutes in the droplet towards the edge of the droplet, regardless of surface-tension gradients, solute diffusion, electrostatic and gravity effects [150]. However, separation based on size might not be applicable towards small molecules, since there is no significant difference in sizes for small molecules.

Currently, there are no reports of applications of the coffee ring effect for the separation of small molecules in the literature. This is probably because potential separation applications based on the coffee ring effect are extremely challenging for the following reasons: 1) The size of the droplet is very small (usually the volume is less than 10 μL); and 2) The capillary flow is too strong to drive all solutes towards the edge. It

seems that in order to achieve a useful separation using the coffee ring effect, the following requirements should be fulfilled. The liquid in the droplet should be able to overcome the constraint of the droplet and migrate into the peripheral region, otherwise the solute will accumulate at the edge of the droplet. Furthermore, the interaction of small molecules in the droplet with the surface should be strong enough to retain small molecules during the migration. Considering that previous work has found that solution in the droplet could be induced to migrate into the peripheral region via the reduction of surface tension [197, 204] and that enhanced interaction of solutes with the surface should be achievable by replacing the surface with nanoparticles (which would increase the surface area significantly), we reason that it may be possible to realize the separation of small molecules using the coffee ring effect.

Here, we propose to explore the separation capability of the coffee ring effect on the silver nanofilm (AgNF) which is composed of closely packed silver nanoparticles. Surfactants will be introduced into the sessile droplet in order to reduce the surface tension. The strong capillary action, resulting from the closely packed nanoparticles at the droplet edge, should be able to facilitate the migration of solution in the droplet into the peripheral region. The solution migration provides a method for mobilizing analytes in the sessile droplet. This proposed method will be employed to study arsenic speciation of four common existing arsenicals were chosen in order to demonstrate the separation capability, including arsenite (As^{III}), arsenate (As^{V}), monomethylarsonic acid (MMA^{V}) and dimethylarsinic acid (DMA^{V}). SERS will be employed to detect the arsenicals, since the closely packed silver nanoparitcles are capable of enhancing the signals of arsenicals by surface plasmon resonance.

3.3 Material and Methods

3.3.1. Materials and Chemicals

Sodium metaarsenite, 98% (As^{III}), sodium arsenate dibasic, 99% (As^{V}), cacodylic acid sodium salt, 98% (DMA^{V}) were purchased from Sigma-Aldrich (St. Louis, MO). Monosodium acid methane arsonate, 99.5% (MMA^{V}) was purchased from Chem Service, USA. Silver nitrate (99.99%) was obtained from STREM chemicals (Newburyport, MA). Sodium citrate dihydrate (Granular certified), NaOH, HCl, K_2HPO_4, KH_2PO_4, ammonium formate, glacial acid were certified A.C.S grade or higher and purchased from Fisher scientific Inc. The phosphate buffer was prepared by mixing equal volume of 0.2 M of K_2HPO_4 and KH_2PO_4. Sodium dodecyl sulfate (SDS, 99.0%) and cetrimonium bromide (CTAB, 99.0%) were purchased from Sigma-Aldrich (St. Louis, MO). (3-Aminopropyl)trimethoxysilane (APTMS), was obtained from Sigma Aldrich (St. Louis, MO). All solutions were prepared in deionized water (DI water) (18.2 MΩ, Barnstead Nanopure Diamond) unless with specific indication. All arsenic stock solutions were prepared in DI water at 1000 ppm (as arsenic). Glass microscope slides, purchased from Fisher Scientific (Pittsburgh, PA), were cut into 1×1 cm^2 pieces as glass substrates. Small size weighing boats were purchased from Cole-Parmer instrument (Vernon Hills, IL) and 25ml clear glass vials with caps were purchased from Fishersci (Hampton, NH).

3.3.2. Instrumentation

Malvern Zetasizer Nano-ZS (Westborough, MA) was employed to obtain the size and zeta potential of nanoparticles synthesized in the laboratory. The average diameters of hydrodynamic nanoparticles were obtained from the "Z-average" intensity peak as a function of size. UV-vis absorption spectra of silver nanoparticles were obtained from a

Cary 300 UV-vis spectrometer. All pH measurements were carried out on a Fisher scientific accumet research AR15 pH/mV/°C meter.

A Veeco multimode nanoscope III D atomic force microscopy (AFM) was employed to obtained surface morphology of the prepared silver nanofilm (AgNF) and to monitor the changes of surface morphology during the cleaning and salinization procedures.

The Raman spectrometer used was the Perkin-Elmer Raman station (Model 400F), which employed a diode laser operating system at 785 nm with an average power of 100 mW at the sample and 100-micron spot size. This Raman station was equipped with one Perkin-Elmer microscopy 300, which had a movable stage and a build-in camera monitoring the sample surface. The laser source was focused on the sample on the stage through fiber optics cable connecting from 400F to microscopy 300. Usually, a 20 × optical lens was employed in order to improve sample focus and Raman signal response. One piece of silicon wafer was employed to calibrate the Raman system at a daily basis, and the Raman signal intensity at 522 cm^{-1} was monitored for calibration purposes. The following SERS measurement parameters used: laser wavelength, 785 nm; exposure time, 1 second; and 4 spectra were averaged per measurement.

3.3.3. Experimental Procedures

3.3.3.1 Fabrication and characterization of AgNF

The fabrication of AgNF is consisted of two major steps, first, synthesis of citrate-coated silver nanoparticles colloidal suspension (AgNPs-Citrate) and second, immobilization of AgNPs-Citrate onto glass substrates. Silver nanoparticles (AgNPs) were synthesized by reducing silver nitrate with sodium citrate [181]. Briefly, all

glassware were emerged in the Aqua Regia solution (HCl/HNO3 = 3:1, v/v) overnight and then rinsed with a large amount of tap water and DI water and finally dried in an oven at 80 °C before use. Then, a 250 ml round bottom flask with 50 ml of 1×10^{-3} M silver nitrate was heated to boil in an oil bath under vigorous stirring with a condenser equipped to reflux. Sodium citrate solution (2 ml, 1% (w/v)) was added dropwise to the hot solution and kept boiling for one hour to yield the greenish yellow AgNPs-Citrate colloidal suspension. The following properties of the colloidal suspension were obtained after the solution cooled down, including size, surface charge and pH.

The immobilization of AgNPs-Citrate onto glass substrates began with the silanol formation on glass substrates. All glass substrates (about 1×1 cm^2) were soaked in Aqua Regia solution overnight, and then sonicated successively in concentrated NaOH solution (2 M) and HCl solution (2 M) for 2 hours. These glass substrates were thoroughly rinsed with large amount of tap water and DI water to wash away excess acid or base. Finally these glass substrates were dried in an 80 °C oven prior to use. Then, the AgNF was fabricated following a two-step procedure [166]. The first step was the silanization reaction on glass substrates surface to attach APTMS molecules catalyzed by a diluted acid [205]. APTMS solutions with different concentrations (0.5, 1.0, 2.5, 5.0 and 10.0% (v/v)) in anhydrous ethanol were first prepared. Then five pieces of glass substrates were soaked in a 25 ml glass vial containing 10 ml of APTMS solution and 100 μL of 1 M HCl solution for 4 hours on an orbital shaker (150 rpm). After the silanization reaction, the glass substrates were cleaned with anhydrous ethanol under sonication for four times of 3-minutes period in order to remove loosely attached APTMS molecules on the glass surface. These treated glass substrates were then dried by nitrogen and heated in an oven

at 80 °C for 30 minutes before the next step. The second step was to immobilize AgNPs-Citrate onto the treated glass substrates. AgNPs-Citrate were immobilized by electrostatic interaction with the glass surface, since the amine groups were facing outwards and positively charged in the solution. The high affinity interaction between silver nanoparticles and amine groups shoud further enhance the attachment [166, 206, 207]. Briefly, five pieces of glass substrates prepared from the first step were placed in a small weighing boat with no overlapping among the slides. Next, 5 ml of AgNPs solution was carefully transferred into a weighing boat and the glass slides were submerged in the solution for different time periods (4, 8, and 24 hours) on an orbital shaker (50 rpm). In order to see the importance of the silinization procedure, a control experiment was carried by soaking untreated glass substrates in the colloidal suspension for the same period of time. DI water was introduced to make up the evaporation. The resulting glass substrates were then cleaned with DI water for three times, dried under N_2 gas, and stored in freezer prior to use.

A UV-vis spectrometer was employed to study surface plasmon resonance of the AgNF with the glass substrate background signal subtracted. Atomic force microscopy (AFM) was used to obtain the surface topology properties of the AgNF, including surface morphology and the AgNF thickness. Two μL of 100 ppm As^{III} was dropped onto the AgNF surface, and SERS signals were immediately collected four times at the center region of the droplet by the Raman spectrometer. For comparison, As^{III} solution was dropped onto a bare glass slide and Raman measurement was carried out. Preparation parameters of AgNF were optimized including the concentration of APTMS and the soaking period in AgNPs-Citrate solution on the basis of the resulting SERS signals.

3.3.3.2 Arsenicals SERS fingerprint signals on the AgNF

Stock solutions of arsenic compounds (1000 ppm) were diluted to 100 ppm with DI water or different buffers, including 0.1 M acetic acid (pH=2.9), 0.1 M phosphate buffer (potassium salt, pH=7.5), and 0.1 M ammonium formate buffer (pH=6.9) as sub-stock solutions. Typically, 2 μL of arsenic solution from sub-stocks were dropped onto the AgNF, and SERS signals were collected randomly at the center region of the sessile droplet. After about 35 minutes of evaporation, the droplet was complete dry and a ring shaped stain was formed on the AgNF. The SERS signals were collected at the edge region of the ring stain.

3.3.3.3 Coffee ring formation on the AgNF

As^{III} was chosen as the arsenic species to explore the coffee ring effect on the AgNF for arsenic determination by using SERS. Two approaches were used to study this phenomenon, including signals changing with time lapse and signals changing with the distance from the center to edge of coffee ring. To study the change of arsenic SERS signal with time lapse, 2 μL of 100 ppm As^{III} in DI water was dropped onto the AgNF and SERS signals were collected every 2 minutes under ambient conditions. Meanwhile, the signals changing with distance was carried out by collecting signals from the center to edge with 100 μm increment 5, 10, and 15 minutes after the sessile droplet dropped onto the AgNF. The SERS signal response of As^{III} on the dry film was poor even at the edge of the coffee ring, thus MMA^{V} was employed to study the coffee ring effect from the center to the edge. A complementary experiment was carried out by dropping 2 μL of 100 ppm MMA^{V} in 0.1 M ammonium formate buffer on the AgNF, and SERS

measurements were carried out along the radius from the center to the edge of the ring stain with 100 μm increments after the complete evaporation.

3.3.3.4 Arsenicals speciation on the AgNF

Mixed arsenic standard solutions containing As^{III}, As^{V}, MMA^{V} and DMA^{V} of 100 ppm for each species, were prepared in different buffer solutions, including 0.1 M acetic acid (pH=2.9), 0.1 M phosphate buffer (pH=7.5) and 0.1 M ammonium formate (pH=6.9), with or without 0.05% of surfactants, including SDS or CTAB. One drop (2 μL) of the solution was dropped onto the AgNF surface and the sessile droplet was allowed to dry on a flat bench under ambient conditions. Different stain patterns were found depending on whether surfactants were applied. The typical coffee ring stain, only having one ring shaped stain, was found for the arsenic solution without surfactants, while the two concentric-ring shaped stain pattern was formed after adding surfactants. Inspired by the previous work of Brochard-Wyart et al. [197, 204], this phenomenon of depositing two concentric-ring shaped stains is named halo coffee ring effect. It is necessary to point out that the three-phase contact line did not move during the evaporation of sessile droplet containing surfactants, only liquid in the sessile droplet permeating into the peripheral region of the sessile droplet. There was a clear boundary between these two concentric rings, named the inner ring (IR) and the outer ring (OR). Typically, SERS measurements on all coffee ring stains were carried out from the center all the way to the OR edge along the radius of the ring and the sampling spots were 100 μm increments. For the two concentric-ring SERS measurements around the boundary region, sampling spots at 10 μm inside and outside the boundary were taken as well.

3.4 Results and Discussions

3.4.1 Optimization of parameters for fabrication and characterization of AgNF

Monolayer fabrication is a well stuided technique [166, 208, 209] to coat with functional end groups, such as $-NH_2$ and $-SH$, on a glass surface. The resulting functionalized glass surface provides a strong binding affinity to gold/silver nanoparticles by electrostatic interaction or metal sulfur bond [210] and thus, uniform nanoparticle film could be prepared. In this study, the glass substrate was modified with APTMS for attaching AgNPs-Citrate onto the surface to prepare AgNF. The pH of the freshly prepared AgNPs-Citrate colloidal solution was 9.0, and the surface of AgNPs-Citrate was negatively charged according to the zeta potential measurement. Because the $-NH_2$ group of APTMS has a very high pKa value (pKa > 10) [211], the lone pair electrons on the nitrogen atom should be able to capture a proton in the pH 9.0 solution to form a positively charged $-NH_3^+$ group [206]. The positively charged surface would facilitate the adsorption of negatively charged AgNPs, and the strong binding between APTMS and AgNPs [206, 207] will further enhance the immobilization of AgNPs-Citrate onto the glass surface.

To optimize the immobilization time of AgNPs-Citrate, glass substrates treated with 2.5% of APTMS were soaked in the AgNPs-Citrate solution for different period of time (Fig. 3.1A).

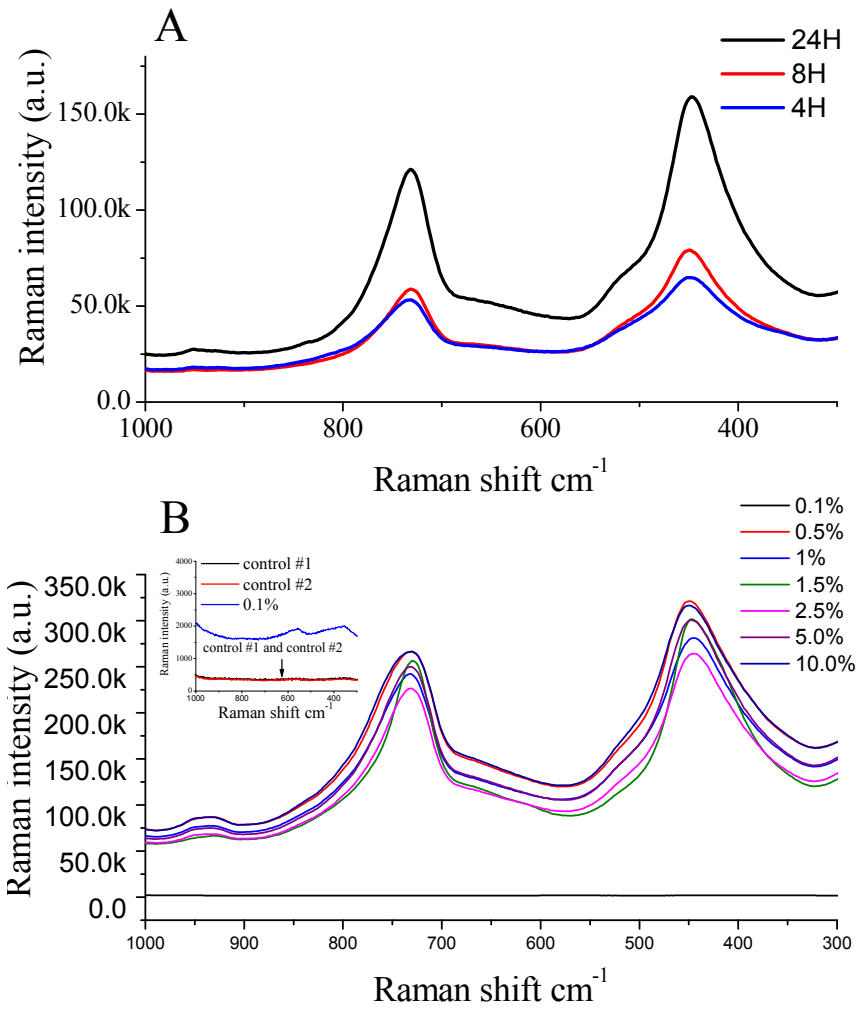

Figure 3.1 Optimization the usage of APTMS. In A, 2μL 100ppm As^{III} SERS signals obtained on AgNF, including two controls (inset), control #1 was 2μL As^{III} on bare glass slides, control #2 was 2μL As^{III} on glass slide without salinization procedure. B, SERS intensity of vibrational band at 732 cm^{-1}, the average intensity was calculated from 4 individual measurements.

It was found that 24 hours of immobilization yields the strongest signal response for 2 μL of 100 ppm As^{III} in DI water, and less strong signal was obtained after immobilization of 8 hours and the weakest signal was obtained for the reaction of 4 hours.

The time of immobilization was selected as 8 hours in the further experiments for the sake of saving time. The amounts of APTMS needed were optimized (Fig. 3.1B). No SERS signals were observed from the two control experiments, including the bare glass slide and the glass slide without APTMS treatment and only minimum signals were obtained by using 0.1% of APTMS. Strong signals were yielded by using 0.5 to 10.0% of APTMS. These results indicated that modification of the glass surface using APTMS was the key factor for the successful fabrication of the AgNF. In addition, it seems that 0.5% of APTMS would be sufficient for the treatment of glass substrates. Eventually, 1% of APTMS was employed for the following experiments.

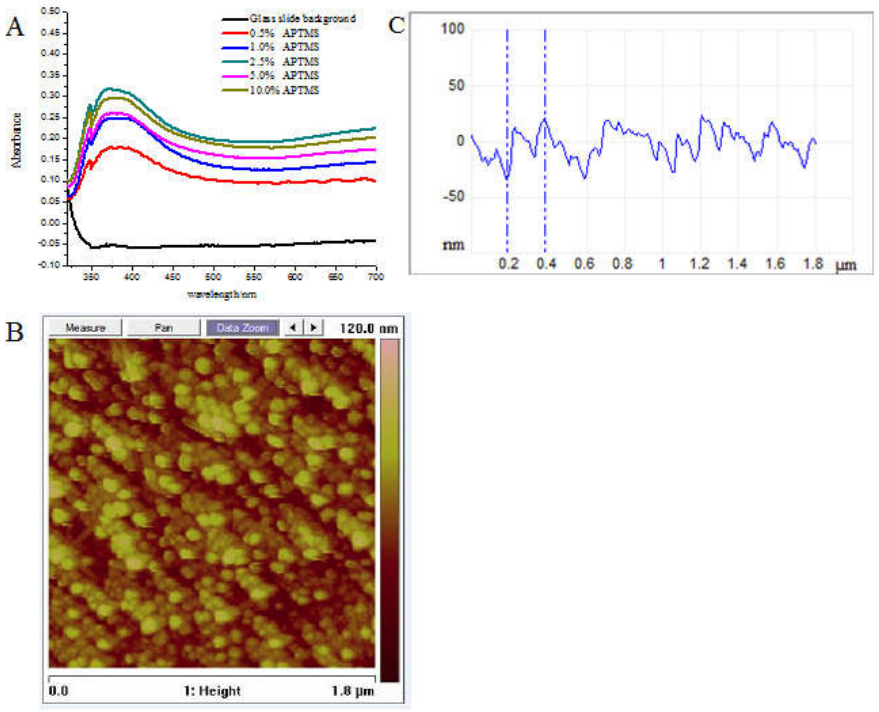

Figure 3.2 Properties of the AgNF. A, UV-vis absorbance of AgNF fabricated using different concentration of APTMS; B, the typical AgNF surface morphology using AFM depth imagine; C, the cross-section profile of the AgNF and the vertical distance was the distance between the valley and the peak as the two dash lines indicated.

UV-vis spectrum was obtained to compare the surface plasmon resonance of the AgNF fabricated using different amount of APTMS (Fig. 3.2A), and the AgNF surface morphology was studied using AFM (Fig. 3.2B). The intensity of surface plasmon resonance should be in positive correlation with the density of AgNPs immobilized on the AgNF. As shown in Fig. 3.2A, the surface plasmon resonance of AgNF increased with higher concentration of APTMS in general with an absorbance exception of the AgNF fabricated using 2.5% APTMS, which was the greatest among all AgNF. This observation of decline in AgNF surface plsmon resonance with APTMS more than 2.5% could be attributed to the limited area of glass substrates. When occupation of alkylsilanes on the glass substrates reached the threshold, excessive APTMS could no longer improve the attachment of AgNPs-Citrate. Once the amount of APTMS was over the threshold, excessive APTMS molecules could react with the amine groups on the surface and thus reduce the binding capacity of AgNPs. As shown in Fig. 3.2B, the AgNF surface was coated thoroughly with AgNPs as bright dots, however, the AgNPs arrangement was not well organized. AFM cross-section of the sample is shown in Fig. 3.2C. Ten random sections were selected in order to calculate the mean vertical distance of the AgNF thickness, which was found to be 48.7 ± 6.7 nm. The average size of AgNPs was about 50 nm according to the z-average measurement by Zetasizer suggesting that the AgNF formed a monolayer film.

3.4.2 SERS response of arsenicals on the AgNF

The typical fingerprint SERS signals of different arsenicals including As^{III}, As^{V}, MMA^{V} and DMA^{V} in different solutions are shown in Fig. 3.3, as well as background

signals of different AgNF surface were studied in the fingerprint signals range (1000~300 cm^{-1}) in Fig. 3.4.

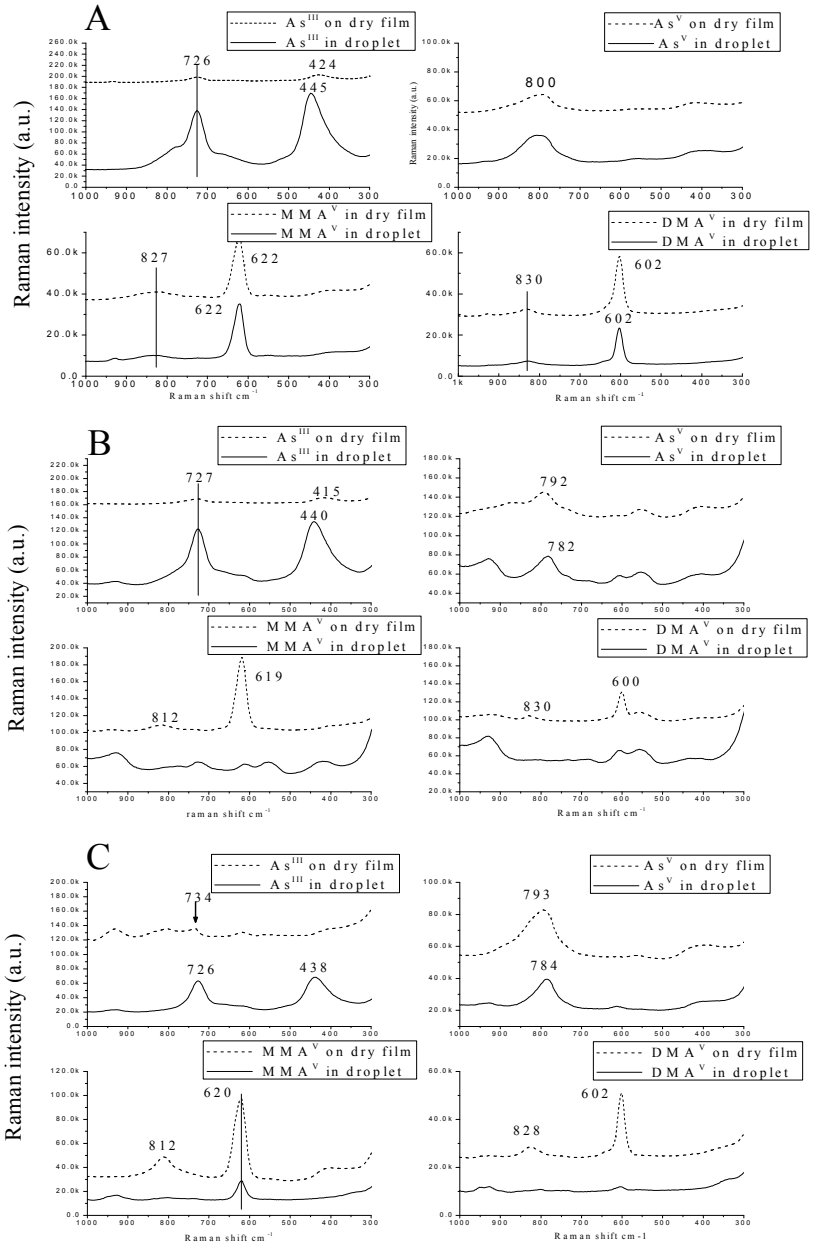

Figure 3.3 Individual arsenic SERS signals on the AgNF as droplet (as black curves) and at the edge of dry film (as red curves). All signals were obtained from 2 μL of 100ppm arsenic solutions in different buffers, A—0.1 M acetic acid (pH=2.9), B—0.1 M phosphate buffer (pH=7.5), C—0.1 M ammonium formate buffer (pH=6.9).

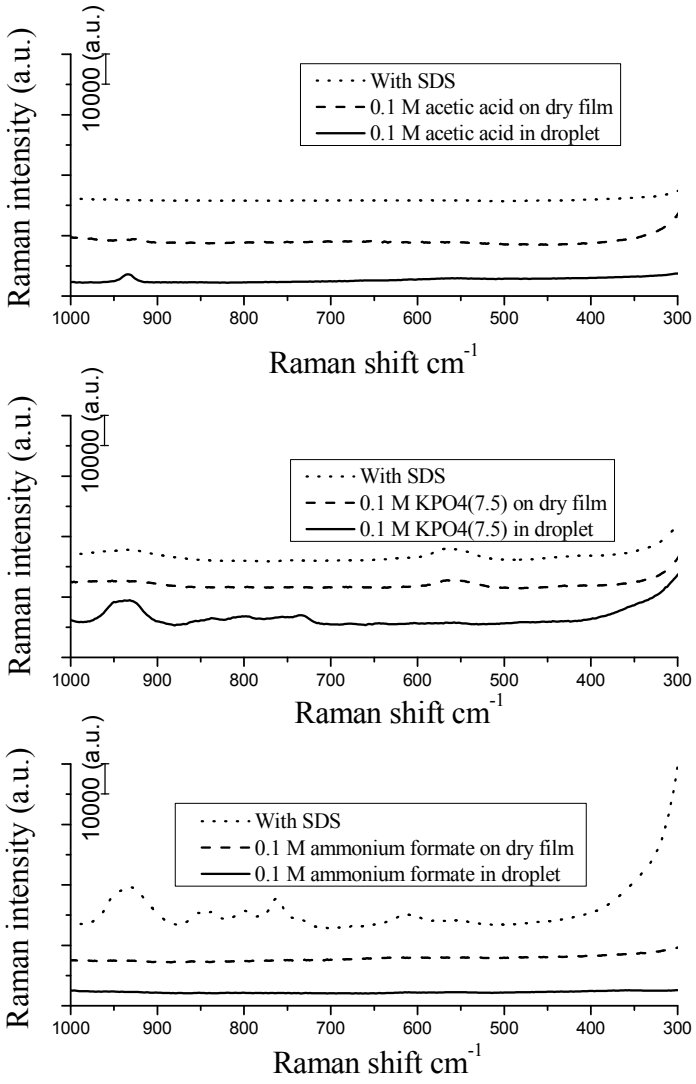

Figure 3.4 Typical SERS background signals from different buffer system with or without SDS including. A—0.1 M acetic acid; B— 0.1 M phosphate buffer (potassium salt, pH=7.5); C—0.1 M ammonium formate.

Signals were collected at the center of droplet once 2 μL of 100 ppm arsenic solution was placed on the AgNF. Because of the coffee ring effect, signals were collected close to the edge region of coffee ring stain after complete evaporation of the sessile droplets. There was no significant interference in the Raman shift range 1000~300

cm^{-1} from these three buffers employed here (Fig. 3.4). In 0.1 M acetic acid (Fig. 3.3A), a characteristic vibrational band at 726 cm^{-1} for As^{III} was observed, which was resulted from As─O stretch mode [184]. The band at 445 cm^{-1} was not reported in literature, and no attempt was made to identify and assign this band. In addition, it was observed that the band at 445 cm^{-1} was always present along with the band at 726 cm^{-1} for As^{III} and usually with stronger intensity. After the sessile droplet dried completely, signal intensities of both bands reduced significantly but were still distinguishable with the unassigned vibrational band shifting to a low vibrational number at 424 cm^{-1}. When As^{III} was present in the sessile droplet, As^{III} could get really close to the AgNF surface due to diffusion and thus the signal intensity was very strong. Although the evaporation of solution should be able to bring As^{III} molecules significantly close to the AgNF, the SERS signal dropped dramatically unexpectedly. The dramatic changes in SERS signals between in the droplet or on the dry film could be due to the fact that As^{III} has a pKa value of 9.2 and it is always protonated in the acetic acid buffer. The fully protonated As^{III} can prevent the complexation of As^{III} with the AgNF surface. For As^{V}, it had a fingerprint signal at 800 cm^{-1} in the sessile droplet or on the dry film and this could be assigned to the As─O symmetric vibration [186]. The superposition stretch of $\nu 2$ and $\nu 5$ of the arsenate molecule was not distinguishable in this buffer solution, which usually appears around 410 cm^{-1} [132]. Due to the similarity in structure for the two organoarsneicals, MMA^{V} and DMA^{V}, being different by one methyl group, their SERS signal profiles were highly resemble. MMA^{V} showed one sharp vibrational band at 622 cm^{-1} due to the As─C stretch (Fig. 3.3C) and one board vibrational band at 820 cm^{-1}, which should be assigned to the vibrational of As─O [188]. For DMA^{V}, the symmetric stretching of As─C was at 602

cm^{-1} since DMA^V has two As─C bonds, while the asymmetric As─O stretching was found at 830 cm^{-1} [135]. Being the only trivalent arsenic compound among these four arsenicals, As^{III} had a poor signal response on the dry film, while the rest had strong signal responses in both conditions. As mentioned previously, the possible reason could be that As^{III} could not form complexation with the AgNF surface while the others could.

Arsenicals SERS signals behaviors were highly similar between phosphate and ammonium formate buffers, since there is minor difference in their pH. In the phosphate buffer (Fig. 3.3B), a slightly different in signal for As^{III} was found with very small changing in vibrational frequency and the signal intensity dropped significantly on the dry film in comparison with that in droplet, while the vibrational frequency of As^V changed much more than As^{III}, from 800 to 782 cm^{-1} in the droplet and to 792 cm^{-1} on the dry film. For the two organoarsenicals, they had poor signal response in the droplet but relatively strong signals on the dry film, being different from their signals in the acetic acid buffer. In the ammonium formate buffer (Fig. 3.3C), these four arsenicals had similar signal response as in the phosphate buffer with minor differences in vibrational frequency with an exception for MMA^V. MMA^V had very strong vibrational intensity on the dry film, but only distinguishable signals in the droplet. When comparing the SERS signal of these two organoarsenicals in acetic acid with the rest two buffers, it was observed that they all have strong signal responses on the dry film, however, the SERS signal responses in the sessile droplet were completely different. In the acetic acid buffer, they have strong signals in the sessile droplet, which was almost the same as on the dry film. However, the signals were fairly poor or barely distinguishable with the pH increase

in other two buffers. The possible reason could be the deprotonation of organoarsenicals and the negatively charged AgNF surface in buffers with high pH.

3.4.3 Changes in arsenic SERS signals during evaporation of solvent

The essential of the coffee ring effect is the enrich capability during the evaporation of the sessile droplet. According to Deegan's work in 1997 [150], all solution will be driven to the edge of the sessile droplet as long as the contact line is pinned. Here two approaches were employed to validate this statement for arsenic analysis by SERS. First, the time lapse for signal changes of As^{III} was obtained (Fig. 3.5A). SERS signals of As^{III} were decreasing with the time at the center of the droplet, indicating that the concentration of As^{III} at the center region reduced with time. This observation should be due to the migration of As^{III} outwards from the center of the sessile droplet during the evaporation. The second approach was to collect SERS signals along the center to edge of the dry coffee ring. However, As^{III} had a poor SERS signal response on the dry film as mentioned in the previous section. Therefore, As^{III} SERS measurements were carried out before the sessile droplet dried completely and the SERS signals were collected from the center to the edge of the droplet with 100 μm increment in 5, 10 and 15 minutes after the As^{III} solution being dropped onto the AgNF surface. Similar results were obtained with 5, 10 and 15 minutes of drying.

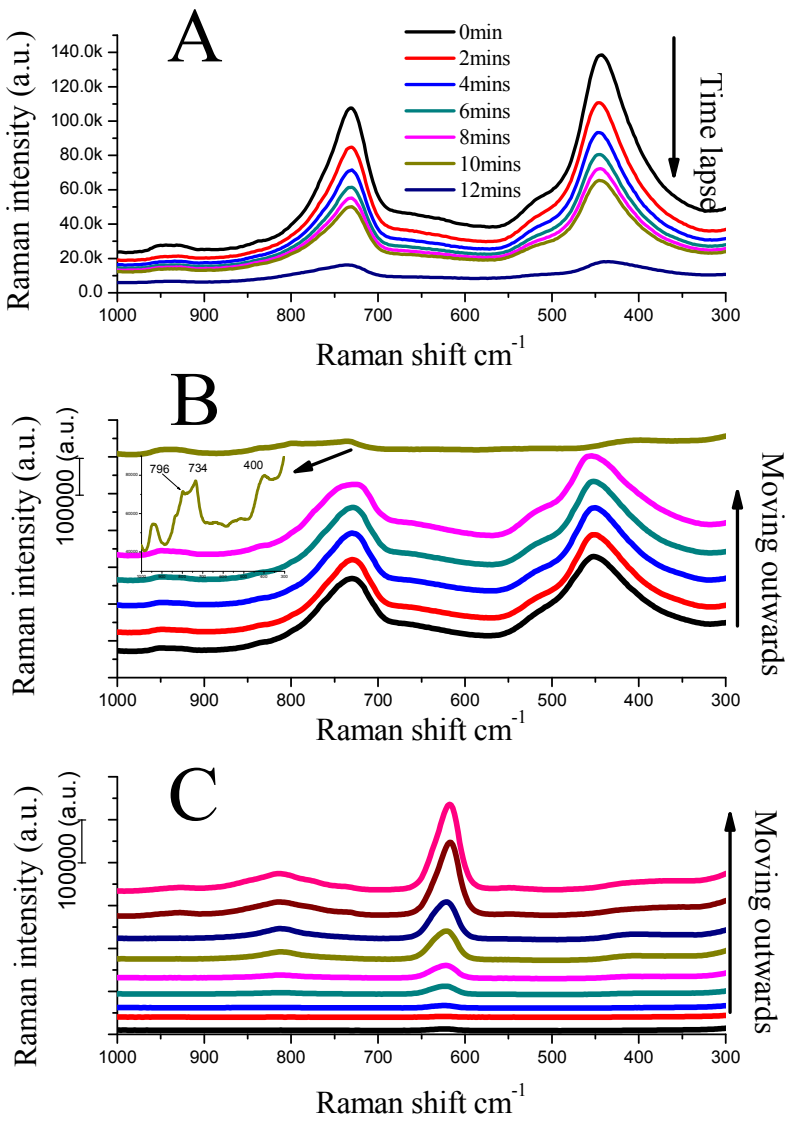

Figure 3.5 The typical coffee ring signal profile of aresnicals on the AgNF. A−Time lapse SERS signals of 2 µL 100ppm As^{III} (prepared in DI water) droplet on AgNF; B−As^{III} SERS signal from the center to edge after 2 µL 100ppm As^{III} was dropped onto the AgNF for 5 minutes. Note, it took around 35 minutes for a 2 µL droplet to evaporate totally on the AgNF.

The results of 5−minute of drying are shown in Fig 4.5B as an example. It was found that there was no significant difference in signal intensity along the radius of the

droplet, except a dramatic change in the signal profile at the edge where As^{V} fingerprint signals were observed. Also, we noticed that the droplet was dried faster during the SERS measurement than that in the air. Therefore, heat generated from laser irradiation could cause the oxidation of As^{III} to As^{V}. Although the signals maintained almost the same along the radius of the sessile droplet, the concentration of As^{III} should be higher near the edge than that of in the center. The reason for the lacking in the signal increase with distance from the center is unknown. Another experiment using MMA^{V} in ammonium formate buffer was carried out to observe the migration of arsenic during the evaporation (Fig. 3.5C). It was found that the SERS signal intensity was increased with the sampling spot moving outwards and the outmost sampling spot has the strongest signal intensity. It was clear that the coffee ring effect drives all solute towards the edge of the sessile droplet during the evaporation.

3.4.4 Arsenic speciation on the AgNF employing the coffee ring effects

3.4.4.1 Arsenic speciation on the AgNF without using surfactants

It was hypothesized that arsenic speciation could be carried out using the outwards capillary flow as a mobile phase and the AgNF area covered by the sessile droplet covering as the stationary phase. Nano-size particles were coated and packed closely on the surface of glass substrate and this property of the AgNF provided the adsorption/desorption interactions with the arsenicals. During the migration of the arsenicals in the droplet toward the edge driven by the capillary flow, different arsenic species might be separated because of different affinities to the AgNF surface. By monitoring the SERS signals from the center to the edge, the separation of arsenic species could be detected, as the fingerprint SERS signals representative of different arsenicals

should appear in the different regions on the AgNF surface. In order to examine the possibility of using this coffee-ring effect for arsenic speciation, arsenic species were prepared in different buffers, including 0.1 M acetic acid (pH=2.9), 0.1 M phosphate buffer (pH=7.5), 0.1 M ammonium formate buffer (pH=6.9), which have shown to have insignficant background signals in the 1000~300 cm^{-1} range. SERS signals were obtained along the radius from the center to the edge of coffee ring after the sessile droplet was dry, and the results are shown in Fig. 3.6.

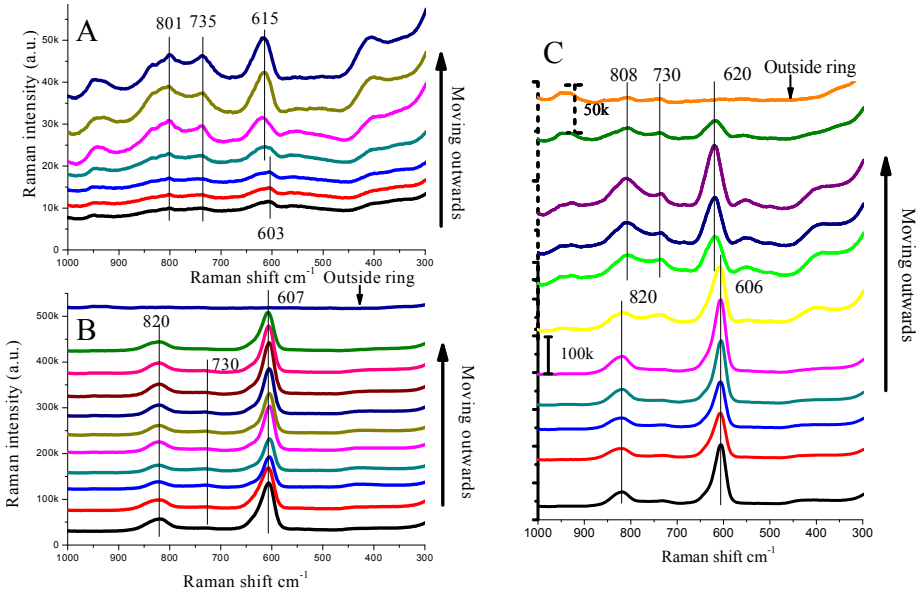

Figure 3.6 Arsenic speciation based on regular coffee ring phenomenon in different buffer solutions.

A—0.1 M acetic acid (pH=2.9), B—0.1 M phosphate buffer (pH=7.5), C—0.1 M ammonium formate buffer (pH=6.9). Note in C, the scale bar of upper section (starts with the yellow curve) is different from lower section.

There were significant differences in arsenic fingerprint signal profiles by using different buffers. For the acetic acid buffer (Fig. 3.6A), the center region had low intensity of fingerprint SERS signals of 603, 735 and 801 cm^{-1}, standing for the As─C

stretching from DMA^V, As─O stretching from As^{III} and As─O symmetric stretching from As^V, respectively. On the contrary, the SERS signals intensity increased dramatically toward the edge, with the strongest signals found at the outmost edge. At the edge region, the As─C vibrational frequency shifted to 615 cm^{-1} which was originated from 603 cm^{-1} at the center. This vibrational band of 615 cm^{-1} might be due to the overlap of the two organoarsenicals (MMA^V and DMA^V), because this vibrational frequency was between the As─C vibrational frequencies of MMA^V and DMA^V. Despite the discrepancies in the SERS signals between the center and the edge, the separation of arsenic species was not observed in the acetic acid buffer, instead the arsenicals were stacked at the edge region, as multiple arsenicals fingerprint signals (and the strongest signals) were found at the edge.

For the phosphate buffer (Fig. 3.6B), three arsenic fingerprint signals were found, including 607, 730 and 820 cm^{-1}, indicative of As─C vibration, As─O stretching from As^{III} and As─O stretching from MMA^V, respectively. Compared to the results using the acetic acid buffer, the signal intensity at 820 cm^{-1} was higher for the organoarsenical using phosphate buffer. No As^V fingerprint signals were found at any spot on the dry film due to possible overlap with the strong organoarsenic signals. It is worth noting that the signal intensity in phosphate buffer maintained stable along the radius with some minor decreasing at the edge, which was against the coffee ring effect. One of possible reasons could be the binding reactions between AgNPs on the AgNF and arsenicals, which occurred because of the high pH of phosphate buffer resulting in the deprotonation of arsenicals. At this pH, the binding of arsenicals with AgNPs could be strong enough to retain arsenicals at the center region.

For the ammonium formate buffer, the SERS signal intensity in the center region was stronger than that in the edge region, as shown by the scale bar changing in Fig. 3.6C. Before the yellow curve, there were two fingerprint signals (820 and 606 cm^{-1}) found close to the center, indicating that both organoarsenicals were present in this region, since neither of these two signals could be solely from MMA^V or DMA^V. After moving outwards, three vibrational bands were detected, including 808, 730 and 620 cm^{-1}. The peak at 730 cm^{-1} can be assigned to As^{III} and the signal at 620 cm^{-1} should be assigned to As─C in MMA^V. The clear red shift for the As─C vibrational band from 606 in the center to 620 cm^{-1} at the edge of the coffee ring suggests that separation of the organoarsenicals happened. No As^V fingerprint signals found in this buffer, but there was a band at 808 cm^{-1} at the edge region. It was believed that this 808 cm^{-1} band was not from As^V or organoarsenicals, instead was the result of vibrational frequency resonance. Probably due to the presence of this 808 cm^{-1} band in ammonium formate buffer, As^V was not detected successfully.

Overall, the results using these three buffers suggest that, without further modifications on the experimental conditions, it was extremely difficult to accomplish arsenic speciation by evaporating a 2 μL sessile droplet on the AgNF. According to the observations, the capillary flow generated during the evaporation could be strong enough that drove all solutes in the sessile droplet towards the edge of coffee ring and thus all arsenicals were stacked at the edge of coffee ring. Although fingerprint signals of multiple arsenicals were observed at the edge, no separation was achieved under this condition. Strong interactions between arsenicals and the AgNF surface were also observed, resulting in that arsenicals SERS intensities are stronger at the center region

than the edge region. The ideal arsenic speciation requires the redistribution of arsenic species of interest along the coffee ring radius through modifying experimental conditions, e.g., addition of surfactants (see below).

3.4.4.2 Arsenic speciation on the AgNF using coffee ring effect under the influence of surfactants

In Deegan's paper about coffee ring mechanism, it was pointed out that surface-tension gradients, solute diffusion, electrostatic and gravity effects are negligible in ring formation [150]. This statement indicates that it could not be effective trying to separate arsenic species during the formation of coffee ring without reshaping the ring. Inspired by previous work [197, 204], the coffee ring phenomenon under the influence of surfactants was explored for potential separation of arsenic species. A small amount of surfactant was introduced into the solution in order to reduce the surface tension, and the liquid in the sessile droplet would be migrated into the peripheral area with the reduced surface tension and strong capillary action from the AgNF surface. The strong capillary action was resulted from the closely packed AgNPs on the AgNF surface. When the liquid in the sessile droplet started permeating into the peripheral region outside the sessile droplet, different arsenicals should be able to move with the capillary flow and migrate different distances on the AgNF surface because of the varying strengths in the interactions of different arsenicals with the AgNPs. As the contact line of the droplet did not move during the evaporation of the droplet, two concentric rings stains were left on the AgNF surface, as shown in Fig. 3.7.

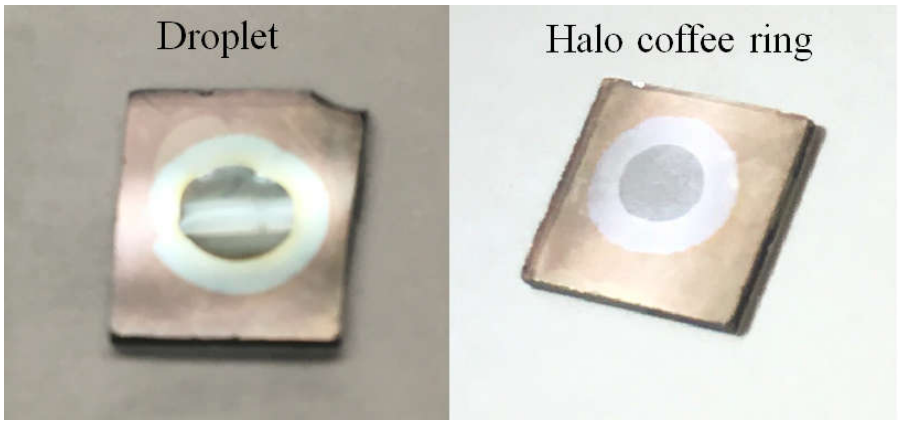

Figure 3.7 Typical halo coffee ring phenomenon as droplet and as dry film using the phosphate buffer system containing 0.05% SDS.

The selection of buffers would play an important role for the potential arsenic separation using this halo coffee ring effect, since the buffer would determine the pH of the sessile droplet and at the meantime affect the adsorption of arsenicals on the AgNF during the evaporation. The key to choose an effective buffer and a surfactant for this halo coffee ring effect mainly depends on the background signals and the SERS signals of individual arsenicals in the buffer after the evaporation. Three buffer systems were tested due to their low background interferences with arsenicals, including 0.1 M acetic acid (pH=2.9), 0.1 M phosphate buffer (potassium salt, pH=7.5) and 0.1 M ammonium formate (pH=6.9). Regarding the surfactants, CTAB strongly adsorbed onto the AgNF and caused strong background signal, and therefore CTAB was not suitable for the generation of halo coffee ring (see details in Fig. 3.8).

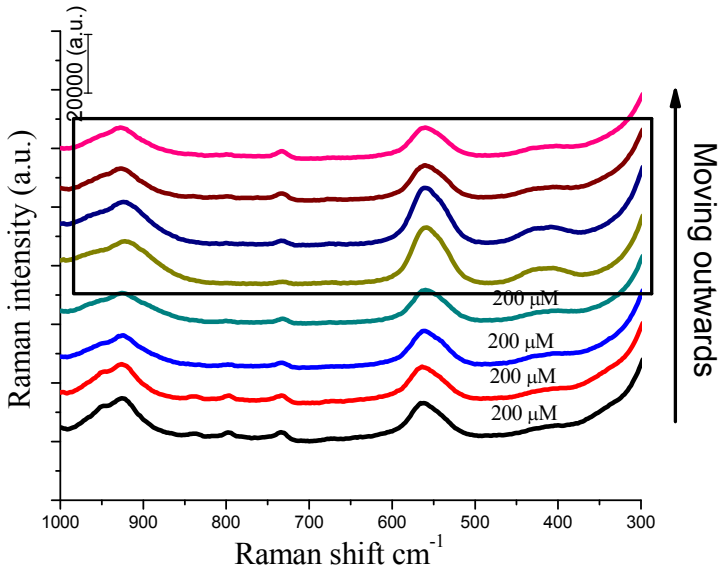

Figure 3.8 SERS signals along the radius of the sessile droplet containing 0.05% CTAB.

On the other hand, SDS was compatible with these three buffer systems and had no interference with arsenic species sensing, especially in the range of 1000 ~ 300 cm^{-1} (Fig. 3.4). Halo coffee ring was observed in these three buffer systems with the addition of 0.05% SDS, and an example using phosphate buffer was shown in Fig. 3.7. This unique halo coffee ring phenomenon featured the following characteristics, including the pinned contact line before the complete evaporation of the sessile droplet (same as the typical coffee ring phenomenon) and the outwards flow driven by capillary action. After the sessile droplet was completely evaporated, the signature halo coffee ring was left on the AgNF surface, which had a darker colored inner ring and a lighter colored halo symmetrically. After carefully controlling the buffer composition and the concentrations of surfactants, liquid from the sessile droplet would overcome the constraint from the surface tension and permeate into the peripheral region of the droplet. This concept

serves as the same principles of circular TLC, but circular TLC typically uses organic solvent as the developing solution. Nano-size AgNPs provided varying retention abilities towards different arsenic compounds during the migration outside the sessile droplet, resulting in different migration distances and thus separation of different arsenicals.

The separation of arsenic species based on the halo coffee ring phenomenon was demonstrated as follows.

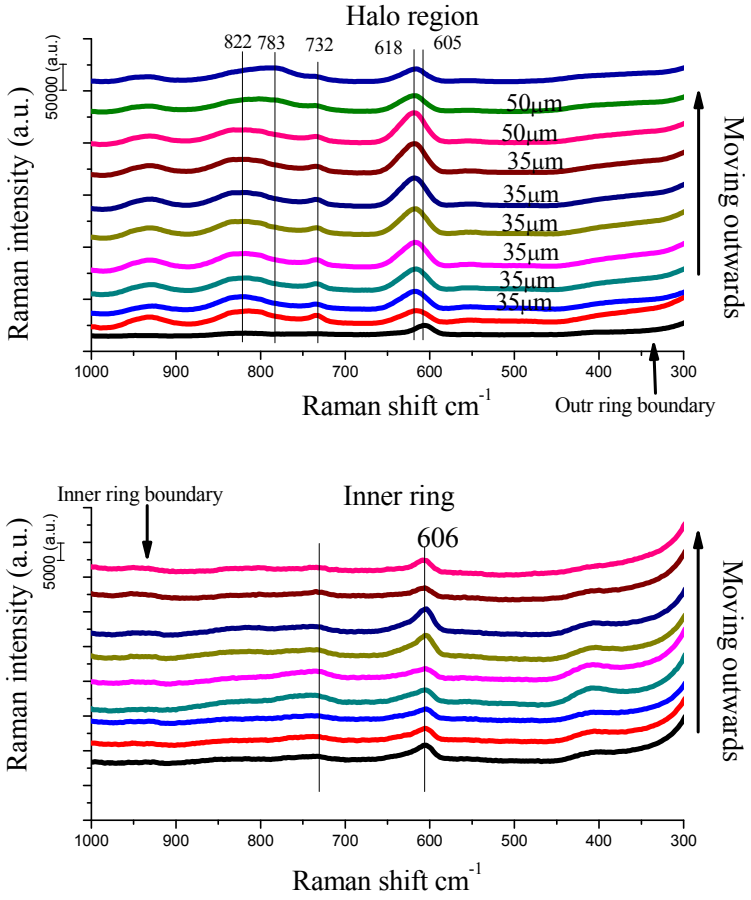

Figure 3.9 Halo coffee ring SERS signal profile of 4 arsenic species in acetic acid.

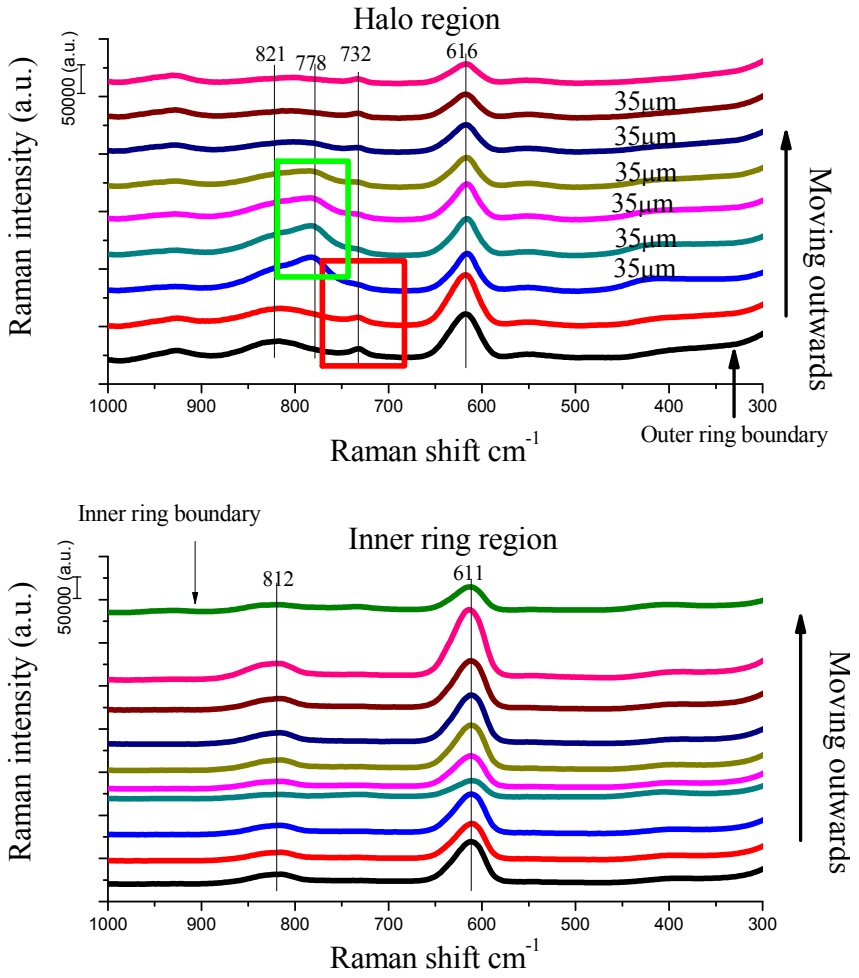

Figure 3.10 Halo coffee ring SERS signal profile of 4 arsenic species in phosphate buffer.

In acetic acid buffer (see Fig. 3.9), only one vibrational band at 606 cm^{-1} was found in the inner ring area, presumably representing DMA^{V}. When the sampling spots moved into the halo ring region, significant changes in SERS profiles were found. Firstly, an obvious red-shift of As─C vibrational band was found, which, together with the appearance of 822 cm^{-1} band (slight blue-shift from original 827 cm^{-1} obtained from

MMA^V coffee ring edge), should indicate that MMA^V dominated in the halo region. A series of weak signals at 732 cm^{-1} were found along the halo region, probably indicative of the presence of As^{III}. At the outmost of the halo region, a 783 cm^{-1} band was found, which should suggest the presence of As^V. In the pH=7.5 phosphate buffer (see Fig. 3.10), only 611 and 812 cm^{-1} vibrational bands were found in the inner ring region. Where it moved outwards, the dominant SERS signal was the band at 616 cm^{-1}. With the sampling spots moving outwards, As^{III} (the band at 732 cm^{-1}) and As^V (the band at 778 cm^{-1}) signals were found subsequently and the As^{III} intensity was fairly weak while the As^V intensity was acceptable. In the ammonium formate buffer (see Fig. 3.11), a similar phenomenon was observed as in previous two buffer systems, in the inner ring region, only one band at 609 cm^{-1} was found. When it moved outwards, the As─C vibrational band shifted to 619 cm^{-1}. Associated with 619 cm^{-1} band, there was s 819 cm^{-1} appearing on the spectra, which indicated the existing of MMA^V. The band at 730 cm^{-1} represented As^{III} showed up earlier than the one at 780 cm^{-1}, indicating As^V.

Generally, the arsenic separation in these three buffer systems is summarized as the following. Only one arsenic compound was left in the inner ring region, which was DMA^V despite there was minor difference in As─C vibrational frequencies in these three buffer systems. In the halo ring region, fingerprint signals of As^{III}, As^V, MMA^V were found with MMA^V dominated in large area and As^V migrated further than As^{III}. Secondly, the signals intensity in the halo region had a universal trend, the signals decreased with the distance heading the halo ring edge, however, this might not be application for As^V since it appeared on the way to the edge. Thirdly, there was significant SERS signals profiles changing between inner ring and halo ring, usually started at the first sampling

sport of the halo ring, sometimes even including the outer ring boundary. Fourthly, these two organoarsenicals might not be separated totally in certain buffer systems, such as phosphate buffer (potassium salt) and ammonium formate, because the AsC fingerprint frequencies were deviated from according solo organoarsenicals. In the phosphate buffer (potassium salt) , the As─C vibrational frequency were found 611 and 616 cm-1 in inner ring and halo respectively. It was believed in the inner ring region some MMA^V was not able to migrate into halo ring and elevated the frequency, while some DMA^V was migrated into the halo ring and reduced the frequency. In the ammonium formate buffer, only some MMA^V left in the inner ring.

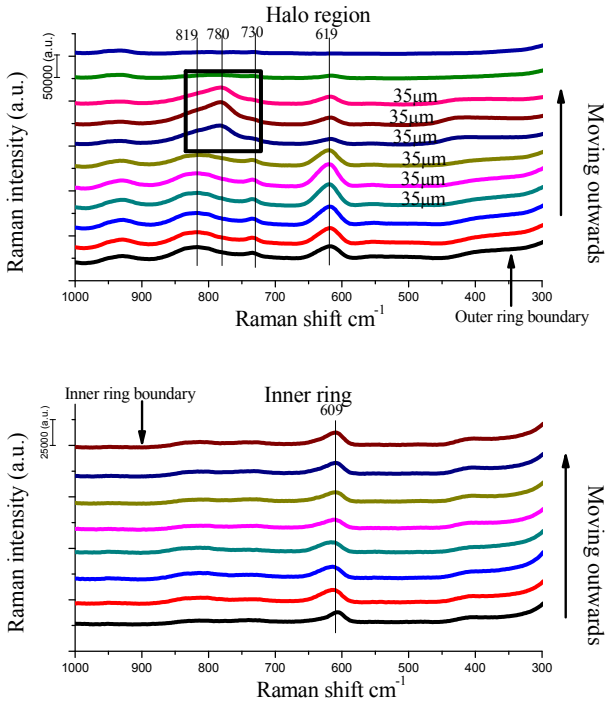

Figure 3.11 Halo coffee ring SERS signal profile of 4 arsenic species in ammonium formate.

The AgNF surface played a significant role for the arsenic separation, and the charge status was the most critical factor. There was no direct method to determine the surface charge of the AgNF, thus, AgNPs from the surface were washed off using NaBH4 under sonication and re-suspend into these three buffer systems used respectively [142]. Zeta potential data obtained from these solutions were all negatively charged. Even through the AgNPs were attached to the surface via amine groups on the surface and the amine groups should have an unneglectable effect on the AgNF surface charge. However, the potential positively charged resulted from the amine groups on the glass substrate is ignored owing to the following reasons. Firstly, the glass surface was coating with close-pack nanoparticles and thus it was believed there is very few free amine groups exposed because they are all binding to the silver nanoparticles. Furthermore, the surface of AgNPs on the AgNF was assumed to be surrounded by buffer solution during the arsenic migration. Therefore, the zeta potential data were used as an alternative for a better understanding of arsenic migration behavior.

DMA^V was mostly left in the inner ring region, and the possible reason could be partially due to the relatively high pKa value (pKa=6.2). It maintained neutral in acetic acid and ammonium formate buffer systems, and as a result it was not migrated into the halo ring region. In the halo ring As^V was usually found in the foremost area despited the prevalent distribution of MMA^V, the strong deprotonation ability could contribute to this. It was negatively charged under these buffer systems and the surface was also negatively charged. Therefore, there was no significant attraction from the AgNF during its migration outwards and it was pushed to front. For the prevalent distribution of MMAV, the possible reason could be loose binding with the AgNPs on the AgNF.

In the capillary electrophoresis separation., arsenic species were separated by their deprotonation status in the buffer [77] and As^{III} eluted first and As^{V} the last. The reason was that As^{III} was neutral and As^{V} was highly deprotonated in the NaH_2PO_4-$Na_2B_4O_7$ buffer (pH=6.5). Similar to the CE technique, As^{V} was eluted the last in the ion chromatography separation due to low pKa value [212]. However, As^{V} was barely migrated in TLC using cellulose as the migration plate [213, 214]. It was reasonable since the migration solution was in high pH and there were lots of hydroxyl grounds existing on the cellulose plate surface, which ensure the active binding of As^{V} onto the surface via chelating complexation. In this study, the electrostatic interactions between arsenicals and the AgNPs on the AgNF plays a critical separation role during the migration along the radius from the center to the edge. At the same time there was non-specific binding found for MMA^{V}, however, the detail reason was not clear.

3.5 Conclusion

In this study, arsenic speciation based on the coffee ring effect was explored and it seems promising to achieve the arsenic separation by using the coffee ring effect under the regulation of surfactants. Due to the strong capillary flow generated by the coffee ring effect, arsenicals accumulated at the edge of the coffee ring and the separation was hard to achieve. In the presence of surfactants, a new ring phenomenon−halo coffee ring effect occurred; solution in the droplet was able to migrate into peripheral region. During the migration into the peripheral region, arsenicals had different interactions with the surface and thus partial separation was achieved. This halo coffee ring effect was demonstrated in different solutions, including 0.1 M acetic acid, phosphate buffer (potassium salt) and ammonium formate. Partial separation of common arsenic species was observed in these

three solutions of different pHs, and the phosphate buffer had the relatively better separation effect. Charge status of individual arsenicals played an important role during the migration and eventually caused the separation, since the interaction between arsenicals and the AgNF surface was mostly depending on the electrostatic interaction. However, there are other factors participate in the arsenic migration and separation during the formation of halo coffee ring.

Chapter 4

Raman Spectra of Thiolated Arsenicals with Biological Importance

4.1 Abstract

Surface enhanced Raman scattering (SERS) has great potential as an alternative tool for arsenic speciation in biological matrices. The SERS measurements have advantages over other techniques because of its ability to maintain the integrity of arsenic species and its minimal requirements for sample preparation. Up to now, very few Raman spectra of arsenic compounds have been reported. This observation in current literature is particularly true for thiolated arsenicals, which have recently been found to be widely present in humans. The lack of data for Raman spectra in arsenic speciation hampers the development of new tools using SERS. Herein, we report the results of a study combining the analysis of experimental Raman spectra with that obtained from computational calculations for some important arsenic metabolites. The results were obtained with a hybrid functional B3LYP approach using different basis sets to calculate Raman spectra of the selected arsenicals. By comparing experimental and calculated spectra of dimethylarsinic acid (DMA^{V}), the basis set 6-311++G** was found to provide computational efficiency and precision in vibrational frequency prediction. The Raman frequencies of a set of six organoarsenicals were studied using this basis set, including monomethylarsonous acid (MMA^{III}), dimethylarsinous acid (DMA^{III}), dimethylmonothioarinic acid ($DMMTA^{V}$), dimethyldithioarsinic acid ($DMDTA^{V}$), S-(Dimethylarsenic) cysteine ($DMA^{III}Cys$) and dimethylarsinous glutathione ($DMA^{III}GS$). The results were compared with fingerprint Raman frequencies from As─O, As─C, and As─S obtained under different chemical environments. These fingerprint vibrational frequencies should prove useful in future measurements of different species of arsenic using SERS.

Key words: Arsenic metabolism • Density functional theory • Raman spectra • Thiolated arsenicals • B3LYP

4.2 Introduction

Arsenic as a notoriously toxic pollutant exists widely in the environment. Extensive arsenic contamination of groundwater has led to widespread poisoning in many regions [30-33]. On the other hand, certain arsenic compounds have been used as medicines for treatment of cancers such as acute promyelocytic leukemia, and lymphoma [215, 216]. Chronic exposure or direct ingestion of arsenicals can result in extensive metabolism and transformation in biological systems, resulting in a wide variety of arsenicals with drastically different chemical properties and toxicities [217-219]. Methylated arsenicals including monomehtylarsonic acid (MMA^V), dimethylarsinic acid (DMA^V), monomethylarsonous acid (MMA^{III}), and dimethylarsinous acid (DMA^{III}) are generally believed to be the major arsenic metabolites [220-222]. However, thiolated arsenicals have been recently identified in various biological samples. Dimethylarsinothioyl glutathione complex ($DMMTA^V(GS)$) was first detected in cabbages following exposure to DMA^V [223] and also identified in human cell lines after darinaparsin (S-dimethylarsino-glutathione) exposure [183, 224, 225]. Monomethylmonothioarsonic acid ($MMMTA^V$) was found in urine of hamsters, rats, human [226-229], and in human gut microbiota [230]. Dimethylmonothioarinic acid ($DMMTA^V$) was also detected in many biological samples [227, 229, 231-235], such as urine, liver and kidney homogenates, plasma, and red blood cells. It is now recognized that more arsenic metabolites may exist in human than previously believed. Identification

of arsenic species in different biological matrices is of great importance in the study and assessment of metabolites of arsenic *in vivo*.

Generally, speciation of arsenic has been carried out by a combination of chromatographic separation and spectroscopic detection. High-performance liquid chromatography (HPLC) [176, 183, 224, 225], ion chromatography (IC) [78, 79] and capillary electrophoresis (CE) [236-238] have been popular separation techniques for these species. Following chromatographic separation, inductively coupled plasma mass spectrometry (ICP-MS) [176, 183, 224, 225], electrospray ionization mass spectrometry (ESI-MS) [72], and time-of-flight mass spectrometry (TOF-MS) [81] have been used for detection, of which ICP-MS and ESI-MS are most widely used. Before analysis can be conducted, extraction of specific arsenicals from different sample matrices usually has to be performed. However, extraction steps employing acid/base or organic solvents may cause alterations in arsenic speciation. For example, it was reported in one sample preparation method that only 55 % of DMA^{III} remained following extraction and cleanup [239]. Speciation analysis of arsenic in biological samples remains a challenging task because of the diversity of arsenic metabolites and their instability. Therefore the development of a method for arsenic speciation that does not require extensive sample preparation would be ideal. Raman spectroscopy provides molecular fingerprint information and should be a good choice for elemental speciation analysis. Raman spectroscopy provides great structural information using vibrational spectra, and unlike infrared methods, water is not an interferent [100], which makes Raman spectroscopy readily adapted to *in vivo* studies [240, 241]. Surface-enhanced Raman spectroscopy (SERS) employs metallic nanostructured substrates to improve the signal sensitivity

using localized surface plasmon resonant field enhancements. In recent years, the use of SERS in bioanalytical fields has increased exponentially as a result of advances in the preparation of nanomaterials [242-245]. It is potentially possible to employ SERS for arsenic speciation analysis *in vivo*. However, reports related to the application of SERS in this area are limited because of the lack of reported Raman spectra and vibrational assignments for most arsenic metabolites. In previous work, the Raman spectra of mixtures of arsenic and sulfur vapors were investigated using high-temperature laser. Complicated interactions between arsenic and sulfur were observed various Raman vibrational bands as shown on the Raman spectra. Unfortunately, potential As─S vibrational movements were not assigned in the paper [246]. The Raman spectra of Na_3AsS_4•8$(D,H)_2O$ and Na_3SbS_4•9$(D,H)_2O$ were measured in salt hydrates, providing valuable information of As─S bonds despite lacking spectrum unfolding [247]. However, with the discovery of new arsenic metabolites, particularly the thiolated organoarsenicals, the information on the Raman spectra of these arsenic compounds is very much needed.

Quantum chemical calculation is an essential method for interpretation of experimental vibrational spectra [248]. Previously, ab initio Hartree-Fock molecular orbital theory was employed to interpret EXAFS and Raman spectral properties of various inorganic sulfur-containing arsenicals [249]. Compared with Hartree-Fock calculations, density functional theory (DFT) including the Becke, 3-parameter, Lee-Yang-Parr (B3LYP) method [162-165], has been demonstrated to yield good performance when used to predict IR and Raman spectra. The Raman spectra of the $As(HCys)_3$ complex was calculated using the DFT method and was compared with Raman frequencies for this same complex observed experimentally. The calculated As─S

frequencies for $As(Hcys)_3$ were approximately 368-402 cm^{-1}, which provides the important structural information as well as the mechanism of arsenite complexation at a molecular level [250]. The As─O, As─OH, As─S, and As─SH vibrational frequencies for some inorganic oxoarsenicals and thioarsenicals have also been calculated using the CBSB7 B3LYP method [251]. Nevertheless, many organic arsenic metabolites and thiolated arsenicals still lack spectral analysis. Previously, most theoretical computations were calculated roughly by low-precision methods [249] and focused mainly on inorganic arsenic compounds [251]. The recent discovery of an extensive variety of arsenic metabolites including new thioarsenicals has resulted in an urgent need for these compounds to be characterized by computational and experimental methods. Raman spectroscopy and especially SERS has great potential in the study of arsenic metabolism, but there is currently a lack of data for these studies.

The objective of the present work was to study the Raman spectra of some key organoarsenicals that have been identified in biological samples or could potentially be important in arsenic metabolism by comparison of computational and experimental results. The selected arsenicals included thiolated arsenicals which were either purchased or synthesized in the laboratory. Raman spectra of the selected compounds were measured experimentally with protection from air oxidation for certain oxygen sensitive species (MMA^{III}, DMA^{III}, $DMMTA^{V}$, $DMDTA^{V}$, $DMA^{III}Cys$, $DMA^{III}GS$. Quantum chemistry methods were employed to simulate molecular vibrations associated with the Raman spectra in order to assist in the assignment of vibrational bands of the arsenicals. Overall this research provides important information on Raman spectra for some

potentially important arsenic metabolites and sheds light on future analysis of arsenic metabolites *in vivo* using SERS.

4.3 Materials and Chemicals

Cacodylic acid sodium salt, 98% (DMA^V-Salt) and cacodylic acid, 98% (DMA^V) were purchased from Sigma-Aldrich, USA. Monosodium acid methane arsonate sesquihydrate, 98% (MMA^V) was purchased from Chem Service, USA. L-Cysteine (cell culture reagent) was purchased from Acros Organics, USA. L-Cystine (Sigma grade) was purchased from Sigma-Aldrich, USA. NaOH, HCl, H_2SO_4, P_2O_5, KI, $Na_2S•9H_2O$ were certified ACS grade and purchased from Fisher Scientific, USA. Sulfur dioxide (SO_2) gas and nitrogen (N_2) gas were purchased from Specialty Gases of America, USA and Airgas, USA, respectively. Anhydrous ethyl alcohol (ACS/USP grade) was purchased from Pharmco-Aaper, USA. Ethyl ether anhydrous (ACS certified) was purchased from Fisher Scientific, USA. DI water (18.2 MΩ) was produced in the laboratory using a Barnstead Nanopure Diamond, USA.

4.4 Experimental procedures

4.4.1 Synthesis of arsenicals in the laboratory

4.4.1.1 MMA^{III} and DMA^{III}

The MMA^{III} and DMA^{III} were prepared from their corresponding iodine forms according to the procedures reported previously [176]. Briefly, MMA^V or DMA^V was mixed with KI in DI water, and then concentrated HCl was added to the solution. The solution was placed on a magnetic stirring plate and a flow of SO_2 was used for reduction of the arsenic compound. For $MMA^{III}I_2$, a yellow precipitate was formed in the aqueous solution as reduction proceded. The yellow precipitate was collected and dissolved in

diethyl ether and dried under a stream of N_2 gas. For $DMA^{III}I$, a yellow oil product was found at bottom of the reaction vial at the end of the reaction. The yellow oil was collected and dried over P_2O_5. The drying in P_2O_5 must be performed cautiously since heat is released when P_2O_5 reacts with water. The dry yellow oil was extracted using diethyl ether and dried under a stream of N_2 gas. Saturated solutions of $MMA^{III}I_2$ and $DMA^{III}I$ were prepared and hydrolyzed in 0.1 M NaOH prior to Raman spectral measurement.

4.4.1.2 $DMMTA^V$ and $DMDTA^V$

The anhydride form of $DMMTA^V$ was prepared by dissolving DMA^V (6.52 g or 47.2 mmol) in 70 ml of 30 % (wt/wt) aqueous ethanol [252]. Dilute H_2SO_4 (2 M) solution was added dropwise onto $Na_2S•9H_2O$ crystals to produce H_2S in a gas generator and the gas was bubbled into the 70 ml of DMA^V solution prepared upon for 15 minutes under stirring without heating. After reaction, the solution was dried using a rotary evaporator and the resultant sample was hydrolyzed in degassed DI water. The hydrolysis product was dried again in a rotary evaporator and the dried powder was collected for further analysis.

Dimethyldithioarsinic acid ($DMDTA^V$) was prepared from sodium dimethyldithioarsinic salt (Sodium-DMDTA) [253]. Sodium-DMDTA was prepared by passing hydrogen sulfide (H_2S) through a boiling ethanol solution of dimethylarsinic (DMA^V-Salt, 0.584 mol/L, 25 ml) for half hour. The H_2S gas was generated by dropping diluted H_2SO_4 into $Na_2S•9H_2O$ crystals and the gas was collected and bubbled into the solution using a gas generator. After the reaction flask cooled down, a large amount of precipitate was found at bottom of the flask. Cold ethanol was used to wash the

precipitate three times and then the precipitate was dried under a stream of N_2 gas. The precipitate (sodium salt form) was dissolved in hot ethanol and 2 M HCl solution was introduced drop by drop in order to yield the product $DMDTA^V$ (acid form) and byproduct NaCl as precipitate. Because NaCl had relatively low solubility in the ethanol solution and it was easily removed by decanting and the organic phase was dried under a stream of N_2 gas.

4.4.1.3 $DMA^{III}Cys$

The S-(Dimethylarsenic) cysteine ($DMA^{III}Cys$) complex was prepared by reduction using a mixture of DMA^V (0.66 mmol) with L-cysteine (0.33 mmol) in 10 ml of degassed DI water under nitrogen. Our synthesis of $DMA^{III}Cys$ used a larger quantity of L-cysteine than DMA^V than described in previous reports [235, 254], however, it was found that the cystine byproduct in the precipitate affects the $DMA^{III}Cys$ Raman spectra (See Figure S5A). Because $DMA^{III}Cys$ hydrolyzed and turned into DMA^{III} during chromatographic separation and ICP-MS detection of ^{75}As in these two previous reports, the co-existing byproduct cystine had no influence on their study. Therefore, a two-fold molar of DMA^V against L-cysteine was employed to reduce the formation of byproduct—cystine. The reaction was carried out at room temperature using magnetic stirring for three hours [225]. After the reaction, the solution was centrifuged and the supernatant was collected. Then the supernatant was evaporated, the white residue powder was carefully collected for further analysis.

4.4.2 Instrumentation

4.4.2.1 High performance liquid chromatography coupling inductively coupled plasma mass spectrometry (HPLC/ICP-MS) for arsenic speciation

The high-performance liquid chromatography (HPLC) (PerkinElmer series 2000) using a C18 reversed-phase column and a mobile phase consisting of 3 mM malonic acid, 5 mM tetrabutylammonium hydroxide, and 5% (v/v) methanol (pH=5.9) with a flow rate of 1 mL/min. Arsenic content was detected by an ELAN DRC-e inductively coupled plasma mass spectrometry (ICP-MS) (PerkinElmer). The concentrations of all standard arsenic standards were 1μM, including As^{III}, MMA^{III}, DMA^{V} and MMA^{V}.

4.4.2.2 Mass spectrometers

A. Bruker fourier transform ion cyclotron resonance mass spectrometry (FT-ICR-MS)

The $DMMTA^{V}$ sample was analyzed on a Bruker Solarix FT-ICR-MS equipped with a 7 T superconducting magnet in the Advanced Mass Spectrometry Facility at Florida International University (Florida, USA). The samples were infused using a Bruker API electrospray source at 6 μL/min by a syringe pump. The instrument parameters were set at 4.6 kV for the capillary column front end voltage, and 200 V capillary end voltage. Ions accumulated for 0.5 s in hexapole with 6.0 V direct-current voltage and 180 Vp-p ratio frequency (RF) amplitude. The optimized mass for quadrupole 1 was set to 100.0 Da. Hexapoles of the Qh interface were operated at 5MHz and 300 Vp-p amplitude, in which ions accumulated for 0.1 s. Ions were transferred to an ICR cell by electrostatic focusing of the transfer optics. The ICR was operated at 100.4-

4000.0 mass range, and 4 MW data size. The time domain data sets were co-added from 50 data acquisitions.

B. Thermo Finnigan LCQ Deca XP MAX LC-MS/MS mass spectrometer

The $DMDTA^{V}$ powder sample was dissolved in 1 mL methanol (50.0 mg/mL) and diluted ten times in 0.1 % ammonium hydroxide in acetonitrile. The sample was analyzed by directed infusion negative ESI mode on the Thermo Finnigan LCQ Deca XP MAX mass spectrometer, and the full scan from 100-1000 Da and the product ion scan from 50-175 Da modes were performed.

C. QTRAP 5500 LC-MS/MS mass spectrometer

The $DMA^{III}Cys$ powder sample was dissolved in 0.3 mL of 66 % ACN and 34 % DI water. An aliquot (50 µL) of the obtained solution was transferred to a glass vial and mixed with 450 µL of ACN. A blank was prepared similarly, substituting the volume of diluted sample with 34 % water in ACN. Using a syringe pump (5 µL/min), the obtained solutions were combined with the output of an LC system (Thermo Surveyor LC pump), which delivered 50 µL/min of 0.1 % FA in ACN (Optima LC/MS grade). The combined flow was infused into the Turbo VTM ESI source of an AB SCIEX QTRAP 5500 triple quadrupole mass spectrometer, operated in the positively mode under full scan (100-500 Da) and the product ion scan (50-300 Da) modes.

4.4.2.3 Proton NMR spectrometer

Proton NMR spectra were recorded at 25 °C on a Bruker 400 FT NMR spectrometer operating at a proton frequency of 400 MHz.

4.4.2.4 Raman spectroscopy measurement

The Raman spectrometer used in this study was a Perkin-Elmer Raman spectroscopy (Raman station 400F), employing a diode laser operating system at 785 nm with an average power of 100mW at the sample and a 100-micron spot size. This Raman station was equipped with a Perkin-Elmer 300 microscope, which has a movable stage. The laser beam was focused on the sample stage through a fiber optic cable connecting the 400F instrument to the microscope. Typically, a 20X optical lens was employed for better sample focusing and response. Raman spectra (3300~200 cm^{-1}) were recorded using a 785 nm laser with 1 second of exposure time, and 4 exposures per measurement. Redox-sensitive arsenicals were sealed in melting point capillary tubes to prevent oxidation during measurement, while for stable arsenicals, the Raman spectra were obtained by placing powder samples directly onto microscopy slides. Most arsenical Raman spectra prepared in this study were obtained using this Perkin-Elmer Raman station 400 F.

Another Raman spectrometer used in this work was a Thermo Scientific FirstDefender RM portable handheld Raman spectroscopy. The portable handheld system was equipped with one 785 nm diode laser and a CCD spectrometer. The Raman shift measurement range for this instrument was 250~2875 cm^{-1}. It had three levels of output power, low, medium and high, corresponding to 75, 125, and 250 mW, respectively. For Raman spectra obtained from the Thermo Scientific portable handheld Raman spectroscopy, samples in glass vials were directly placed in front of the laser output probe, exposure time was set to 50 seconds and high output power was employed during sample measurement.

4.4.3 Theoretical calculation

The B3LYP functional hybrid software with five different basis sets was employed for arsenic molecular geometry optimization. Subsequently, Raman spectra were calculated at the same level of theory using the optimized molecular structures. Two of Pople's split valence basis sets with different dispersion and polarization levels were first used, including 6-31G* and 6-311++G**. Considering that arsenic is an element belonging to the fourth period, the scalar relativistic effects might have important influences on the chemical properties of arsenic compounds [255]. The Stuttgart/Dresden double-ζ (SDD) basis set was employed to describe the arsenic atom in these arsenic compounds, while other atoms were described using 6-31G* or 6-311++G** basis sets. The resultant mixed basis sets were denoted as SDD/6-31G* and SDD/6-311++G**, which were examined to evaluate whether considering relativistic effects would increase the accuracy of computational results. Lastly, a high resource-demanding and all electron basis set of triple-ζ valence quality, def2-TZVPP [256, 257] was also employed in comparison of basis sets.

All calculations were performed using Gaussian 09 (Revision B.01) running on Florida International University's HPC facility usually using two processors. The MOLDEN program [258] was employed to visualize individual arsenic molecular vibrations at specific vibrational frequencies, while the Multiwfn program was used to convert the Raman activities from Gaussian output files into Raman intensities in order to plot the simulated Raman spectra for arsenicals [259]. The vibrational modes in the DFT Raman spectra were assigned via MOLDEN molecular simulation, while assignments from crystal Raman spectra were employed to verify MOLDEN assignments [187].

Raman frequencies of the same vibrational modes from experimental and calculated Raman spectra were extracted for further comparisons. Different empirical scaling factors for Raman frequencies were used in order to reduce the disagreement between calculated and experimental Raman frequencies: 0.9614 for 6-31G* and SDD/6-31G* [260], and 0.9679 for 6-311++G** and SDD/ 6-311++G** [165]. Corrected Raman frequencies were obtained once the scaling factors were applied. However, the empirical scaling factor for the def2-TZVPP basis set was not available. Usually, two sets of errors ratios were calculated, which were between the experimental and calculated Raman frequencies with or without scaling factors. For example, the error ratio between an experimental and a calculated Raman frequency was determined by dividing absolute difference between the calculated and e experimental Raman frequencies by the experimental frequencies accordingly. A root mean square error (RMS) [165, 260] was adopted to evaluate the performance of basis sets.

4.5 Results

4.5.1 Comparison of theoretical and experimental Raman spectra

The molecular structures of DMA^{V}, DMA^{III}, MMA^{III}, $DMMTA^{V}$, $DMDTA^{V}$, $DMA^{III}GS$, and $DMA^{III}Cys$ are shown in Fig.4.1.

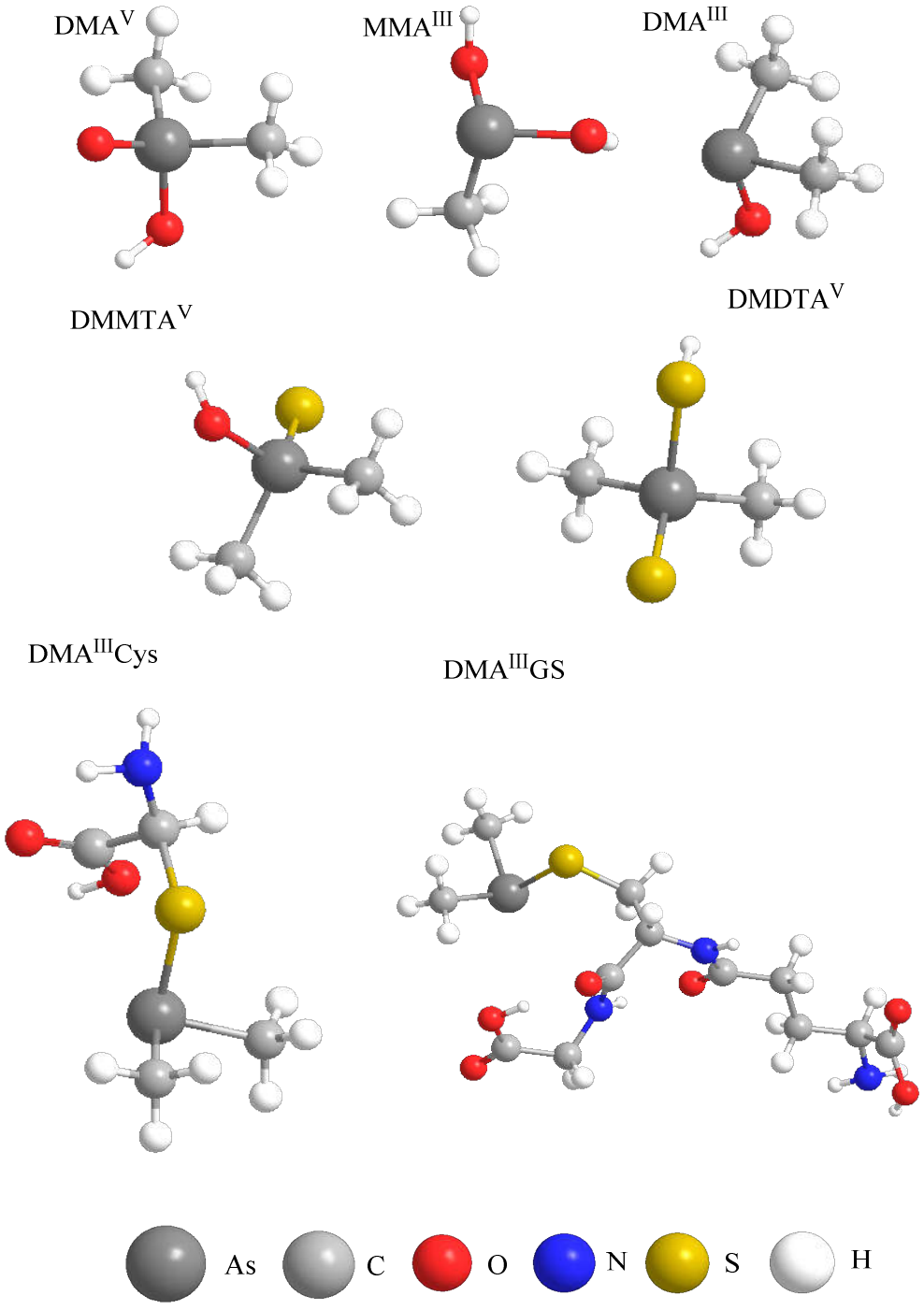

Figure 4.1 3D structures of arsenicals optimized by DFT

Table 4.1 Comparison of experimental and calculated Raman frequencies for DMA^V using all basis set

A	6-311++G**			No scaling factor			With scaling factor		
Assignment	Reported Raman frequency (cm^{-1})	Experimental Raman frequency (cm^{-1})	Error ratio between reported and experimental Raman frequency (%)	6-311++G** (cm^{-1})	Difference between experimental and theoretical Raman frequency (cm^{-1})	Error ratio (%)	Scaled frequency (cm^{-1})	Difference between experimental and scalled theoretical Raman frequency (cm^{-1})	Error ratio with scaling factor (%)
$V_s(AsC_2)$	616	611	0.8	573	38	6.2	555	56	9.2
$V_{as}(AsC_2)$	655	636	3.1	611	25	3.9	591	45	7.0
V(As─O)	754	752	0.3	634	118	15.7	614	138	18.4
V(As═O)	822	820	0.3	932	112	13.7	902	82	10.0
$\delta_g(CH_3)$	1282	1279	0.5	1301	22	1.7	1259	20	1.5
$\delta_a(CH_3)$	1423	1420	0.5	1453	33	2.3	1406	14	1.0
$V_s(CH_3)$	2920	2915	0.8	3054	139	4.8	2956	41	1.4
$V_{as}(CH_3)$	2997	2995	0.3	3148	153	5.1	3047	52	1.7
V(H─O)	NA	NA	NA	3815	NA	NA	3693	NA	NA

B	6-31G*			No scaling factor			With scaling factor		

Assignment	Reported Raman frequency (cm^{-1})	Experimental Raman frequency (cm^{-1})	Error ratio between reported and experimental Raman frequency (%)	6-31G* (cm^{-1})	Difference between experimental and theoretical Raman frequency (cm^{-1})	Error ratio (%)	Scaled frequency (cm^{-1})	Difference between experimental and scaled theoretical Raman frequency (cm^{-1})	Error ratio with scaling factor (%)
$V_s(AsC_2)$	616	611	0.8	578	33	5.4	556	55	9.1
$V_{as}(AsC_2)$	655	636	3.1	611	25	3.9	587	49	7.6
V(As─O)	754	752	0.3	698	54	7.2	671	81	10.8
V(As═O)	822	820	0.3	986	166	20.2	948	128	15.6
$\delta_g(CH_3)$	1282	1279	0.5	1331	52	4.1	1280	1	0.0
$\delta_a(CH_3)$	1423	1420	0.5	1492	72	5.1	1434	14	1.0
$V_s(CH_3)$	2920	2915	0.8	3081	166	5.7	2962	47	1.6
$V_{as}(CH_3)$	2997	2995	0.3	3178	183	6.1	3055	60	2.0
V(H─O)	NA	NA	NA	3744	NA	NA	3599	NA	NA

C	SDD/6-31G*			No scaling factor			With scaling factor		
Assignment	Reported Raman frequency (cm^{-1})	Experimental Raman frequency (cm^{-1})	Error ratio between reported and experimental Raman frequency (%)	SDD/ 6-31G* (cm^{-1})	Difference between experimental and theoretical Raman frequency (cm^{-1})	Error ratio between experimental and theoretical (%)	Scaled frequency (cm^{-1})	Difference between experimental and scaled theoretical Raman frequency (cm^{-1})	Error ratio with scaling factor (%)
$V_s(AsC_2)$	616	611	0.8	569	42	6.9	547	64	10.5

$V_{as}(AsC_2)$	655	636	3.1	611	25	3.9	587	49	7.6
V(As─O)	754	752	0.3	659	93	12.4	634	118	15.7
V(As═O)	822	820	0.3	932	112	13.7	896	76	9.3
$\delta_g(CH_3)$	1282	1279	0.5	1342	63	4.9	1290	11	0.9
$\delta_a(CH_3)$	1423	1420	0.5	1484	64	4.5	1427	7	0.5
$V_s(CH_3)$	2920	2915	0.8	3083	168	5.8	2964	49	1.7
$V_{as}(CH_3)$	2997	2995	0.3	3179	184	6.1	3056	61	2.0
V(H─O)	NA	NA	NA	3737	NA	NA	3593	NA	NA

D	SDD/6-311++G**			No scaling factor			With scaling factor		
Assignment	Reported Raman frequency (cm^{-1})	Experimental Raman frequency (cm^{-1})	Error ratio between reported and experimental Raman frequency (%)	SDD/ 6-311++G** (cm^{-1})	Difference between experimental and theoretical Raman frequency (cm^{-1})	Error ratio between experimental and theoretical (%)	Scaled frequency (cm^{-1})	Difference between experimental and scaled theoretical Raman frequency (cm^{-1})	Error ratio with scaling factor (%)
$V_s(AsC_2)$	616	611	0.8	559	52	8.5	541	70	11.4
$V_{as}(AsC_2)$	655	636	3.1	606	30	4.7	587	49	7.8
V(As─O)	754	752	0.3	613	139	18.5	593	159	21.1
V(As═O)	822	820	0.3	859	39	4.8	831	11	1.4
$\delta_g(CH_3)$	1282	1279	0.5	1313	34	2.7	1271	8	0.6
$\delta_a(CH_3)$	1423	1420	0.5	1452	32	2.3	1405	15	1.0
$V_s(CH_3)$	2920	2915	0.8	3060	145	5.0	2962	47	1.6
$V_{as}(CH_3)$	2997	2995	0.3	3156	161	5.4	3055	60	2.0
V(H─O)	NA	NA	NA	3823	NA	NA	3700	NA	NA

E	def2-TZVPP			No scaling factor			With scaling factor		
Assignment	Reported Raman frequency (cm^{-1})	Experimental Raman frequency	Error ratio between reported and experimental Raman frequency (%)	def2-TZVPP (cm^{-1})	Difference between experimental and theoretical Raman frequency (cm^{-1})	Error ratio between experimental and theoretical (%)	Scaled frequency (cm^{-1})	Difference between experimental and scaled theoretical Raman frequency (cm^{-1})	Error ratio with scaling factor (%)
$V_s(AsC_2)$	616	611	0.8	580	31	5.1	NA		
$V_{as}(AsC_2)$	655	636	3.1	615	21	3.3			
V(As─O)	754	752	0.3	674	78	10.4			
V(As═O)	822	820	0.3	961	141	17.2			
$\delta_g(CH_3)$	1282	1279	0.5	1298	19	1.5			
$\delta_a(CH_3)$	1423	1420	0.5	1454	34	2.4			
$V_s(CH_3)$	2920	2915	0.8	2915	0	0.0			
$V_{as}(CH_3)$	2997	2995	0.3	2995	0	0.0			
V(H─O)	NA	NA	NA	3811	NA	NA			

Table 4.2 Comparisons of computational performance of all basis sets

Basis Set	6-31G*	Scaled 6-31G* (0.9614)	6-311++G**	Scaled 6-311++G** (0.9679)	SDD/ 6-31G*	Scaled SDD/ 6-31G* (0.9614)	SDD/ 6-311++G**	Scaled SDD/6-311++G** (0.9679)	def2-TZVPP
RMS (cm^{-1})	112.4	65.6	90.9	59.4	108.2	63.8	95.9	69.5	60.1
Number of error ratios over 10%	1	2	2	1	2	2	1	2	1
computational cost	2m, 24s	2m, 24s	11m, 29s	11m, 29s	1m, 37s	11m, 29s	4m, 58s	11m, 29s	43m, 5s

The representative arsenic compound DMA^V was employed to explore the discrepancy between the DFT Raman spectra, and the experimental Raman spectra using its crystalline Raman spectra [187] as well as to determine which basis set was best for the DFT Raman spectra simulation. The DMA^V was selected because it is relatively stable and literature results on its Raman frequency were available for comparison. The experimental and calculated Raman frequencies obtained in current study, as well as those reported in the literature for Raman frequencies of DMA^V [187] along with error ratios using all basis sets are shown in Table 4.1. The employed basis sets were compared and evaluated by the RMS, number of error ratios over 10% between experimental and calculated Raman frequencies in DMA^V, and the computational cost (in term of time consumption) (Table 4.2). It was obvious that using scaling factors greatly reduced the RMS values and improved the precision of the theoretical result, mainly because of the scaling factors being smaller than 1.0. Among all basis sets tested, the basis set 6-311++G** yielded the smallest RMS values after applying the scaling factor, other basis sets yielded comparable results. On the other hand, it was found that basis sets 6-31G* and SDD/6-31G* were not able to correctly predict the intensity of CH_3 vibrations from 1600~1200 cm^{-1} (Fig. 4.2) as a result of systematic errors, and the basis set def2-TVZPP was not cost effective (Table 4.2). The Raman spectra of DMA^V measured in this study was in good agreement with that previously reported, having an error ratio of the reported vs. the experimental being less than 3.1% (Table 4.1). The error ratios of the experimentally obtained vs the calculated Raman frequencies of DMA^V were generally less than 10%, which is acceptable according to previous studies [260-262]. However, an over 10% deviation was observed for the Raman frequencies of As─O and As═O. The Raman frequencies obtained from experimental measurement and theoretical calculations were 752 and 667 cm^{-1} for As─O, and 820 and 932 cm^{-1} for As═O, respectively

(Table 4.1). The large discrepancy could be attributed to the systematic error occurring during theoretical computation. These types of errors were also found in a series of arsenicals with similar structure (Table 4.3). Furthermore, while application of the scaling factor substantially reduced the RMS, there was a fairly limited impact on error ratios, with the average error ratio being only reduced by 6.l to 5.8% following the application of scaling factors (Table 4.2).

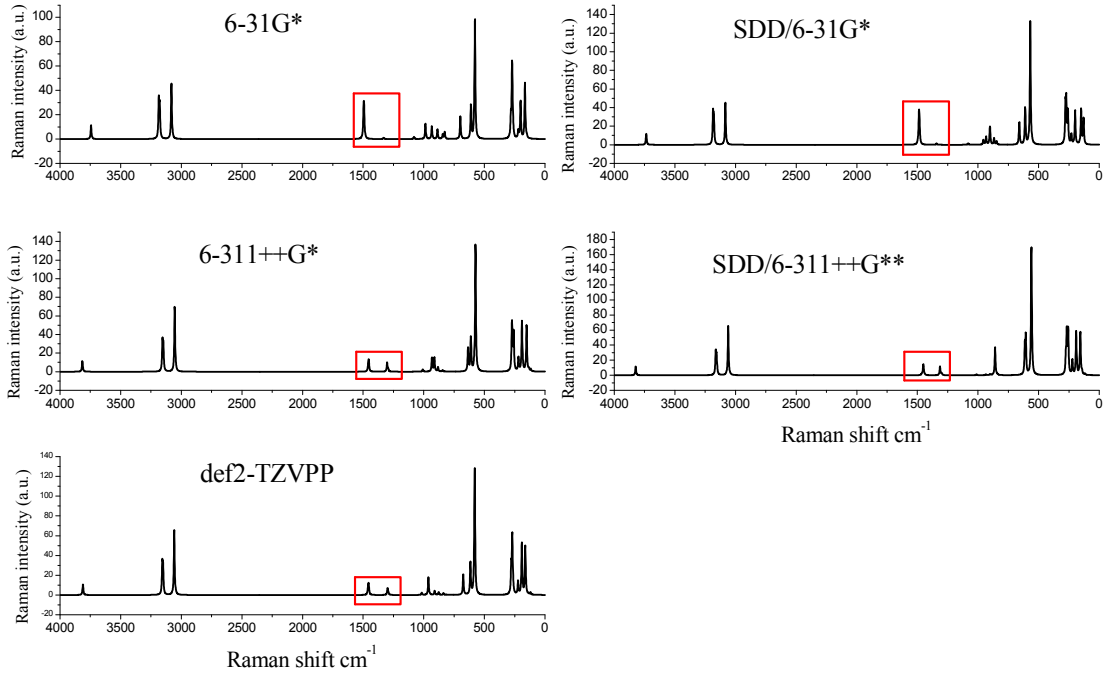

Figure 4.2 Theoretical DMA^V Raman spectra calculated from different basis sets. It was found two basis sets, including 6-31G and SDD/6-31G, had a significant bias in prediction the intensities of bands from 1600~1200 cm^{-1} (with red frame marks in upon spectra), however, these two bands had almost identical intensity in the Raman spectra. It is the major reason that these two basis sets were not chosen.

.

Table 4.3 Comparison of all As─O bonds Raman frequencies between experimental and calculated Raman spectra

Arsenical	Assignment	Experimental Raman frequency (cm^{-1})	6-311++G**, (cm^{-1})
As^V	As═O	842	965
DMA^V		838	932
MMA^V		811	940
As^V	As─O	730	665 sym, 685, 705 asym
DMA^V	As─O	748	634
MMA^V	As─O(Va, Vs)	710	661 sym, 664 asym

Note, sym stands for symmetric stretch, asym stands for asymmetric stretch.

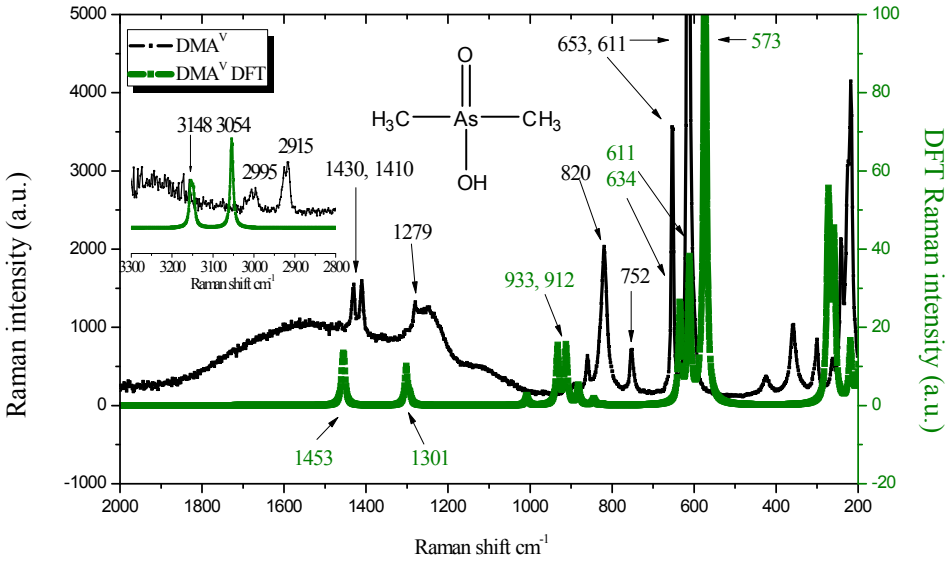

Figure 4.3 Raman spectra of DMA^V obtained via experimental measurement and calculation

Judging from the number of frequency error ratios over 10%, the medium-sized basis set 6-311++G** (Table 4.1A) yielded the best results, while the use of mixed basis

sets that included relativistic effects did not improve the outcome. Although the all electron basis set def2-TZVPP consumed the most computational resources, high demanding basis sets are affordable these days with advances in computational technology. Furthermore, the basis set def2-TZVPP also offers highly comparable RMS results (Table 4.2) without a scaling factor; however, it is difficult to evaluate the results without the scaling factor. Overall, Raman frequencies calculated by the B3LYP with basis set 6-311++G** gave the optimal result for the identification of DMA^V Raman spectra. A superimposed Raman spectra of the experimental and the calculated result is shown in Fig. 4.3.

For the Raman vibrational band assignment of the rest of the arsenicals, only following molecular fingerprint vibrational modes were calculated and interpreted in order to characterize arsenicals: As─C stretch (including symmetry and asymmetry), As═O stretch, As─O stretch, and the As─S stretch (including single and double bonds). The omission of general molecular vibrational bonds was determined by the following reasons: First, most of these arsenicals were synthesized in the laboratory and used without further purification. Therefore, impurities could generate many unknown vibrational bands, creating interpretational issues. Second, many vibrations in these molecules are weak and difficult to identify. Focusing on these molecular fingerprint vibrational modes will greatly reduce problems with the identification of molecules since these fingerprint vibrations usually yield strong bands for easy identification. Most of the arsenicals studied contain the following bonds, As─O, As═O, As─C, As─S, As═S, thus according to previous studies, the Raman shifts of interest would range from 1000~300 cm^{-1} [186-188, 263-265]. Frequencies less than 300 cm^{-1} were omitted because of the

complexity of the vibrational modes. Therefore, in the following discussion, only frequencies in the range of 1000~300 cm^{-1} are utilized for Raman spectra interpretation.

4.5.2 Raman spectra interpretation of MMA^{III} and DMA^{III}

The fingerprint vibrational frequencies and corresponding vibrational mode assignments for MMA^{III} and DMA^{III} are summarized in Table 4.4 and their DFT Raman spectra and experimental Raman spectra are illustrated in Fig. 4.4.

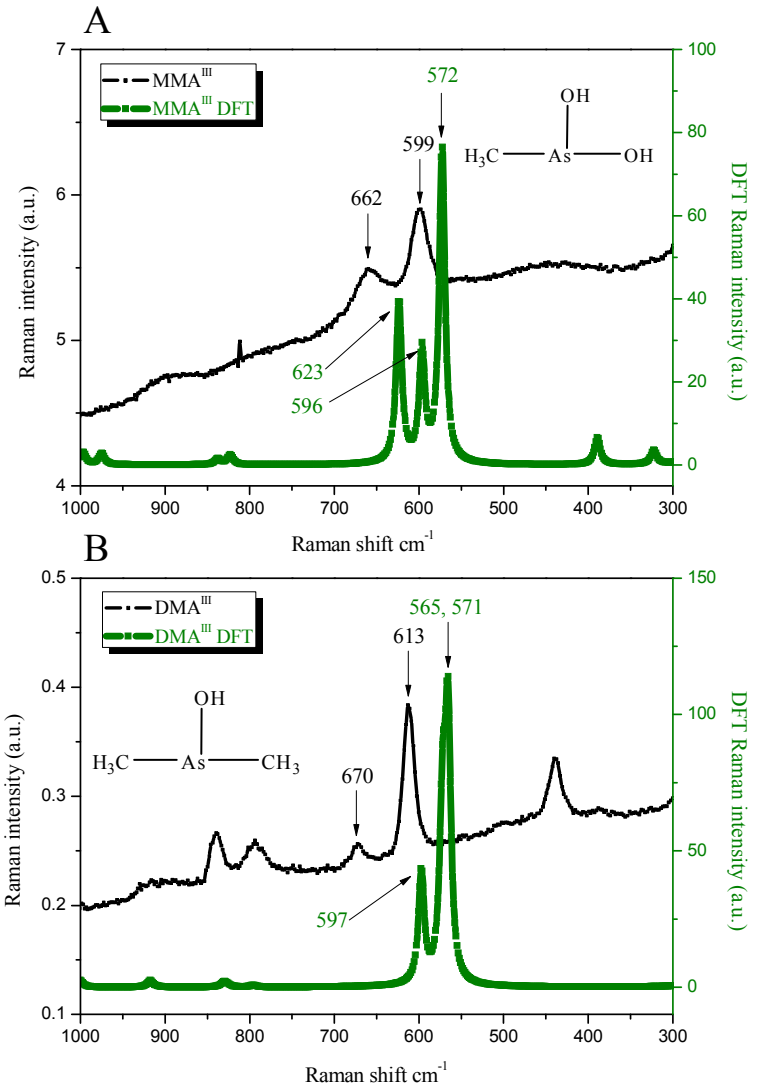

Figure 4.4 Experimental and calculated Raman spectra of MMA^{III} (A) and DMA^{III} (B). (Note Raman spectra was obtained using Thermo FirstDefender RM)

Table 4.4 Vibrational frequencies assignment for MMA^{III} and DMA^{III}

Arsenical	MOLDEN assignment	Experimental Raman frequency (cm^{-1})	Calculated Raman frequency (cm^{-1})	Corrected Raman frequency (cm^{-1})	Frequency difference (cm^{-1})	Error ratio (%)
MMA^{III}	As—C stretch	599	572	554	45.4	7.6
	O—As—O asym stretch	NA	596	577	NA	NA
	O—As—O sym stretch	662	623	603	59.0	8.9
DMA^{III}	C—As—C sym stretch	613	565	547	66.1	10.8
	C—As—C asym stretch	NA	571	553	NA	NA
	As—O stretch	670	597	578	92.2	13.8

The purity of MMA^{III} was confirmed by comparing its retention time to that of an arsenic standard (Fig. 4.5). The DMA^{III} characterization was carried out by using the proton NMR (Fig. 4.6).

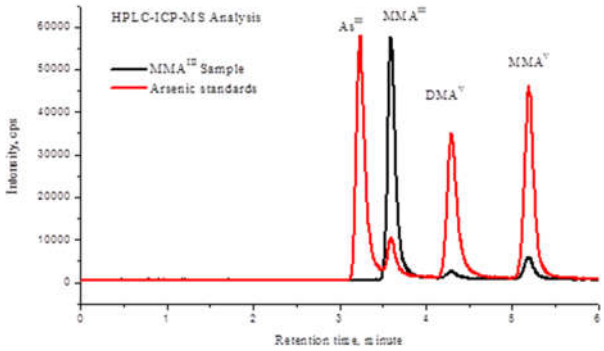

Figure 4.5 HPLC-ICP-MS chromatograms of arsenic standards and MMA^{III} synthesized in the laboratory showing the identity and purity

The purity of MMA^{III} accoring to the peak area in Fig. 4.5 was about 84%. Small amounts of MMA^{V} and DMA^{V} were found in the MMA^{III} synthesized possibly due to the

impurity of MMA^{V} used as starting material and the incomplete reduction during synthesis.

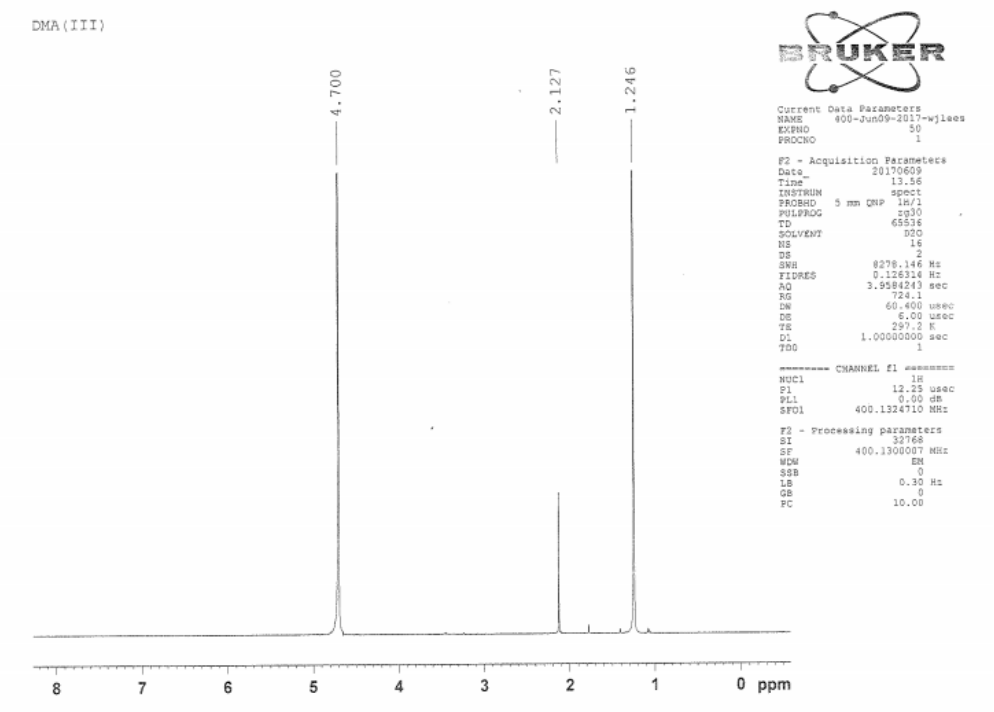

Figure 4.6 Proton NMR spectra for the confirmation of DMAIII synthesized in the laboratory

The chemical shift values in Fig. 4.6 were referenced to the HDO signal at 4.70 ppm. The appearance of DMA^{III} was confirmed by the chemical shift of the methyl protons at 1.25 ppm, which was consistent with the value in the previous report [201].

Both MMA^{III} (Fig. 4.4A) and DMA^{III} (Fig. 4.4B) have characteristic As─C vibration. The DMA^{III} produced characteristic asymmetric and symmetric vibrational modes of As─C because of the presence of two methyl groups, while MMA^{III} did not show these bands. Experimental Raman spectra were measured in water using a portable Raman spectrometer. While the Raman signal intensities were weak all vibrational bands were distinguishable from the baseline. In the experimental spectra of MMA^{III}, the

vibrational band at 599 cm^{-1} was assigned to the As─C stretch, while the band at 662 cm^{-1} was assigned to the symmetric vibration of As─O. The corresponding calculated As─C and As─O vibrational frequencies were 572 and 623 cm^{-1}, respectively. No asymmetric vibrational modes of As─O were found in the experimental spectra, while there was an asymmetric vibration of As─O at 596 cm^{-1} in the calculated Raman spectra. In the experimental Raman spectra of DMA^{III}, a vibrational band at 613 cm^{-1} was assigned to the symmetric As─C stretch, and a vibrational band at 670 cm^{-1} was assigned to the As─O stretch. The corresponding calculated As─C and As─O vibrational frequencies were 565 and 597 cm^{-1}, respectively. The asymmetric As─C vibrational band in DMA^{III} did not appear as a distinguishable band in the experimental Raman spectra, possiblly a result of the the fact that the symmetric and asymmetric vibrational frequencies were very close as demonstrated from the DFT calculation (565 and 571 cm^{-1}). The disappreance of the assymetric vibration of As─O in DMA^{III} might casue the error ratio of the As─O frequency in the DMA^{III} molecule over 10 %.

4.5.3 Raman spectra interpretation of $DMMTA^V$ and $DMDTA^V$

The structure of $DMMTA^V$ and $DMDTA^V$ were confirmed by their molecule ion in the mass spectrum (Fig. 4.7).

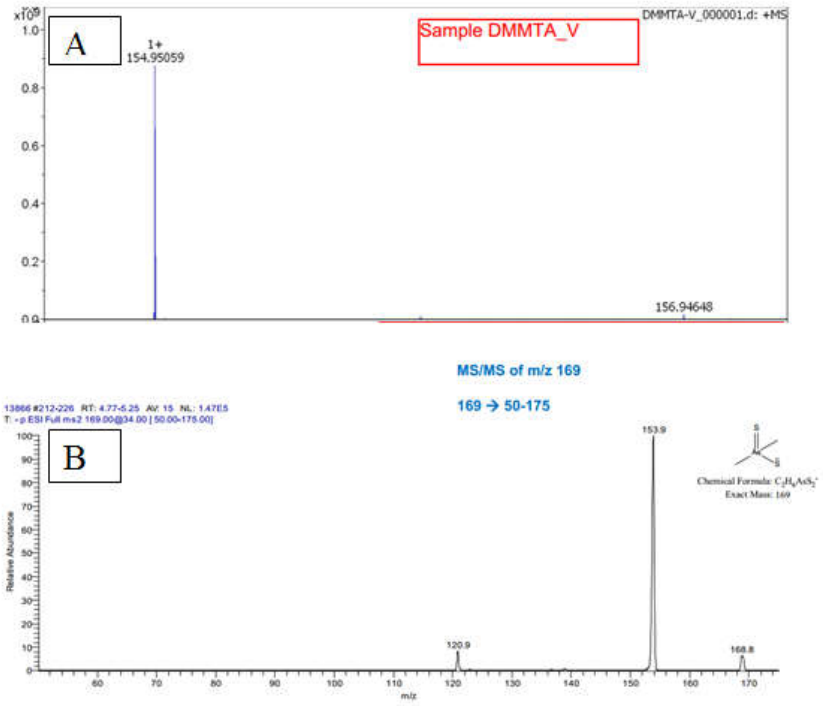

Figure 4.7 Molecular ion peaks confirmation of $DMMTA^V$ (A) and $DMDTA^V$ (B)

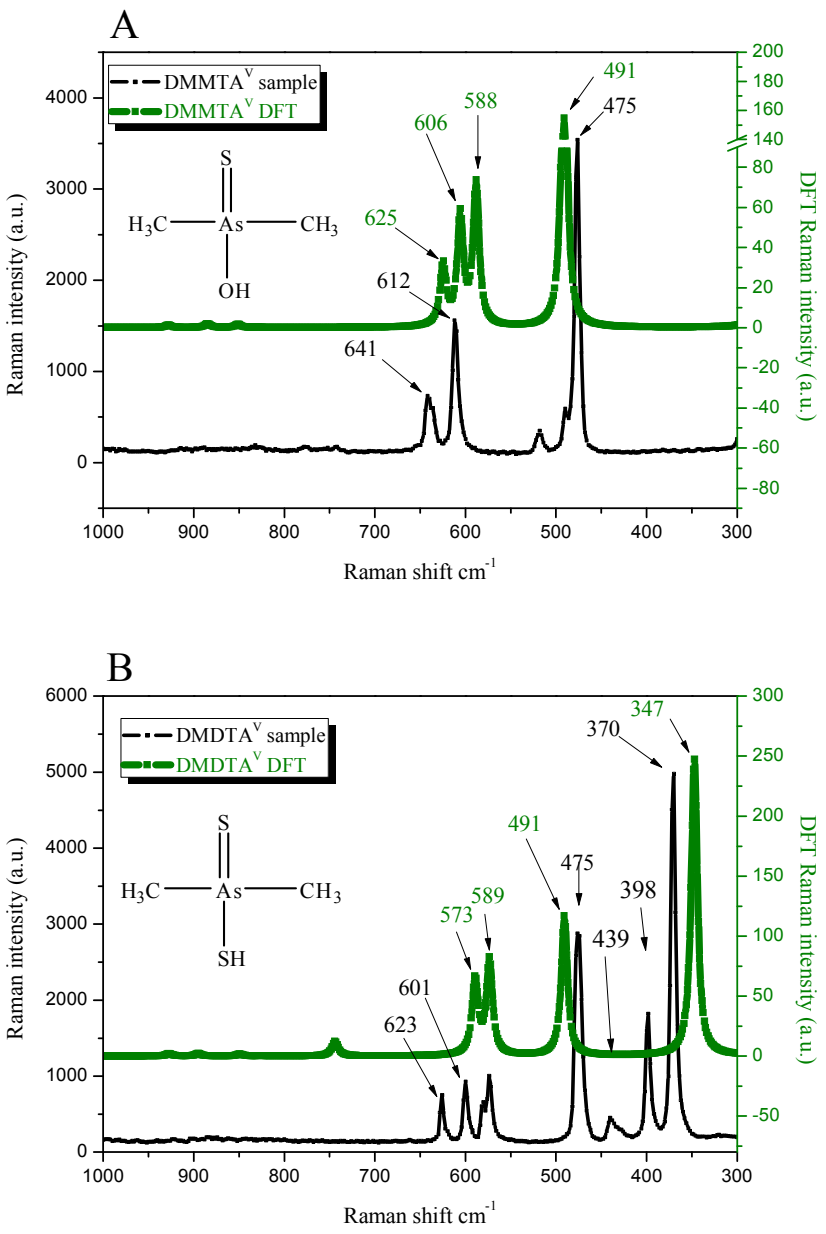

Figure 4.8 Experimental and calculated Raman spectra of DMMTA^V (A) and DMDTA^V (B)

Table 4.5 Vibrational frequencies assignment for $DMMTA^V$ and $DMDTA^V$

Arsenical	MOLDEN assignment	Experimental Raman frequency (cm^{-1})	Calculated Raman frequency (cm^{-1})	Corrected Raman frequency (cm^{-1})	Frequency difference (cm^{-1})	Error ratio (%)
$DMMTA^V$	As═S stretch	475	491	475	0.2	0.1
	C─As─C sym stretch	612	588	569	43	7.0
	C─As─C asym stretch	NA	606	587	NA	NA
	As─O stretch	641	625	605	36	5.6
$DMDTA^V$	As─S stretch	370	347	336	34	9.2
	As═S stretch	475	491	475	0	0.1
	C─As─C sym stretch	601	573	555	46	7.7
	C─As─C asym stretch	623	589	570	53	8.5

Both $DMMTA^V$ and $DMDTA^V$ have two methyl groups and one As═S bond (Fig. 4.8 and Table 4.5). The major differences between these two compounds are the As─S bond in $DMDTA^V$ and As─O bond in $DMMTA^V$. Both of these compounds had very strong Raman signal in the 1000~300 cm^{-1} range. In the experimental spectral results for $DMMTA^V$, three major bands were observed at 475, 612 and 641 cm^{-1}. These were assigned as the As─S stretch, the As─C symmetric vibration and the As─O stretch, respectively (Fig. 4.8A). The corresponding calculated vibrational frequencies of the As═S stretch, the As─C symmetric and asymmetric vibrations and the As─O stretches are at 491, 588, 606 and 625 cm^{-1} respectively. The asymmetric vibrational mode of As─C did not appear in the experimental spectra, but was observed in the DFT spectra due to the vibration overlap aforementioned. For $DMDTA^V$ (Fig. 4.8B), four major bands were found at 370, 475, 601 and 623 cm^{-1}, and they were assigned as the As─S

stretch, the As═S stretch, the As─C symmetric vibration and the As─C asymmetric vibrations, while the band around 400 and 575 cm^{-1} may be due to the presence of sodium-DMDTA [266]. There were also some unknown vibrational bands in the $DMDTA^{V}$ experimental Raman spectra located between 600~550 cm^{-1}. No effort was made to investigate the appearance of these vibrational bands, and it was assumed that they originated from impurities. The corresponding calculated As─S and As═S stretches and As─C symmetric and asymmetric vibrational bands are at 347, 491, 573 and 589 cm^{-1}, respectively. The major differences in the Raman spectra between $DMMTA^{V}$ and $DMDTA^{V}$ were that the As─S stretch which occurred at 370 cm^{-1} appeared only in the $DMDTA^{V}$, while both molecules showed an As═S stretch at 475 cm^{-1}. All error ratios between experimental and corrected Raman frequencies were with 10%.

4.5.4 Raman spectra interpretation of $DMA^{III}GS$ and $DMA^{III}Cys$

$DMA^{III}Cys$ was prepared in the laboratory using excess of DMA^{V} against L-cysteine and was confirmed by mass spectrometry (Fig. 4.9). As in the diagram, m/z=226 was found to be the molecular ion peak, also the mass fragmentation showed ions of losing amine and losing cysteine group from the molecule at m/z=209 and 137.

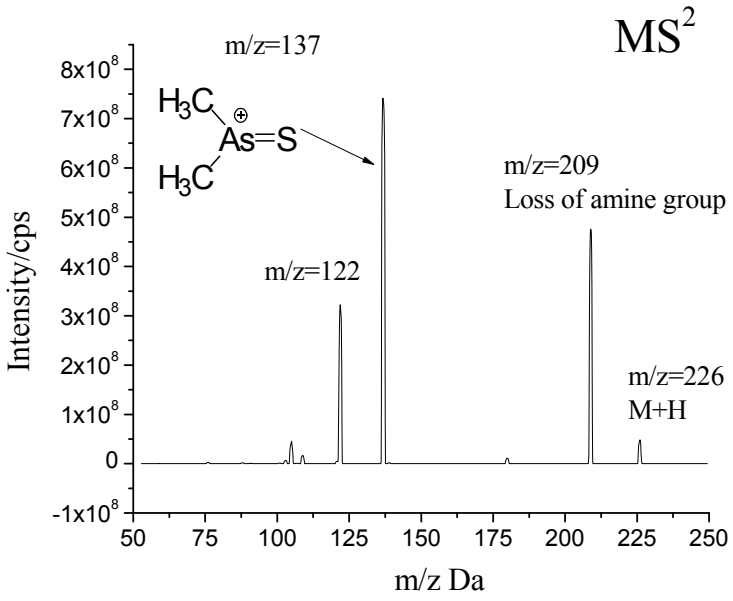

Figure 4.9 Mass spectrum fragmentations of $DMA^{III}Cys$ by ESI-MS. Mass spectrum fragmentations of $DMA^{III}Cys$ by ESI-MS. The appearance of m/z peak of 226 can be used to confirm the existing of $DMA^{III}Cys$ molecule in the reaction product, the fragmentation of m/z= 209 and 137 were the proof of losing the amine group and cysteine group respectively.

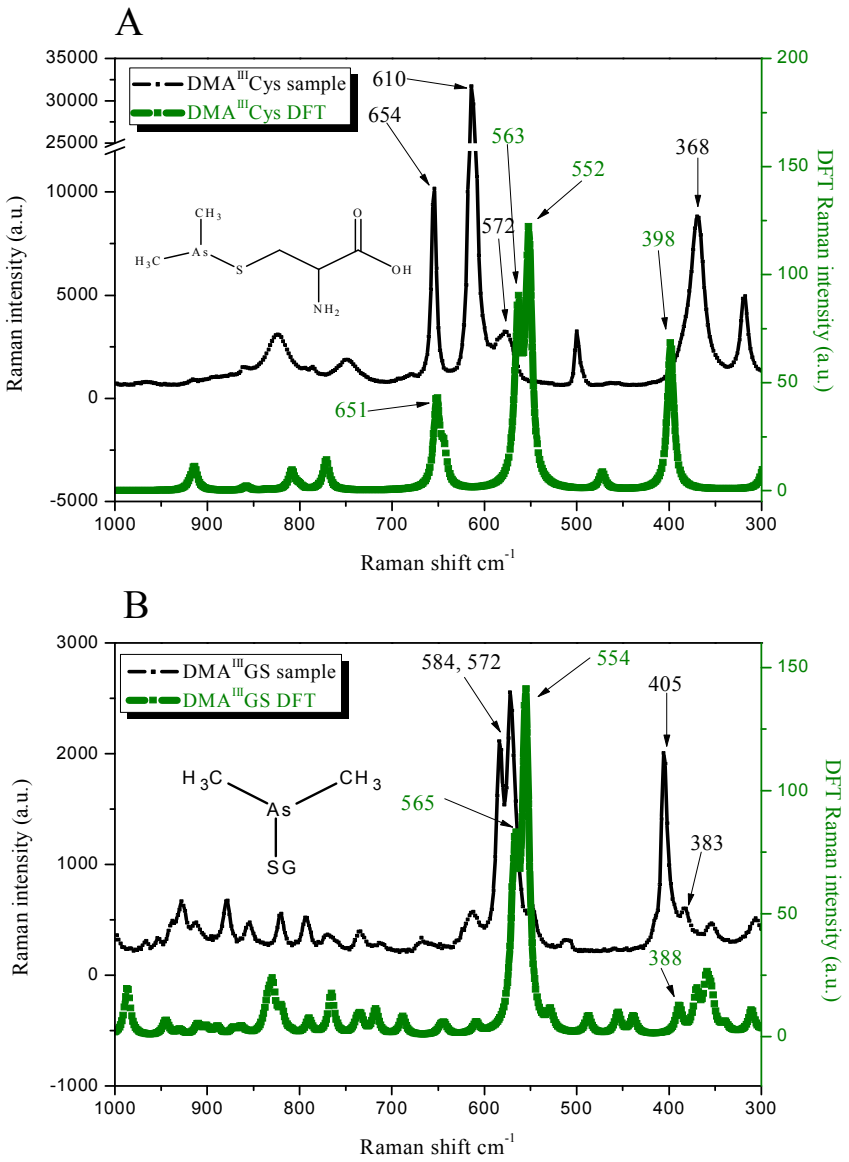

Figure 4.10 Experimental and calculated Raman spectra of $DMA^{III}GS$ (A) and $DMA^{III}Cys$ (B)

The results for $DMA^{III}GS$ and $DMA^{III}Cys$ are summarized in Table 4.6 and Fig. 4.10. $DMA^{III}GS$ was commercially available and used as received. In the experimental spectra of $DMA^{III}GS$, three bands were found at 383, 572 and 584 cm^{-1} representing the

As─S stretch, the As─C symmetric vibration and the As─C asymmetric vibration, respectively. The corresponding calculated As─S stretch, As─C symmetric and asymmetric stretch appeared at 388, 554, 565 cm^{-1}. A band at 405 cm^{-1} also appeared which should be the δ(C─S) deformations of the glutathione molecule [267]. Four major bands were observed at 368, 572, 610 and 654 cm^{-1} in the experimental spectra of DMA^{III}Cys. These were assigned as the As─S stretch, the As─C asymmetric vibration and the As─C symmetric vibration and C─S stretch, respectively. The corresponding calculated As─S stretch, As─C symmetric and asymmetric stretch, and C─S stretch were 398, 552, 563 and 651 cm^{-1} respectively. Extra bands appeared around 500 and 300 cm^{-1} in DMA^{III}Cys Raman spectra and were not assigned as they may be the result of impurities associated with synthetic procedures. It can be seen that different patterns were observed between the spectra of DMA^{III}GS and DMA^{III}Cys, although the only difference in their chemical structure was the complexing ligand. The major difference between the two compounds was that the C─S stretch in the DMA^{III}Cys appeared around 654 cm^{-1} (Fig. 4.10A), while it was at 405 cm^{-1} for DMA^{III}GS due to deformations originated from the δ(C─S) (Fig. 4.10B).

Table 4.6 Vibrational frequencies assignment for $DMA^{III}GS$ and $DMA^{III}Cys$

Arsenical	MOLDEN assignment	Experimental Raman frequency (cm^{-1})	Calculated Raman frequency (cm^{-1})	Corrected Raman frequency (cm^{-1})	Frequency difference (cm^{-1})	Error ratio (%)
$DMA^{III}Cys$	As─S stretch	368	398	385	17	4.7
	C─As─C sym stretch	572	552	534	38	6.6
	C─As─C asym stretch	610	563	545	65	10.7
	C─S stretch	654	651	630	24	3.7
$DMA^{III}GS$	As─S stretch	383	388	376	7	1.9
	C─As─C sym stretch	572	554	536	36	6.3
	C─As─C asym stretch	584	565	547	37	6.4

4.6 Discussion

4.6.1 Validation of the theoretical computation assisted Raman spectra interpretation method

In this study, a methodology involving the combination of a theoretical simulation of each arsenic compound's fingerprint Raman vibrational modes and its experimental Raman spectra were used for the identification and assignment the spectra of known arsenic compounds. For the validation of our proposed method, the molecule DMA^{V} was employed as a standard molecule for the comparison between experimental and calculated Raman frequencies. Computationally, the B3LYP functional with different basis sets was employed for molecular geometry optimization and calculated Raman spectra simulation of all compounds. Among the basis sets used, including 6-31G*, 6-

311++G**, SDD/6-31G*, SDD/6-311++G**, and def2-TZVPP, the basis set 6-311++G** yielded the most optimal results in terms of consistency with previous reports regarding molecular geometry optimization and Raman spectral prediction [164, 268]. The average error ratio between experimental and corrected Raman frequencies was about 5.8%, which was lower than the threshold value of 10%, indicating that this method is reliable [260-262]. Discrepancies were found in the Raman frequencies of As─O bonds (including single bond and double bonds.) This was most likely due to a systematic error during calculation in which the calculated Raman spectra only considered the isolated molecules in vacuum, while the experimental Raman spectra was obtained in crystalline form with constrained geometry. The RMS value was also an important parameter used to evaluate the performance of a basis set, and the application of a scaling factor was able to significantly reduce the RMS, indicating that the scaling factor was useful in minimizing the discrepancy between experimental and calculated Raman frequencies. The RMS (with scaling factor) for 6-311++G** was 49 cm^{-1}, being significantly higher than 26 cm^{-1} in the previous report [260], and this could be due to the limited number of Raman frequencies used for the calculation. Overall, calculated Raman spectra matched the experimental Raman spectra of DMA^V well with an average error ratio of 5.8% in Raman frequencies. This result indicated that using the calculated Raman spectra is a reliable method to simulate the experimental Raman spectra and thus this methodology can be used in the identification and assignment of unknown arsenic Raman spectra.

4.6.2 Comparison of the basis sets employed for vibrational spectra prediction

The B3LYP functional with double-zeta or triple-zeta basis sets have achieved admirable accuracy and efficient calculations in other studies [260]. In this work, the B3LYP function with different basis sets was investigated in order to determine how different modes performed when the basis set was changed. Due to the existence of arsenic atom, mixed basis sets of SDD/6-31G* and SDD/6-311++G** were also employed to study whether considering relativistic effects could improve accuracy of calculation. The all electron triple-zeta basis set def2-TZVPP was used to in an effort to improve the accuracy of calculations by increasing the size of the basis set. Due to its available crystalline Raman spectra and known structure, DMA^V was employed as a reference to determine the most precise and efficient basis set.

The accuracy of calculated Raman frequencies depends on the size and quality of the chosen basis set [165]. Different basis sets were employed to process computational geometry optimization of arsenic molecules and simulation of DFT Raman spectra, in which different dispersion, polarization and relativistic effects were considered, in an effort to improve the accuracy of the computational calculation. Two parameters were employed to evaluate the discrepancy of calculated and experimental Raman frequencies, including RMS and numbers of spectra with error ratios over 10% [260-262].

As shown in Table 4.1A and Table 4.2, the calculated Raman spectra of DMA^V are fundamentally consistent with the experimental data. When no scaling factors were employed in the RMS calculation, the RMS was reduced from 112.4, 90.9 to 60.1 with the basis sets increasing (Table 4.2). The all electron basis set def2-TZVPP also yielded satisfactory outcome with only one error ratio above 10% and a low RMS value. It was

found that increasing the dispersion and polarization in basis sets could improve the outcome of RMS calculation. When a scaling factor was applied, the Raman prediction accuracy in all basis sets was improved as shown in Table 4.2, mainly because the calculated Raman frequencies overestimated the experimental data [260]. Earlier work has demonstrated that the error ratio of calculated Raman frequencies against the experimental Raman frequencies is greatly reduced when a scaling factor is applied [269]. The mixed basis sets which take the relativistic effects into consideration such as SDD/6-31G* and SDD/6-311++G** did not yield improved results. This is perhaps due to the fact that arsenic belongs in the group of fourth period elements, for which the relativistic effects are not very important in determining vibrational frequencies. Computational efficiency is also a critical parameter in the comparison of performance among these basis sets, although many resource-consuming basis sets are still affordable for most researchers. Extra dispersion and polarization will significantly increase the need for computational resources especially for larger systems such as $DMA^{III}Cys$ and $DMA^{III}GS$. The time consumption associated with each basis set is shown in Table 4.2. The all electron basis set def2-TZVPP basis set was the most computationally demanding basis set. In addition, the computational costs were greatly reduced when the relativistic effects of the arsenic atom were included during theoretical calculations, since the time consumed in mixed basis sets was shorter than their corresponding counterparts.

Taking the above parameters into consideration, including number of error ratios over 10%, computational efficiency and Raman intensity prediction, 6-311++G** was the optimal basis set used in this study. It is worth mentioning that the all electron basis

set def2-TZVPP would be the method of choice if there was no restriction in computational resources.

4.6.3 Fingerprint Raman frequencies of the arsenicals in different chemical environments

The As─O bond widely exists in inorganic and organic arsenicals present in biological systems and is closely related to arsenic metabolism. As─O vibrational frequencies in pentavalent arsenicals were generally larger than 700 cm^{-1} except in $DMMTA^{V}$, whose As─O frequency was 641 cm^{-1} (Table 4.7). On the other hand, frequencies in trivalent arsenicals were all less than 700 cm^{-1}. The difference in vibrational frequencies for trivalent and pentavalent arsenicals may be partially due to the force constant difference in these two types of compounds. Arsenicals are completely protonated in pentavalent arsenicals since in the solid acidic form, the arsenic atoms are actually attached to hydroxyl groups (As─OH) [149].

Table 4.7 Summary of As─O Raman frequencies

Arsenical	Assignment	Experimental Raman spectra (cm^{-1})	Calculated Raman frequency (cm^{-1})	Corrected Raman frequency (cm^{-1})	Frequency difference (cm^{-1})	Error ratio (%)
MMA^{III}	O─As─O sym stretch	662	661	640	22	3.4
DMA^{III}	As─O stretch	670	597	578	92	13.8
$DMMTA^{V}$	As─O stretch	641	624	604	37	5.8
iAs^{V}	As─O stretch	769 [186]	NA	NA	NA	NA
MMA^{V}	As─O(Va, Vs)	769, 780 (Va, Vs) [188]	NA	NA	NA	NA
DMA^{V}	As─O stretch	748	667	646	102	13.7

However, trivalent arsenicals, such as MMA^{III} and DMA^{III}, are hydrolyzed in excess base and they were fully deprotonated when their Raman spectra were measured. Thus their arsenic atoms were only linked to oxygen atoms (As─O) [149]. The force constant increased from As─O to As─OH as reported previously [189] and the vibrational frequency was positively correlated to the force constant between the two atoms, i.e. arsenic and oxygen. The valence of arsenicals is likely the major reason for the obvious difference in As─O vibrational frequencies between trivalent and pentavalent arsenic species. A similar result was found in the Se─O vibrational frequencies for selenic acid (H_2SeO_4) and selenous acid (H_2SeO_3) [270, 271]. Among all pentavalent arsenicals studied, $DMMTA^V$ was the only compound containing an As─O bond, and its As─O vibrational frequency was less than 700 cm^{-1}. The only difference between DMA^V and $DMMTA^V$ was the substitution of the oxygen atom by a sulfur atom. The possible reason for As−O frequency less than 700 cm^{-1} in the pentavalent $DMMTA^V$ could be the difference in electronegativity between oxygen and sulfur atoms, in which sulfur atom was weaker than oxygen. When sulfur is substituted for oxygen, the electropositivity of the arsenic atom in the molecule $DMMTA^V$ is reduced and thus the force constant of As─O should also be reduced when compared to DMA^V. Furthermore, the calculated Raman frequencies of As─O were mostly smaller than the experimental values. This observation was unusual since the scaling factors were all reported less than 1.0 and the calculated Raman frequencies were generally bigger than the experimental Raman frequencies. However, according to the previous studies, the differences between experimental and corrected frequencies produced a normal distribution [272] and this this result could be interpreted as systematic error during DFT calculation.

All As─C Raman frequencies were summarized in Table 4.8. There was also a positive correlation between the arsenic valency and the As─C experimental Raman frequencies with the exception of DMA^{III}, in which the As─C Raman frequencies in pentavalent arsenicals were larger than trivalent ones. Among all Raman spectra, MMA^{III} and DMA^{III} were the only two obtained from aqueous solution (hydrolyzed by 0.1 M NaOH) while the rest of the compounds were measured as solid samples. The Raman frequencies of As─C in MMA^{III} and DMA^{III} were significantly higher than those trivalent arsenicals containing sulfur. The reason could be due to the abundant hydroxyl ions existing in the aqueous solution. Only the symmetric vibrational frequencies of As─C were selected for comparison because the symmetric As─C intensities were found to be stronger than those from asymmetric vibrations in this study. This positive correlation was consistent with the finding by Zingaro et al [273], whose conclusion was based on the summary of Cullen's work [274]. In Cullen's work the carbon-arsenic stretching frequencies in trimethylarsine were from 572~582 cm^{-1}, while in tetramethylarsonium compounds the frequencies were approximately 650 cm^{-1} [274].

Table 4.8 Summary of As─C Raman frequencies

Arsenical	MOLDEN assignment	Experimental Raman spectra (cm^{-1})	Calculated Raman frequency (cm^{-1})	Corrected Raman frequency (cm^{-1})	Frequency difference (cm^{-1})	Error ratio (%)
MMA^{III}	As─C	599	572	554	45	7.6
DMA^{III}	C─As─C sym stretch	613	565	547	66	10.8
	C─As─C asym stretch	NA	571	553	NA	NA
$DMA^{III}Cys$	C─As─C sym stretch	572	552	534	38	6.6
	C─As─C asym stretch	610	563	545	65	10.7
$DMA^{III}GS$	C─As─C sym stretch	572	554	536	36	6.3
	C─As─C asym stretch	584	565	547	37	6.4
$DMMTA^{V}$	C─As─C sym stretch	612	588	569	43	7.0
	C─As─C asym stretch	NA	606	587	NA	NA
$DMDTA^{V}$	C─As─C sym stretch	601	573	555	46	7.7
	C─As─C asym stretch	623	589	570	53	8.5
DMA^{V}	C─As─C sym stretch	611	573	555	56	9.2
	C─As─C asym stretch	636	611	591	45	7.0

Vibrational spectra of several methylated arsenicals containing sulfur have been reported [252, 253, 264-266]. Unfortunately, fingerprint Raman frequencies were not clearly assigned. In a previous study [59], two strong vibrational frequencies located at

602 and 624 cm^{-1} were observed in the Raman spectra of NaS_2AsMe_2, a thiolated arsenical similar to $DMDTA^V$ used in this study. These Raman frequencies were similar to the As─C bands at 601 and 623 cm^{-1} observed in $DMDTA^V$, whose Raman spectrum was measured and vibrational frequencies were assigned in this study. Similarly, a vibrational frequency of 612 cm^{-1} with medium intensity was reported in the Raman spectrum of $(CH_3)_2As(S)OAs(S)(CH_3)_2$ [252]. This is identical to Raman frequency assigned to an As─C symmetrical stretch found in the $DMMTA^V$ shown in this work. It appears that thiolation of these arsenicals did not significantly impact the As─C Raman frequencies, while clear differences in the Raman frequencies of the As─O stretch were observed in $DMMTA^V$. Furthermore, no difference in Raman frequency was found in the As─C symmetric frequencies of DMA^V (611 cm^{-1}) and $DMMTA^V$ (612 cm^{-1}), which may indicate that thiolation has a limited impact on the As─C symmetric frequencies among these aresnicals. However, the As─C symmetric frequency in $DMDTA^V$ was significantly lower than in DMA^V or $DMMTA^V$. Therefore, the single As─S bond also has a substantial impact on the As─C symmetric vibrational frequencies. Overall, both reducing the valency of arsenic and the presence of a single As─S bond should reduce As─C symmetric vibrational frequencies. Furthermore arsenic valence has a similar impact on the Raman frequencies of As─O and As─C, resulting in a positive correlation between the arsenic valence and the Raman frequencies of As─O or As─C. It is believed that the electropositivity of arsenic atoms in these pentavalent and trivalent arsenicals has a significant impact, since outer electrons in pentavalent ones are all paired while there is a lone pair of electrons in these trivalent species. The existence of a lone pair of electrons will reduce the electropositivity of arsenic atoms in these trivalent arsenicals [275].

Table 4.9 Summary of As─S Raman frequencies

Arsenical	Assignment	Frequency (cm^{-1})	Calculated Ramanfrequency (cm^{-1})	Corrected Raman frequency (cm^{-1})	Frequency difference (cm^{-1})	Error ratio (%)
$DMMTA^{V}$	As═S	475	491	475	0	0.1
$DMDTA^{V}$	As═S	475	491	475	0	0.1
	As─S	370	347	336	34	9.2
$DMA^{III}Cys$	As─S	368	398	385	17	4.7
$DMA^{III}GS$	As─S	383	388	376	7	1.9

Sulfur-containing arsenicals studied in this study can be categorized into two groups, one is arsenic complexes with sulfur-containing ligands and another is the pentavalent oxoarsenicals with oxygen being substituted by sulfur. Thiol-containing molecules, such as glutathione (GSH), cysteine (Cys) or sulfhydryl containing proteins, are widely present in cellular environment. Trivalent arsenicals can bind to these thiol-containing molecules and form As─S single bonds. Both single bond (As─S) and double bond (As═S) can be found in the arsenicals studied (Table 4.9). The Raman frequencies of As═S obtained via experiments and DFT calculation were always higher than those found in As─S and this result was consistent with the results reported elsewhere [264, 273, 276]. This observation is the same as the Raman frequency of As═O is higher than the As─O in DMA^{V}. The reason for this pattern is that the force constant between diatoms increases with bond order, [275]. Thus the Raman frequencies of double bonds are always bigger than the respectively single bonds. Similar effects are seen in dithiocacodylate complexes (sulfur containing arsenic chelating ligands $(CH_3)_2AsS_2^-$) known for their malodor [264, 276-278]. In earlier work, Zingaro had calculated the harmonically vibrational frequencies for As─S and As═S, as 372 and 555

cm^{-1} respectively [279]. Raman spectra of dithiocacodylate complexes were usually obtained using their salt accordingly. Due to the distribution of π-electrons over the whole S─As─S fragment, there were other As─S Raman bands within 400~500 cm^{-1} besides the existence of two regular As─S vibrational frequencies [276]. These extra As─S bands were found in $DMDTA^V$ (Fig. 4.8B), between 475 and 370 cm^{-1}. This is important because the $DMDTA^V$ should be in ionic form in the cellular environment.

4.7 Conclusion

In this study, we identified and assigned the fingerprint Raman frequencies for some potentially important compounds involved in arsenic metabolism by comparing experimental data with DFT calculations. Of all basis sets employed for DFT Raman spectra simulation, the basis set 6-311++G** provided the most efficient and accurate result for the standard molecule—DMA^V calculation and therefore was utilized for the calculation of all arsenicals. The results of theoretical calculations matched well with the experimental data after an empirical scaling factor applied. The As─O and As─C vibrational frequencies were higher in pentavalent than in trivalent arsenicals. For the thiolated arsenicals, the fingerprint Raman frequencies of As─S (including single and double bonds) were identified, of which the Raman frequency of As═S was about 475 cm^{-1} and the frequency of As─S was around 370 cm^{-1}. This study provides much needed fundamental information on Raman spectrometry for some potentially important arsenicals associated with biological systems. The fingerprint Raman frequencies identified and assigned in these compounds should assist in the development of SERS for arsenic speciation in biological and environmental matrices.

Chapter 5

Summary, Significance, and Future Research Directions

5.1 Summary

In this project, arsenic speciation analysis by SERS for As^{III}, As^{V}, MMA^{V} and DMA^{V}, was carried out under the influence of a cellular matrix. Two different types of silver nanoparticles with different surface coating molecules were employed with varying SERS signal response resulting from different electrostatic interactions with the nanoparticle surface. Each of the four compounds measured generated fingerprint SERS signals, which were distinguishable even in mixed samples. The interactions between arsenic compounds and silver nanoparticles in the colloidal suspensions were studied using adsorption experiments to better understand their respective spectral differences. Increase arsenic adsorption was found in the positively charged nanoparticles, and only the positively charged silver nanoparticles were able to achieve simultaneous detection of arsenicals in the colloidal suspension without separation. However, MMA^{V} and DMA^{V} had identical SERS signal response in the positively charged nanoparticles. The limit of detections (LOD) was calculated based on a measurement of three times of standard deviation of the blank samples and was determined to be 1.0, 2.8, and 9.9 ppb for As^{V}, As^{III}, and MMA^{V}/DMA^{V}, respectively. The work demonstrated that positively charged silver nanoparticles could be a promising SERS substrate for studying arsenic metabolism in a biological matrix, reducing the bias caused by traditional techniques that involve sample preparation and pretreatment.

Secondly, arsenic speciation on silver nanofilms was explored by examining the spectral response of the same four common arsenicals, As^{III}, As^{V}, MMA^{V} and DMA^{V}. A coffee ring effect was observed during the evaporation of a liquid drop on the silver nanofilm. The unique effect coffee ring drove all solute in the droplet towards the edge of

the coffee ring. At first this coffee ring effect was employed for separation of arsenicals in solutions of different pHs. However, the capillary flow generated in the coffee ring effect was strong and hard to control. No separation was found in these initial experiments and the arsenicals were observed to stack at the edge of coffee ring. To improve separation efficiency, the coffee ring was examined under the influence of surfactants. The introduction of small amounts of surfactants (0.05%) caused a continual migration of liquid into the peripheral region of the droplet and increased the migration distance for arsenic separation. This unique coffee ring phenomenon left two concentric-ring stain patterns after the complete evaporation and it was described as a halo coffee ring effect. The arsenic separation using the halo coffee ring effect was successfully demonstrated in three solutions, including, 0.1 M acetic acid (pH=2.9), 0.1 M phosphate (pH=7.5) and 0.1 M ammonium formate (pH=6.9). As the sampling spot moved from the center to the edge of the coffee ring, a clear SERS signal pattern changes were observed at the halo ring region and the inner ring region, indicating that arsenicals were separated along the radius. Moreover, the results illustrated that the electrostatic interactions between arsenicals and the AgNF surface played a major role in the arsenicals separation. This work provides a novel approach for using the coffee ring effect in chemical separations.

Thirdly, fingerprint Raman frequencies of some potentially important arsenic metabolites were assigned and identified by comparing experimental Raman spectra with theoretical Raman spectra obtained from DFT calculations. Most of the arsenicals studied in this work were unstable in ambient conditions, including, MMA^{III}, DMA^{III}, $DMMTA^{V}$, $DMDTA^{V}$, $DMA^{III}GS$ and $DMA^{III}GS$. Through this study, the DFT was demonstrated to

be helpful in providing simulated Raman spectra and vibrational modes for the identification of spectra from unknown arsenicals. DMA^V was employed as a representative compound to optimize the computational method. Different basis sets were used to simulate DFT Raman spectra and Raman frequencies were extracted from the calculated results to determine the best basis set. The basis set 6-311++G** was found to provide the most efficient and precise results for the representative molecule calculation and also used for the computation of all arsenicals. To reduce the discrepancy between theoretical and experimental results, an empirical scaling factor was used and improved matching results were observed. In addition to the identification and assignment of unknown arsenicals' fingerprint Raman spectra, it was also possible to observe Raman frequencies changing rules under the chemical and structural effect. Raman frequencies changing rules were observed. Generally, the As─O and As─C vibrational frequencies were higher in pentavalent than that in trivalent arsenicals. In addition, the Raman frequencies of As═S and As─S were measured to be about 475 and 370 cm^{-1}, respectively. The study contributes Raman spectral information for some potentially important arsenicals involved in arsenic metabolism in biological systems. The fingerprint Raman frequencies identified and assigned for these arsenicals could help the method development when using SERS for arsenic speciation in biological and environmental matrices.

5.2 Significance of this study

The research reported in this work is original, since no report about SERS studies of organoarsenicals found in cells is available. Arsenic speciation is important in the evaluation of arsenic bioavailability and toxicity towards human health. Currently, most

analytical methods for the arsenic speciation involve chromatographic separation coupled with mass spectrometry detection. However, the requirement of sample preparation/pretreatment before instrumental measurements could compromise the integrity of arsenicals present in the sample. SERS overcomes many drawbacks of the prevalent analytical methods, because SERS can minimize sample preparation procedures. Previous SERS studies of arsenic were mostly focused on the determination of inorganic arsenic compounds in environmental samples, and organoarsenicals were barely reported. In addition, the study of arsenic speciation in biological matrices using SERS has not previously been explored. This study explored the possibility of arsenic speciation using metallic colloidal suspensions and fundamental parameters were studied. This work included the examination of the interactions between arsenicals and charged nanoparticles, as well as determination arsenicals SERS signals in nanoparticles with different coatings, surface charge, and size in a cellular matrix. In addition, this study unveiled that in addition to aggregation, electrostatic interactions are also important as the nanoparticles aggregation for strong SERS signal generation in the colloidal solutions.

In the second part of this work, a novel arsenic speciation technique using the coffee ring effect was developed. This part of work was highly challenging, because the coffee ring size was very small. It was produced by dropping only 2 μL solution onto the AgNF and allowing the strong capillary flow to drive the analytes in the droplet towards the edge. This study demonstrated that two important requirements should be fulfilled for coffee ring separation of small molecules. Firstly, the liquid in the droplet should be able to migrate into peripheral region to increase the arsenicals' migration distance. Secondly, the interactions between the surface and arsenicals should be strong enough to retain the

arsenicals. To fulfill these two requirements, surfactants were introduced into the droplet to reduce surface tension and permit the liquid to migrate into peripheral region by capillary action. Coating the surface with nanoparticles enhanced the interaction between arsenicals and the surface. The electrostatic interaction played a significant role here since these arsenicals have different deprotonation abilities. This work provides a novel approach for the arsenic speciation by SERS, especially for a small volume of biological samples.

The third part of this work provided valuable information for Raman spectra of potential arsenic metabolites. This work contributes Raman spectra for six potential arsenic metabolites, including MMA^{III}, DMA^{III}, $DMMTA^{V}$, $DMDTA^{V}$, $DMA^{III}GS$ and $DMA^{III}Cys$ though the assignment of unknown arsenicals' Raman spectra. Using DMA^{V} as a representative molecule, detailed Raman spectra analysis and Raman spectra comparisons between experimental and theoretical results were performed. The theoretical calculations were found to provide useful Raman spectra predictions for the experimental spectra, and computational simulations also provided detailed molecular movements for the identification of vibrational modes. Since most of relevant arsenicals were not commercially available, these compounds were mostly synthesized in the laboratory. A new method was validated to synthesize $DMA^{III}Cys$ using excessive of DMA^{V} against L-cysteine. This approach avoided serious signal interference of the by-product cystine, which is usualy produced in the typical synthetic recipe using a molar excess of L-cysteine against DMA^{V}.

5.3 Future research directions

The experiments involving arsenic speciation with silver colloidal suspensions developed in this work was a preliminary study. Only four commonly existing redox-inert arsenicals were selected to demonstrate the possibility of arsenic speciation using SERS. The study should be expanded to investigate other potential arsenic metabolites found in arsenic metabolism, such as MMA^{III}, DMA^{III}, $DMMTA^{V}$, $DMDTA^{V}$, $DMA^{III}GS$ and $DMA^{III}Cys$.. However, the stability of these unstable arsenicals in term of SERS enhancement in different colloidal suspensions should be studied prior to this work.

There are additional potential arsenic metabolites found in arsenic metabolism, such as, monomethyl monothioarsonate ($MMMTA^{V}$), monomethyldithioarsonic acid ($MMDTA^{V}$), monomethylarsenic diglutathione ($MMA^{III}(GS)_2$), dimethylarsinothioyl glutathione ($DMMTA^{V}(GS)$) etc. It would be useful to study their Raman spectra by employing density functional theory computation.

Arsenic speciation inside cells can potentially be carried out by using the introduction of nanoparticles into cells. Gold nanoshells may be fabricated and optimized to permit determination of molecules *in vivo*. Protection of the surface of these gold nanoshells may be necessary to prevent biomolecules from attaching to their surface when in the cytoplasm.

Arsenic speciation using the coffee ring effect, especially the halo coffee ring effect, could be expanded towards use in other elements' speciation. In addition complementary studies on the mechanism of this halo coffee ring effect should be carried out to obtain comprehensive understanding of the phenomenon. For example, the question about surface tension changes of the sessile droplet during the formation of halo

coffee ring stain need to be studied. It would be interesting to discover the correlation between the droplet surface tension and the size of the halo region to improve separation. Meanwhile, the interactions between analytes and the surface can be improved by using nanoparticles with different surface coatings or though the applying of AgNF surface modification.

Reference

[1] K.A. Francesconi and D. Kuehnelt, Arsenic compounds in the environment, Environmental chemistry of arsenic, in: W.T.W.T. Frankenberger, Marcel Dekker. New York, pp. 51-94.

[2] I. Gaballah, N. Menad, D. Hartmann, G. Lyaudet, and P. Michel, Decontamination as important step towards recycling, Resources, Conservation and Recycling. 10 (1994) 107-116.

[3] J. Nriagu, P. Bhattacharya, A. Mukherjee, J. Bundschuh, R. Zevenhoven, and R. Loeppert, Arsenic in soil and groundwater: an overview, Trace Metals and other Contaminants in the Environment, in, pp. 3-60.

[4] P. Smedley and D. Kinniburgh, A review of the source, behaviour and distribution of arsenic in natural waters, Applied geochemistry. 17 (2002) 517-568.

[5] R. Nickson, J. McArthur, W. Burgess, K.M. Ahmed, P. Ravenscroft, and M. Rahman, Arsenic poisoning of Bangladesh groundwater, Nature. 395 (1998) 338.

[6] A. Krysiak and A. Karczewska, Arsenic extractability in soils in the areas of former arsenic mining and smelting, SW Poland, Sci. Total Environ. 379 (2007) 190-200.

[7] A. Davis, M.V. Ruby, and P.D. Bergstrom, Bioavailability of Arsenic and Lead in Soils from the Butte, Montana, Mining District, Environ. Sci. Technol. 26 (1992) 461-468.

[8] J. Lever, Paget's disease of bone in Lancashire and arsenic pesticide in cotton mill wastewater: a speculative hypothesis, Bone. 31 (2002) 434-436.

[9] R. Wauchope, Fixation of arsenical herbicides, phosphate, and arsenate in alluvial soils, J. Environ. Qual. 4 (1975) 355-358.

[10] M. Flues, I.M. Sato, M.A. Scapin, M.E.B. Cotrim, and I.M.C. Camargo, Toxic elements mobility in coal and ashes of Figueira coal power plant, Brazil, Fuel. 103 (2013) 430-436.

[11] B.P. Jackson and P.M. Bertsch, Determination of arsenic speciation in poultry wastes by IC-ICP-MS, Environ. Sci. Technol. 35 (2001) 4868-4873.

[12] H. Garelick, H. Jones, A. Dybowska, and E. Valsami-Jones, Arsenic pollution sources, Reviews of Environmental Contamination and Toxicology, in, Springer. New York, pp. 17-60.

[13] J. Liu, B. Zheng, H.V. Aposhian, Y. Zhou, M.-L. Chen, A. Zhang, and M.P. Waalkes, Chronic arsenic poisoning from burning high-arsenic-containing coal in Guizhou, China, Environ. Health Persp. 110 (2002) 119-122.

[14] G. Sun, Arsenic contamination and arsenicosis in China, Toxicol. Appl. Pharmacol. 198 (2004) 268-271.

[15] B.K. Mandal and K.T. Suzuki, Arsenic round the world: a review, Talanta. 58 (2002) 201-235.

[16] J.O. Nrtagu, Arsenic poisoning through the ages, Environmental chemistry of arsenic, in: J. William T. Frankenberger, Marcel Dekker. New York, pp. 1-26.

[17] S. Strom, F.D.A. Bans Three Arsenic Drugs Used in Poultry and Pig Feeds, The New York Times. (2013). http://www.nytimes.com/2013/10/02/business/fda-bans-three-arsenic-drugs-used-in-poultry-and-pig-feeds.html

[18] K. Lew, J.P. Acker, S. Gabos, and X.C. Le, Biomonitoring of Arsenic in Urine and Saliva of Children Playing on Playgrounds Constructed from Chromated Copper Arsenate-Treated Wood, Environ. Sci. Technol. 44 (2010) 3986-3991.

[19] J.A. Hingston, C.D. Collins, R.J. Murphy, and J.N. Lester, Leaching of chromated copper arsenate wood preservatives: a review, Environ. Pollut. 111 (2001) 53-66.

[20] A.H. Smith, E.O. Lingas, and M. Rahman, Contamination of drinking-water by arsenic in Bangladesh: a public health emergency, Bull. W.H.O. 78 (2000) 1093-1103.

[21] T.-H.L.Y.-L. Huang and M.-Y. Wang, Arsenic species in drinking water, hair, fingernails, and urine of patients with blackfoot disease, J. Toxicol. Env. Heal. A. 53 (1998) 85-93.

[22] K. Farzana Akter, Z. Chen, L. Smith, D. Davey, and R. Naidu, Speciation of arsenic in ground water samples: A comparative study of CE-UV, HG-AAS and LC-ICP-MS, Talanta. 68 (2005) 406-415.

[23] C.-p. Liu, C.-l. Luo, Y. Gao, F.-b. Li, L.-w. Lin, C.-a. Wu, and X.-d. Li, Arsenic contamination and potential health risk implications at an abandoned tungsten mine, southern China, Environ. Pollut. 158 (2010) 820-826.

[24] G. Li, G.-X. Sun, P.N. Williams, L. Nunes, and Y.-G. Zhu, Inorganic arsenic in Chinese food and its cancer risk, Environ. Int. 37 (2011) 1219-1225.

[25] S. Kar, J.P. Maity, J.-S. Jean, C.-C. Liu, C.-W. Liu, J. Bundschuh, and H.-Y. Lu, Health risks for human intake of aquacultural fish: Arsenic bioaccumulation and contamination, Journal of Environmental Science and Health Part A. 46 (2011) 1266-1273.

[26] A.Q. Shah, T.G. Kazi, J.A. Baig, M.B. Arain, H.I. Afridi, G.A. Kandhro, S.K. Wadhwa, and N.F. Kolachi, Determination of inorganic arsenic species (As3+ and As5+) in muscle tissues of fish species by electrothermal atomic absorption spectrometry (ETAAS), Food Chem. 119 (2010) 840-844.

[27] G. Okkenhaug, Y.-G. Zhu, J. He, X. Li, L. Luo, and J. Mulder, Antimony (Sb) and arsenic (As) in Sb mining impacted paddy soil from Xikuangshan, China: differences in mechanisms controlling soil sequestration and uptake in rice, Environ. Sci. Technol. 46 (2012) 3155-3162.

[28] M.A. Rahman and H. Hasegawa, High levels of inorganic arsenic in rice in areas where arsenic-contaminated water is used for irrigation and cooking, Sci. Total Environ. 409 (2011) 4645-4655.

[29] Z. Cheng, K.-C. Chen, K.-B. Li, X.-P. Nie, S.C. Wu, C.K.-C. Wong, and M.-H. Wong, Arsenic contamination in the freshwater fish ponds of Pearl River Delta: bioaccumulation and health risk assessment, Environ. Sci. Pollut. R. (2012) 1-12.

[30] Tsuruta, Hamada, Mochida, Nakagawa, Kobayashi, and Ishii, Merkel cell carcinoma, Bowen's disease and chronic occupational arsenic poisoning, Br. J. Dermatol. 139 (1998) 291-294.

[31] A.M. Lee and J.F. Fraumeni, Arsenic and respiratory cancer in man: an occupational study, J. Natl. Cancer Inst. 42 (1969) 1045-1052.

[32] J.G. Farmer and L.R. Johnson, Assessment of Occupational Exposure to Inorganic Arsenic Based on Urinary Concentrations and Speciation of Arsenic, Br. J. Ind. Med. 47 (1990) 342-348.

[33] Y. Yoshimura, Y. Endo, Y. Shimoda, K. Yamanaka, and G. Endo, Acute Arsine Poisoning Confirmed by Speciation Analysis of Arsenic Compounds in the Plasma and Urine by HPLC-ICP-MS, J. Occup. Health. 53 (2011) 45-49.

[34] L. Järup, G. Pershagen, and S. Wall, Cumulative arsenic exposure and lung cancer in smelter workers: a dose-response study, Am. J. Ind. Med. 15 (1989) 31-41.

[35] V.C. Pandey, J.S. Singh, R.P. Singh, N. Singh, and M. Yunus, Arsenic hazards in coal fly ash and its fate in Indian scenario, Resources, Conservation and Recycling. 55 (2011) 819-835.

[36] D. Jolliffe, A history of the use of arsenicals in man, J. R. Soc. Med. 86 (1993) 287-289.

[37] T.D. Zhang, [Treatment of acute granulocytic leukemia with "Ai ling No. 1"--clinical analysis and experimental research], Zhong xi yi jie he za zhi = Chinese journal of modern developments in traditional medicine. 4 (1984) 19-20.

[38] S.A. Lerman, T.W. Clarkson, and R.J. Gerson, Arsenic uptake and metabolism by liver cells is dependent on arsenic oxidation state, Chem-Biol Interact. 45 (1983) 401-406.

[39] M. Vahter, Species differences in the metabolism of arsenic compounds, Appl. Organomet. Chem. 8 (1994) 175-182.

[40] R.-N. Huang and T.-C. Lee, Cellular uptake of trivalent arsenite and pentavalent arsenate in KB cells cultured in phosphate-free medium, Toxicol. Appl. Pharmacol. 136 (1996) 243-249.

[41] C.-H. Tseng, C.-K. Chong, C.-J. Chen, and T.-Y. Tai, Dose-response relationship between peripheral vascular disease and ingested inorganic arsenic among residents in blackfoot disease endemic villages in Taiwan, Atherosclerosis. 120 (1996) 125-133.

[42] R.N. Ratnaike, Acute and chronic arsenic toxicity, Postgrad. Med. J. 79 (2003) 391-396.

[43] M.R. Karagas, T.D. Tosteson, J. Blum, B. Klaue, J.E. Weiss, V. Stannard, V. Spate, and J.S. Morris, Measurement of low levels of arsenic exposure: a comparison of water and toenail concentrations, Am. J. Epidemiol. 152 (2000) 84-90.

[44] B.K. Mandal, Y. Ogra, and K.T. Suzuki, Speciation of arsenic in human nail and hair from arsenic-affected area by HPLC-inductively coupled argon plasma mass spectrometry, Toxicol. Appl. Pharmacol. 189 (2003) 73-83.

[45] A.G. Gault, H.A. Rowland, J.M. Charnock, R.A. Wogelius, I. Gomez-Morilla, S. Vong, M. Leng, S. Samreth, M.L. Sampson, and D.A. Polya, Arsenic in hair and nails of individuals exposed to arsenic-rich groundwaters in Kandal province, Cambodia, Sci. Total Environ. 393 (2008) 168-176.

[46] M.M. Rahman, J.C. Ng, and R. Naidu, Chronic exposure of arsenic via drinking water and its adverse health impacts on humans, Environ. Geochem. Health. 31 Suppl 1 (2009) 189-200.

[47] J.C. States, S. Srivastava, Y. Chen, and A. Barchowsky, Arsenic and Cardiovascular Disease, Toxicol. Sci. 107 (2009) 312-323.

[48] Y. Chen, J.H. Graziano, F. Parvez, M. Liu, V. Slavkovich, T. Kalra, M. Argos, T. Islam, A. Ahmed, M. Rakibuz-Zaman, R. Hasan, G. Sarwar, D. Levy, A. van Geen, and H. Ahsan, Arsenic exposure from drinking water and mortality from cardiovascular disease in Bangladesh: prospective cohort study, BMJ. 342 (2011).

[49] M. Rahman, M. Tondel, S.A. Ahmad, and O. Axelson, Diabetes Mellitus Associated with Arsenic Exposure in Bangladesh, Am. J. Epidemiol. 148 (1998) 198-203.

[50] A. Navas-Acien, E.K. Silbergeld, R. Pastor-Barriuso, and E. Guallar, ARsenic exposure and prevalence of type 2 diabetes in us adults, JAMA. 300 (2008) 814-822.

[51] J.K. Levin-Scherz, J.D. Patrick, F.H. Weber, and C. Garabedian, Acute arsenic ingestion, Ann. Emerg. Med. 16 (1987) 702-704.

[52] A. Dueñas-Laita, M. Pérez-Miranda, M.A. González-López, J.C. Martín-Escudero, M. Ruiz-Mambrilla, and J. Blanco-Varela, Acute arsenic poisoning, The Lancet. 365 (2005) 1982.

[53] D. Trachootham, W. Lu, M.A. Ogasawara, R.D. Nilsa, and P. Huang, Redox regulation of cell survival, Antioxid. Redox Signal. 10 (2008) 1343-1374.

[54] H.P. Indo, M. Davidson, H.-C. Yen, S. Suenaga, K. Tomita, T. Nishii, M. Higuchi, Y. Koga, T. Ozawa, and H.J. Majima, Evidence of ROS generation by mitochondria in cells with impaired electron transport chain and mitochondrial DNA damage, Mitochondrion. 7 (2007) 106-118.

[55] T. Finkel and N.J. Holbrook, Oxidants, oxidative stress and the biology of ageing, Nature. 408 (2000) 239-247.

[56] Y. Kobayashi, X. Cui, and S. Hirano, Stability of arsenic metabolites, arsenic triglutathione [As(GS)(3)] and methylarsenic diglutathione [CH3As(GS)(2)], in rat bile, Toxicology. 211 (2005) 115-123.

[57] C. Jung and A. Rothstein, Arsenate uptake and release in relation to the inhibition of transport and glycolysis in yeast, Biochem. Pharmacol. 14 (1965) 1093-1112.

[58] J. Pi, H. Yamauchi, Y. Kumagai, G. Sun, T. Yoshida, H. Aikawa, C. Hopenhayn-Rich, and N. Shimojo, Evidence for induction of oxidative stress caused by chronic exposure of Chinese residents to arsenic contained in drinking water, Environ. Health Persp. 110 (2002) 331-336.

[59] S. Das, A. Santra, S. Lahiri, and D.G. Mazumder, Implications of oxidative stress and hepatic cytokine (TNF-α and IL-6) response in the pathogenesis of hepatic collagenesis in chronic arsenic toxicity, Toxicol. Appl. Pharmacol. 204 (2005) 18-26.

[60] G.M. Cooper, The central role of enzymes as biological catalysts, (2000).

[61] T. Samikkannu, C.-H. Chen, L.-H. Yih, A.S. Wang, S.-Y. Lin, T.-C. Chen, and K.-Y. Jan, Reactive oxygen species are involved in arsenic trioxide inhibition of pyruvate dehydrogenase activity, Chem. Res. Toxicol. 16 (2003) 409-414.

[62] I. Lehnman, DNA ligase: structure, mechanism, and function, Science. 186 (1974) 790-797.

[63] C. Bernstein, A.R. Prasad, V. Nfonsam, and H. Bernstein, DNA damage, DNA repair and cancer, New Research Directions in DNA Repair. InTech. doi:10.5772/53919

[64] M. Kessel, S.X. Liu, A. Xu, R. Santella, and T.K. Hei, Arsenic induces oxidative DNA damage in mammalian cells, Mol. Cell. Biochem. 234 (2002) 301-308.

[65] T. Schwerdtle, I. Walter, I. Mackiw, and A. Hartwig, Induction of oxidative DNA damage by arsenite and its trivalent and pentavalent methylated metabolites in cultured human cells and isolated DNA, Carcinogenesis. 24 (2003) 967-974.

[66] K.T. Kitchin and S. Ahmad, Oxidative stress as a possible mode of action for arsenic carcinogenesis, Toxicol. Lett. 137 (2003) 3-13.

[67] A. Hartwig, Carcinogenicity of metal compounds: possible role of DNA repair inhibition, Toxicol. Lett. 102 (1998) 235-239.

[68] A.D. Kligerman, C.L. Doerr, A.H. Tennant, K. Harrington-Brock, J.W. Allen, E. Winkfield, P. Poorman-Allen, B. Kundu, K. Funasaka, and B.C. Roop, Methylated trivalent arsenicals as candidate ultimate genotoxic forms of arsenic: induction of chromosomal mutations but not gene mutations, Environ. Mol. Mutagen. 42 (2003) 192-205.

[69] S. Nesnow, B.C. Roop, G. Lambert, M. Kadiiska, R.P. Mason, W.R. Cullen, and M.J. Mass, DNA damage induced by methylated trivalent arsenicals is mediated by reactive oxygen species, Chem. Res. Toxicol. 15 (2002) 1627-1634.

[70] M.J. Mass, A. Tennant, B.C. Roop, W.R. Cullen, M. Styblo, D.J. Thomas, and A.D. Kligerman, Methylated trivalent arsenic species are genotoxic, Chem. Res. Toxicol. 14 (2001) 355-361.

[71] Y. Yoshimura, Y. Endo, Y. Shimoda, K. Yamanaka, and G. Endo, Acute Arsine Poisoning Confirmed by Speciation Analysis of Arsenic Compounds in the Plasma and Urine by HPLC-ICP-MS, J. Occup. Health. 53 (2010) 45-49.

[72] Y.-J. Hsieh and S.-J. Jiang, Application of HPLC-ICP-MS and HPLC-ESI-MS Procedures for Arsenic Speciation in Seaweeds, J. Agric. Food Chem. 60 (2012) 2083-2089.

[73] P. Alava, F. Tack, G.D. Laing, and T.V. de Wiele, HPLC-ICP-MS method development to monitor arsenic speciation changes by human gut microbiota, Biomed. Chromatogr. 26 (2012) 524-533.

[74] J.L. Gómez-Ariza, D. Sánchez-Rodas, I. Giráldez, and E. Morales, A comparison between ICP-MS and AFS detection for arsenic speciation in environmental samples, Talanta. 51 (2000) 257-68.

[75] C. Niegel, S.A. Pfeiffer, M. Grundmann, U. Arroyo-Abad, J. Mattusch, and F.-M. Matysik, Fast separations by capillary electrophoresis hyphenated to electrospray ionization time-of-flight mass spectrometry as a tool for arsenic speciation analysis, Analyst. 137 (2012) 1956-1962.

[76] L. Liu, B. He, Z. Yun, J. Sun, and G. Jiang, Speciation analysis of arsenic compounds by capillary electrophoresis on-line coupled with inductively coupled plasma mass spectrometry using a novel interface, J. Chromatogr. A. 1304 (2013) 227-233.

[77] G. Yang, J. Xu, J. Zheng, X. Xu, W. Wang, L. Xu, G. Chen, and F. Fu, Speciation analysis of arsenic in Mya arenaria Linnaeus and Shrimp with capillary electrophoresis-inductively coupled plasma mass spectrometry, Talanta. 78 (2009) 471-6.

[78] A.A. Ammann, Arsenic speciation by gradient anion exchange narrow bore ion chromatography and high resolution inductively coupled plasma mass spectrometry detection, J. Chromatogr. A. 1217 (2010) 2111-2116.

[79] V. Dufailly, M. Nicolas, J.R. Payot, and E. Poitevin, Validation of a method for arsenic speciation in food by ion chromatography-inductively coupled plasma/mass spectrometry after ultrasonic-assisted enzymatic extraction, J. AOAC Int. 94 (2011) 947-958.

[80] J. Morton and E. Leese, Arsenic speciation in clinical samples: urine analysis using fast micro-liquid chromatography ICP-MS, Anal. Bioanal. Chem. 399 (2011) 1781-1788.

[81] U. Arroyo-Abad, S. Lischka, C. Piechotta, J. Mattusch, and T. Reemtsma, Determination and identification of hydrophilic and hydrophobic arsenic species in methanol extract of fresh cod liver by RP-HPLC with simultaneous ICP-MS and ESI-Q-TOF-MS detection, Food Chem. 141 (2013) 3093-3102.

[82] S.D. Conklin, M.W. Fricke, P.A. Creed, and J.T. Creed, Investigation of the pH effects on the formation of methylated thio-arsenicals, and the effects of pH and temperature on their stability, J. Anal. Atom. Spectrom. 23 (2008) 711-716.

[83] H.R. Hansen, A. Raab, M. Jaspars, B.F. Milne, and J. Feldmann, Sulfur-Containing Arsenical Mistaken for Dimethylarsinous Acid [DMA(III)] and Identified as a Natural Metabolite in Urine: Major Implications for Studies on Arsenic Metabolism and Toxicity, Chem. Res. Toxicol. 17 (2004) 1086-1091.

[84] T. Hayakawa, Y. Kobayashi, X. Cui, and S. Hirano, A new metabolic pathway of arsenite: arsenic–glutathione complexes are substrates for human arsenic methyltransferase Cyt19, Arch. Toxicol. 79 (2005) 183-191.

[85] K. Rehman and H. Naranmandura, Arsenic metabolism and thioarsenicals, Metallomics : integrated biometal science. 4 (2012) 881-892.

[86] M.G. Mason, A.S. Ball, B.J. Reeder, G. Silkstone, P. Nicholls, and M.T. Wilson, Extracellular heme peroxidases in actinomycetes: a case of mistaken identity, Appl. Environ. Microbiol. 67 (2001) 4512-4519.

[87] R. Kar and C.B. Sharma, Bilirubin peak can be mistaken as Hb Bart's or Hb H on High-performance liquid chromatography, Hemoglobin. 35 (2011) 171-174.

[88] P.G. Smith, I. Koch, R.A. Gordon, D.F. Mandoli, B.D. Chapman, and K.J. Reimer, X-ray Absorption Near-Edge Structure Analysis of Arsenic Species for Application to Biological Environmental Samples, Environ. Sci. Technol. 39 (2004) 248-254.

[89] C.S. Kim, G.E. Brown Jr, and J.J. Rytuba, Characterization and speciation of mercury-bearing mine wastes using X-ray absorption spectroscopy, Sci. Total Environ. 261 (2000) 157-168.

[90] I.J. Pickering, G.E. Brown, and T.K. Tokunaga, Quantitative Speciation of Selenium in Soils Using X-Ray-Absorption Spectroscopy, Environ. Sci. Technol. 29 (1995) 2456-2459.

[91] D. Paktunc, A. Foster, and G. Laflamme, Speciation and characterization of arsenic in Ketza River mine tailings using x-ray absorption spectroscopy, Environ. Sci. Technol. 37 (2003) 2067-2074.

[92] P.G. Smith, I. Koch, R.A. Gordon, D.F. Mandoli, B.D. Chapman, and K.J. Reimer, X-ray absorption near-edge structure analysis of arsenic species for application to biological environmental samples, Environ. Sci. Technol. 39 (2005) 248-254.

[93] R. Andrahennadi, M. Wayland, and I.J. Pickering, Speciation of selenium in stream insects using x-ray absorption Spectroscopy, Environ. Sci. Technol. 41 (2007) 7683-7687.

[94] A.L. Foster, G.E. Brown, T.N. Tingle, and G.A. Parks, Quantitative arsenic speciation in mine tailings using X-ray absorption spectroscopy, Am. Mineral. 83 (1998) 553-568.

[95] A.A. Meharg, E. Lombi, P.N. Williams, K.G. Scheckel, J. Feldmann, A. Raab, Y.G. Zhu, and R. Islam, Speciation and localization of arsenic in white and brown rice grains, Environ. Sci. Technol. 42 (2008) 1051-1057.

[96] E. Lombi, K.G. Scheckel, J. Pallon, A.M. Carey, Y.G. Zhu, and A.A. Meharg, Speciation and distribution of arsenic and localization of nutrients in rice grains, New Phytol. 184 (2009) 193-201.

[97] T. Bacquart, G. Devès, and R. Ortega, Direct speciation analysis of arsenic in sub-cellular compartments using micro-X-ray absorption spectroscopy, Environ. Res. 110 (2010) 413-416.

[98] T. Bacquart, G. Devès, A. Carmona, R. Tucoulou, S. Bohic, and R. Ortega, Subcellular Speciation Analysis of Trace Element Oxidation States Using Synchrotron Radiation Micro-X-ray Absorption Near-Edge Structure, Anal. Chem. 79 (2007) 7353-7359.

[99] J.P. Scaffidi, M.K. Gregas, V. Seewaldt, and T. Vo-Dinh, SERS-based plasmonic nanobiosensing in single living cells, Anal. Bioanal. Chem. 393 (2009) 1135-1141.

[100] D.I. Ellis and R. Goodacre, Metabolic fingerprinting in disease diagnosis: biomedical applications of infrared and Raman spectroscopy, Analyst. 131 (2006) 875-885.

[101] F. Inscore, C. Shende, A. Sengupta, H. Huang, and S. Farquharson, Detection of drugs of abuse in saliva by surface-enhanced Raman spectroscopy (SERS), Appl. Spectrosc. 65 (2011) 1004-1008.

[102] M. Casella, A. Lucotti, M. Tommasini, M. Bedoni, E. Forvi, F. Gramatica, and G. Zerbi, Raman and SERS recognition of β-carotene and haemoglobin fingerprints in human whole blood, Spectrochim. Acta A. 79 (2011) 915-919.

[103] D. Drescher, T. Büchner, D. McNaughton, and J. Kneipp, SERS reveals the specific interaction of silver and gold nanoparticles with hemoglobin and red blood cell components, Phys. Chem. Chem. Phys. 15 (2013) 5364-5373.

[104] C. Leordean, V. Canpean, and S. Astilean, Surface-enhanced Raman scattering (SERS) analysis of urea trace in urine, fingerprint, and tear samples, Spectrosc. Lett. 45 (2012) 550-555.

[105] R. Stosch, A. Henrion, D. Schiel, and B. Güttler, Surface-enhanced Raman scattering based approach for quantitative determination of creatinine in human serum, Anal. Chem. 77 (2005) 7386-7392.

[106] B. ZHENG, J.-c. DONG, L.-z. SU, M. Meng, Y.-j. ZHANG, and J.-f. LI, Surface-Enhanced Raman Spectroscopy Study of Fresh Human Urine: A Preliminary Study, Spectrosc. Spect. Anal. 36 (2016) 1987-1991.

[107] Y. Wang, J. Chen, Y. Wu, Y. Chen, J. Pan, J. Lei, Y. Chen, L. Sun, S. Feng, and R. Chen. Surface-enhanced Raman spectroscopy of creatinine in silver colloid. SPIE (2012), doi:10.1117/12.918990.

[108] T.L. Wang, K.C. Hui-hua, and H.-h. Lu. SERS quantitative urine creatinine measurement of human subject. SPIE (2005), doi: 10.1117/12.591393.

[109] S. Feng, D. Lin, J. Lin, B. Li, Z. Huang, G. Chen, W. Zhang, L. Wang, J. Pan, and R. Chen, Blood plasma surface-enhanced Raman spectroscopy for non-invasive optical detection of cervical cancer, Analyst. 138 (2013) 3967-3974.

[110] G. Del Mistro, S. Cervo, E. Mansutti, R. Spizzo, A. Colombatti, P. Belmonte, R. Zucconelli, A. Steffan, V. Sergo, and A. Bonifacio, Surface-enhanced Raman spectroscopy of urine for prostate cancer detection: a preliminary study, Anal. Bioanal. Chem. 407 (2015) 3271-3275.

[111] S. Feng, J. Lin, Z. Huang, G. Chen, W. Chen, Y. Wang, R. Chen, and H. Zeng, Esophageal cancer detection based on tissue surface-enhanced Raman spectroscopy and multivariate analysis, Appl. Phys. Lett. 102 (2013), doi:10.1063/1.4789996.

[112] C.J. Saatkamp, M.L. de Almeida, J.A.M. Bispo, A.L.B. Pinheiro, A.B. Fernandes, and L. Silveira, Quantifying creatinine and urea in human urine through Raman spectroscopy aiming at diagnosis of kidney disease, J. Biomed. Opt. 21 (2016) 037001-037001. doi:10.1117/1.JBO.21.3.037001.

[113] J. Wang, Y.Y. Zeng, J.Q. Lin, L. Lin, X.C. Wang, G.N. Chen, Z.F. Huang, B.H. Li, H.S. Zeng, and R. Chen, SERS spectroscopy and multivariate analysis of globulin in human blood, Laser Phys. 24 (2014), doi: 10.1088/1054-660X/24/6/065602.

[114] Z. Huang, X. Chen, Y. Chen, J. Chen, M. Dou, S. Feng, H. Zeng, and R. Chen, Raman spectroscopic characterization and differentiation of seminal plasma, J. Biomed. Opt. 16 (2011), doi:10.1117/1.3650310.

[115] Z. Ye, H. Meizhen, W. Kehui, S. Biao, W. Yang, C. Jie, L. Xi, L. Xia, L. Lulu, and H. Gaozhong, Urine surface-enhanced Raman spectroscopy for non-invasive diabetic detection based on a portable Raman spectrometer, Laser Phys. Lett. 13 (2016), doi: 10.1088/1612-2011/13/6/065604.

[116] M. Li, Y. Du, F. Zhao, J. Zeng, C. Mohan, and W.-C. Shih, Reagent-and separation-free measurements of urine creatinine concentration using stamping surface enhanced Raman scattering (S-SERS), Biomed. Opt. Express. 6 (2015) 849-858.

[117] S. Shanmukh, L. Jones, J. Driskell, Y. Zhao, R. Dluhy, and R.A. Tripp, Rapid and sensitive detection of respiratory virus molecular signatures using a silver nanorod array SERS substrate, Nano Lett. 6 (2006) 2630-2636.

[118] H. Wang, N. Malvadkar, S. Koytek, J. Bylander, W.B. Reeves, and M.C. Demirel, Quantitative analysis of creatinine in urine by metalized nanostructured parylene, J. Biomed. Opt. 15 (2010), doi:10.1117/1.3369002.

[119] L. Guerrini, E. Pazos, C. Penas, M.E. Vazquez, J.L. Mascarenas, and R.A. Alvarez-Puebla, Highly sensitive SERS quantification of the oncogenic protein c-Jun in cellular extracts, J. Am. Chem. Soc. 135 (2013) 10314-10317.

[120] M.Y. Sha, H. Xu, M.J. Natan, and R. Cromer, Surface-enhanced Raman scattering tags for rapid and homogeneous detection of circulating tumor cells in the presence of human whole blood, J. Am. Chem. Soc. 130 (2008) 17214-17215.

[121] H. Chon, S. Lee, S.W. Son, C.H. Oh, and J. Choo, Highly sensitive immunoassay of lung cancer marker carcinoembryonic antigen using surface-enhanced Raman scattering of hollow gold nanospheres, Anal. Chem. 81 (2009) 3029-3034.

[122] B.-H. Jun, M.S. Noh, G. Kim, H. Kang, J.-H. Kim, W.-J. Chung, M.-S. Kim, Y.-K. Kim, M.-H. Cho, and D.H. Jeong, Protein separation and identification using magnetic beads encoded with surface-enhanced Raman spectroscopy, Anal. Biochem. 391 (2009) 24-30.

[123] H. Chon, S. Lee, S.-Y. Yoon, S.-I. Chang, D.W. Lim, and J. Choo, Simultaneous immunoassay for the detection of two lung cancer markers using functionalized SERS nanoprobes, Chem. Commun. 47 (2011) 12515-12517.

[124] V.K. Gupta, N. Atar, M.L. Yola, M. Eryılmaz, H. Torul, U. Tamer, İ.H. Boyacı, and Z. Üstündağ, A novel glucose biosensor platform based on Ag@ AuNPs modified graphene oxide nanocomposite and SERS application, J. Colloid. Interf. Sci. 406 (2013) 231-237.

[125] K.V. Kong, Z. Lam, W.K.O. Lau, W.K. Leong, and M. Olivo, A transition metal carbonyl probe for use in a highly specific and sensitive sers-based assay for glucose, J. Am. Chem. Soc. 135 (2013) 18028-18031.

[126] S.J. Greaves and W.P. Griffith, Surface-enhanced Raman scattering (SERS) from silver colloids of vanadate, phosphate and arsenate, J. Raman Spectrosc. 19 (1988) 503-507.

[127] J. Li, L. Chen, T. Lou, and Y. Wang, Highly sensitive SERS detection of As3+ ions in aqueous media using glutathione functionalized silver nanoparticles, ACS Appl. Mater. Inter. 3 (2011) 3936-3941.

[128] J. Du, J. Cui, and C. Jing, Rapid in situ identification of arsenic species using a portable Fe_3O_4@ Ag SERS sensor, Chem. Commun. 50 (2014) 347-349.

[129] L. Ye, G. Wen, J. Dong, Y. Luo, Q. Liu, A. Liang, and Z. Jiang, A simple label-free rhodamine 6G SERS probe for quantitative analysis of trace As 3+ in an aptamer–nanosol, RSC Adv. 4 (2014) 32960-32964.

[130] L. Song, K. Mao, X. Zhou, and J. Hu, A novel biosensor based on Au@ Ag core–shell nanoparticles for SERS detection of arsenic (III), Talanta. 146 (2016) 285-290.

[131] W. Wang, Y. Yin, Z. Tan, and J. Liu, Coffee-ring effect-based simultaneous SERS substrate fabrication and analyte enrichment for trace analysis, Nanoscale. 6 (2014) 9588-9593.

[132] M. Mulvihill, A. Tao, K. Benjauthrit, J. Arnold, and P. Yang, Surface-Enhanced Raman Spectroscopy for Trace Arsenic Detection in Contaminated Water, Angew. Chem. Int. Ed. 47 (2008) 6456-6460.

[133] Z.H. Xu, J.M. Hao, F.S. Li, and X.G. Meng, Surface-enhanced Raman spectroscopy of arsenate and arsenite using Ag nanofilm prepared by modified mirror reaction, J. Colloid. Interf. Sci. 347 (2010) 90-95.

[134] D. Gloria, G. Moran, and D.B. Hibbert. Detection of Arsenobetaine: A Step Towards SERS-based Arsenic Speciation. AIP conference proceedings. 510 (2010), doi: 10.1063/1.3482645

[135] J. Olavarría-Fullerton, S. Wells, W. Ortiz-Rivera, M.J. Sepaniak, and M.A. De Jesus, Surface-Enhanced Raman Scattering (SERS) Characterization of Trace Organoarsenic Antimicrobials Using Silver/Polydimethylsiloxane Nanocomposites, Appl. Spectrosc. 65 (2011) 423-428.

[136] J.M. Hao, M.J. Han, Z.H. Xu, J.W. Li, and X.G. Meng, Fabrication and evolution of multilayer silver nanofilms for surface-enhanced Raman scattering sensing of arsenate, Nanoscale Res. Lett. 6 (2011) 263.

[137] Z. Xu, X. Meng, Y. Zhang, and F. Li, Effects and mechanisms of water matrix on surface-enhanced Raman scattering analysis of arsenite on silver nanofilm, Colloid. Surface. A. 497 (2016) 117-125.

[138] Z. Xu, C. Jing, J. Hao, C. Christodoulatos, G.P. Korfiatis, F. Li, and X. Meng, Effect of bonding interactions between arsenate and silver nanofilm on surface-enhanced Raman scattering sensitivity, J. Phys. Chem. C. 116 (2011) 325-329.

[139] A.M. Fales, H. Yuan, and T. Vo-Dinh, Development of Hybrid Silver-Coated Gold Nanostars for Nonaggregated Surface-Enhanced Raman Scattering, J Phys Chem C 118 (2014) 3708-3715.

[140] H. Yuan, C.G. Khoury, C.M. Wilson, G.A. Grant, A.J. Bennett, and T. Vo-Dinh, In vivo particle tracking and photothermal ablation using plasmon-resonant gold nanostars, Nanomed. Nanotechnol. Biol. Med. 8 (2012) 1355-1363.

[141] H. Park, S. Lee, L. Chen, E.K. Lee, S.Y. Shin, Y.H. Lee, S.W. Son, C.H. Oh, J.M. Song, S.H. Kang, and J. Choo, SERS imaging of HER2-overexpressed MCF7 cells using antibody-conjugated gold nanorods, Phys. Chem. Chem. Phys. 11 (2009) 7444-7449.

[142] Z. Xu, J. Hao, F. Li, and X. Meng, Surface-enhanced Raman spectroscopy of arsenate and arsenite using Ag nanofilm prepared by modified mirror reaction, J. Colloid. Interf. Sci. 347 (2010) 90-95.

[143] R. Haresh, D. Philip, and G. Aruldhas, Infrared, Raman, and SERS spectra of betaine arsenate, Spectrosc. Lett. 28 (1995) 11-28.

[144] Z. Ji, X. Jin, S. George, T. Xia, H. Meng, X. Wang, E. Suarez, H. Zhang, E.M. Hoek, H. Godwin, A.E. Nel, and J.I. Zink, Dispersion and stability optimization of TiO2 nanoparticles in cell culture media, Environ. Sci. Technol. 44 (2010) 7309-7314.

[145] C. Schulze, C. Schulze, A. Kroll, C. Schulze, A. Kroll, C.-M. Lehr, U.F. Schäfer, K. Becker, J. Schnekenburger, C. Schulze Isfort, R. Landsiedel, and W. Wohlleben, Not ready to use – overcoming pitfalls when dispersing nanoparticles in physiological media, Nanotoxicology. 2 (2008) 51-61.

[146] M.P. Monopoli, D. Walczyk, A. Campbell, G. Elia, I. Lynch, F.B. Bombelli, and K.A. Dawson, Physical-chemical aspects of protein corona: relevance to in vitro and in vivo biological impacts of nanoparticles, J. Am. Chem. Soc. 133 (2011) 2525-2534.

[147] M.J. Han, J.M. Hao, Z.H. Xu, and X.G. Meng, Surface-enhanced Raman scattering for arsenate detection on multilayer silver nanofilms, Anal. Chim. Acta. 692 (2011) 96-102.

[148] J. Hao, Z. Xu, M.-J. Han, S. Xu, and X. Meng, Surface-enhanced Raman scattering analysis of perchlorate using silver nanofilms deposited on copper foils, Colloid. Surface. A. 366 (2010) 163-169.

[149] K. Müller, V.S.T. Ciminelli, M.S.S. Dantas, and S. Willscher, A comparative study of As(III) and As(V) in aqueous solutions and adsorbed on iron oxy-hydroxides by Raman spectroscopy, Water Res. 44 (2010) 5660-5672.

[150] R.D. Deegan, O. Bakajin, T.F. Dupont, G. Huber, S.R. Nagel, and T.A. Witten, Capillary flow as the cause of ring stains from dried liquid drops, Nature. 389 (1997) 827-829.

[151] J.T. Wen, C.-M. Ho, and P.B. Lillehoj, Coffee ring aptasensor for rapid protein detection, Langmuir. 29 (2013) 8440-8446.

[152] E. Kočišová, M. Procházka, and H. Šípová, Thiol-modified gold-coated glass as an efficient hydrophobic substrate for drop coating deposition Raman (DCDR) technique, J. Raman Spectrosc. 47 (2016) 1394-1396.

[153] P. Šimáková, M. Procházka, and E. Kočišová, SERS Microspectroscopy of Biomolecules on Dried Ag Colloidal Drops, Spectrosc. Int. J. 27 (2012) 449-453.

[154] X. Pan, J. Dong, Y. Li, X. Sun, C. Yuan, and W. Qian, The strategy of two-scale interface enrichment for constructing ultrasensitive SERS substrates based on the coffee ring effect of AgNP@ β-CD, RSC Adv. 6 (2016) 29586-29591.

[155] S. Yang, X. Dai, B.B. Stogin, and T.-S. Wong, Ultrasensitive surface-enhanced Raman scattering detection in common fluids, P. Natl. Acad. Sci. 113 (2016) 268-273.

[156] D.M. Kuncicky, B.G. Prevo, and O.D. Velev, Controlled assembly of SERS substrates templated by colloidal crystal films, J. Mater. Chem. 16 (2006) 1207-1211.

[157] J. Xu, J. Du, C. Jing, Y. Zhang, and J. Cui, Facile detection of polycyclic aromatic hydrocarbons by a surface-enhanced Raman scattering sensor based on the Au coffee ring effect, ACS Appl. Mater. Inter. 6 (2014) 6891-6897.

[158] P.J. Yunker, T. Still, M.A. Lohr, and A. Yodh, Suppression of the coffee-ring effect by shape-dependent capillary interactions, Nature. 476 (2011) 308-311.

[159] L. Cui, J. Zhang, X. Zhang, L. Huang, Z. Wang, Y. Li, H. Gao, S. Zhu, T. Wang, and B. Yang, Suppression of the coffee ring effect by hydrosoluble polymer additives, ACS Appl. Mater. Inter. 4 (2012) 2775-2780.

[160] T.S. Wong, T.H. Chen, X.Y. Shen, and C.M. Ho, Nanochromatography Driven by the Coffee Ring Effect, Anal. Chem. 83 (2011) 1871-1873.

[161] N.R. Devlin, K. Loehr, and M.T. Harris, The separation of two different sized particles in an evaporating droplet, AICHE J. 61 (2015) 3547-3556.

[162] D. Michalska and R. Wysokiński, The prediction of Raman spectra of platinum (II) anticancer drugs by density functional theory, Chem. Phys. Lett. 403 (2005) 211-217.

[163] D. Michalska, W. Zierkiewicz, D.C. Bienko, W. Wojciechowski, and T. Zeegers-Huyskens, "Troublesome" Vibrations of Aromatic Molecules in Second-Order Möller-Plesset and Density Functional Theory Calculations: Infrared Spectra of Phenol and Phenol-OD Revisited, J. Phys. Chem. A. 105 (2001) 8734-8739.

[164] S.Z. Fairchild, C.F. Bradshaw, W. Su, and S.K. Guharay, Predicting Raman spectra using density functional theory, Appl. Spectrosc. 63 (2009) 733-741.

[165] M.P. Andersson and P. Uvdal, New scale factors for harmonic vibrational frequencies using the B3LYP density functional method with the triple-ζ basis set 6-311+ G (d, p), J. Phys. Chem. A. 109 (2005) 2937-2941.

[166] R.G. Freeman, K.C. Grabar, K.J. Allison, and R.M. Bright, Self-assembled metal colloid monolayers: an approach to SERS substrates, Science. 267 (1995) 1629.

[167] C. Steinmaus, Y. Yuan, D. Kalman, O.A. Rey, C.F. Skibola, D. Dauphine, A. Basu, K.E. Porter, A. Hubbard, and M.N. Bates, Individual differences in arsenic metabolism and lung cancer in a case-control study in Cordoba, Argentina, Toxicol. Appl. Pharmacol. 247 (2010) 138-145.

[168] L.M. Knobeloch, K.M. Zierold, and H.A. Anderson, Association of arsenic-contaminated drinking-water with prevalence of skin cancer in Wisconsin's Fox River Valley, Journal of Health, Population and Nutrition. 24 (2011) 206-213.

[169] C. Ferreccio, A.H. Smith, V. Durán, T. Barlaro, H. Benítez, R. Valdés, J.J. Aguirre, L.E. Moore, J. Acevedo, M.I. Vásquez, L. Pérez, Y. Yuan, J. Liaw, K.P. Cantor, and C. Steinmaus, Case-Control Study of Arsenic in Drinking Water and Kidney Cancer in Uniquely Exposed Northern Chile, Am. J. Epidemiol. 178 (2013) 813-818.

[170] K. Jomova and M. Valko, Advances in metal-induced oxidative stress and human disease, Toxicology. 283 (2011) 65-87.

[171] Y. Sun, G. Liu, and Y. Cai, Thiolated arsenicals in arsenic metabolism: Occurrence, formation, and biological implications, J. Environ. Sci. 49 (2016) 59-73.

[172] T.W. Gebel, Arsenic methylation is a process of detoxification through accelerated excretion, Int J Hyg Envir Heal. 205 (2002) 505-508.

[173] H.V. Aposhian, E.S. Gurzau, X.C. Le, A. Gurzau, S.M. Healy, X. Lu, M. Ma, L. Yip, R.A. Zakharyan, R.M. Maiorino, R.C. Dart, M.G. Tircus, D. Gonzalez-Ramirez, D.L. Morgan, D. Avram, and M.M. Aposhian, Occurrence of Monomethylarsonous Acid in Urine of Humans Exposed to Inorganic Arsenic, Chem. Res. Toxicol. 13 (2000) 693-697.

[174] X.C. Le, X. Lu, M. Ma, W.R. Cullen, H.V. Aposhian, and B. Zheng, Speciation of key arsenic metabolic intermediates in human urine, Anal. Chem. 72 (2000) 5172-5177.

[175] B. Moe, H. Peng, X. Lu, B. Chen, L.W.L. Chen, S. Gabos, X.-F. Li, and X.C. Le, Comparative cytotoxicity of fourteen trivalent and pentavalent arsenic species determined using real-time cell sensing, J. Environ. Sci. 49 (2016) 113-124.

[176] L. Yehiayan, M. Pattabiraman, K. Kavallieratos, X.T. Wang, L.H. Boise, and Y. Cai, Speciation, formation, stability and analytical challenges of human arsenic metabolites, J. Anal. Atom. Spectrom. 24 (2009) 1397-1405.

[177] L.W.L. Chen, X. Lu, and X.C. Le, Complementary chromatography separation combined with hydride generation–inductively coupled plasma mass spectrometry for arsenic speciation in human urine, Anal. Chim. Acta. 675 (2010) 71-75.

[178] Z. Gong, X. Lu, W.R. Cullen, and X. Chris Le, Unstable trivalent arsenic metabolites, monomethylarsonous acid and dimethylarsinous acid, J. Anal. Atom. Spectrom. 16 (2001) 1409-1413.

[179] Z. Sun, J. Du, and C. Jing, Recent progress in detection of mercury using surface enhanced Raman spectroscopy — A review, J. Environ. Sci. 39 (2016) 134-143.

[180] J. Hao, M.-J. Han, S. Han, X. Meng, T.-L. Su, and Q.K. Wang, SERS detection of arsenic in water: A review, J. Environ. Sci. 36 (2015) 152-162.

[181] P. Lee and D. Meisel, Adsorption and surface-enhanced Raman of dyes on silver and gold sols, J. Phys. Chem. 86 (1982) 3391-3395.

[182] D. van Lierop, Z. Krpetic, L. Guerrini, I.A. Larmour, J.A. Dougan, K. Faulds, and D. Graham, Positively charged silver nanoparticles and their effect on surface-enhanced Raman scattering of dye-labelled oligonucleotides, Chem. Commun. 48 (2012) 8192-8194.

[183] L. Yehiayan, N. Membreno, S. Matulis, L.H. Boise, and Y. Cai, Extraction tool and matrix effects on arsenic speciation analysis in cell lines, Anal. Chim. Acta. 699 (2011) 187-192.

[184] T.M. Loehr and R.A. Plane, Raman spectra and structures of arsenious acid and arsenites in aqueous solution, Inorg. Chem. 7 (1968) 1708-1714.

[185] S.C. Myneni, S.J. Traina, G.A. Waychunas, and T.J. Logan, Experimental and theoretical vibrational spectroscopic evaluation of arsenate coordination in aqueous solutions, solids, and at mineral-water interfaces, Geochim. Cosmochim. Acta. 62 (1998) 3285-3300.

[186] F.K. Vansant, B.J. Van Der Veken, and H.O. Desseyn, Vibrational analysis of arsenic acid and its anions: I. Description of the Raman spectra, J. Mol. Struct. 15 (1973) 425-437.

[187] F. Vansant, B. Van der Veken, and M. Herman, Vibrational analysis of dimethylarsinic acid, Spectrochim. Acta A-M. 30 (1974) 69-78.

[188] F. Vansant, B. Van der Veken, and M. Herman, The vibrational analysis of methylarsonic acid, trideuteromethylarsonic acid and their anions, J. Mol. Struct. 35 (1976) 191-200.

[189] S. Cowen, M. Duggal, T. Hoang, and H.A. Al-Abadleh, Vibrational spectroscopic characterization of some environmentally important organoarsenicals-A guide for understanding the nature of their surface complexes, Can. J. Chem. 86 (2008) 942-950.

[190] H. Wang, C.S. Levin, and N.J. Halas, Nanosphere arrays with controlled sub-10-nm gaps as surface-enhanced Raman spectroscopy substrates, J. Am. Chem. Soc. 127 (2005) 14992-14993.

[191] C. Jing, X. Meng, S. Liu, S. Baidas, R. Patraju, C. Christodoulatos, and G.P. Korfiatis, Surface complexation of organic arsenic on nanocrystalline titanium oxide, J. Colloid. Interf. Sci. 290 (2005) 14-21.

[192] P. Gao and M.J. Weaver, Surface-enhanced Raman spectroscopy as a probe of adsorbate-surface bonding: benzene and monosubstituted benzenes adsorbed at gold electrodes, J. Phys. Chem. 89 (1985) 5040-5046.

[193] A. Campion and P. Kambhampati, Surface-enhanced Raman scattering, Chem. Soc. Rev. 27 (1998) 241-250.

[194] X.-M. Lin, Y. Cui, Y.-H. Xu, B. Ren, and Z.-Q. Tian, Surface-enhanced Raman spectroscopy: substrate-related issues, Anal. Bioanal. Chem. 394 (2009) 1729-1745.

[195] M. Rahman, S. Laurent, N. Tawil, L.H. Yahia, and M. Mahmoudi, Nanoparticle and Protein Corona, Protein-Nanoparticle Interactions: The Bio-Nano Interface, in, Springer Berlin Heidelberg. Berlin, Heidelberg, pp. 21-44.

[196] P. Ball, Fluid dynamics - How coffee leaves its mark, Nature. 389 (1997) 788-788.

[197] R. Fondecave and F.B. Wyart, Wetting laws for polymer solutions, EPL (Europhysics Letters). 37 (1997) 115.

[198] H.Y. Erbil, Evaporation of pure liquid sessile and spherical suspended drops: A review, Adv. Colloid Interfac. 170 (2012) 67-86.

[199] E. Tekin, P.J. Smith, and U.S. Schubert, Inkjet printing as a deposition and patterning tool for polymers and inorganic particles, Soft Matter. 4 (2008) 703-713.

[200] W. Han and Z. Lin, Learning from “Coffee Rings”: Ordered Structures Enabled by Controlled Evaporative Self-Assembly, Angew. Chem. Int. Ed. 51 (2012) 1534-1546.

[201] T. Still, P.J. Yunker, and A.G. Yodh, Surfactant-induced Marangoni eddies alter the coffee-rings of evaporating colloidal drops, Langmuir. 28 (2012) 4984-4988.

[202] D. Soltman and V. Subramanian, Inkjet-Printed Line Morphologies and Temperature Control of the Coffee Ring Effect, Langmuir. 24 (2008) 2224-2231.

[203] X. Zhong, A. Crivoi, and F. Duan, Sessile nanofluid droplet drying, Adv. Colloid Interfac. 217 (2015) 13-30.

[204] F. Brochard-Wyart, R. Fondecave, and M. Boudoussier, Wetting of antagonist mixtures: the `leak out' transition, Int. J. Eng. Sci. 38 (2000) 1033-1047.

[205] J.J. Cras, C.A. Rowe-Taitt, D.A. Nivens, and F.S. Ligler, Comparison of chemical cleaning methods of glass in preparation for silanization, Biosens. Bioelectron. 14 (1999) 683-688.

[206] S. Bharathi, N. Fishelson, and O. Lev, Direct Synthesis and Characterization of Gold and Other Noble Metal Nanodispersions in Sol−Gel-Derived Organically Modified Silicates, Langmuir. 15 (1999) 1929-1937.

[207] K. Aslan, P. Holley, and C.D. Geddes, Metal-enhanced fluorescence from silver nanoparticle-deposited polycarbonate substrates, J. Mater. Chem. 16 (2006) 2846-2852.

[208] N. Hajduková, M. Procházka, J. Štěpánek, and M. Špírková, Chemically reduced and laser-ablated gold nanoparticles immobilized to silanized glass plates: preparation, characterization and SERS spectral testing, Colloid. Surface. A. 301 (2007) 264-270.

[209] N. Nath and A. Chilkoti, Label-free biosensing by surface plasmon resonance of nanoparticles on glass: optimization of nanoparticle size, Anal. Chem. 76 (2004) 5370-8.

[210] G. Chumanov, K. Sokolov, B.W. Gregory, and T.M. Cotton, Colloidal metal films as a substrate for surface-enhanced spectroscopy, J. Phys. Chem. 99 (1995) 9466-9471.

[211] I. Toshikazu, I. Yasushi, and T. Jiro, Nucleophilic Substitution of Aromatic Halides with Amines under High Pressure, Chem. Lett. 16 (1987) 1187-1190.

[212] M.F. Hughes, M. Menache, and D.J. Thompson, Dose-Dependent Disposition of Sodium Arsenate in Mice Following Acute Oral Exposure, Fundam. Appl. Toxicol. 22 (1994) 80-89.

[213] G.K.H. Tam, S.M. Charbonneau, F. Bryce, and E. Sandi, Excretion of a single oral dose of fish-arsenic in man, Bull. Environ. Contam. Toxicol. 28 (1982) 669-673.

[214] G.K.H. Tam, S.M. Charbonneau, G. Lacroix, and F. Bryce, Confirmation of inorganic arsenic and dimethylarsinic acid in urine and plasma of dog by ion-exchange and TLC, Bull. Environ. Contam. Toxicol. 21 (1979) 371-374.

[215] S. Gibaud and G. Jaouen, Arsenic-based drugs: from fowler's solution to modern anticancer chemotherapy, Medicinal organometallic chemistry, in, Springer, pp. 1-20.

[216] S.A. Stice, Speciation, Metabolism, Toxicity, and Protein-binding of Different Arsenic Species in Human Cells, edition ed, Florida International University, Miami. 1203. http://digitalcommons.fiu.edu/etd/1203.

[217] T.R. Radabaugh and H.V. Aposhian, Enzymatic reduction of arsenic compounds in mammalian systems: reduction of arsenate to arsenite by human liver arsenate reductase, Chem. Res. Toxicol. 13 (2000) 26-30.

[218] B.K. Mandal, Y. Ogra, and K.T. Suzuki, Identification of dimethylarsinous and monomethylarsonous acids in human urine of the arsenic-affected areas in West Bengal, India, Chem. Res. Toxicol. 14 (2001) 371-378.

[219] R. Xie, W. Johnson, S. Spayd, G.S. Hall, and B. Buckley, Arsenic speciation analysis of human urine using ion exchange chromatography coupled to inductively coupled plasma mass spectrometry, Anal. Chim. Acta. 578 (2006) 186-194.

[220] C.A. Loffredo, H.V. Aposhian, M.E. Cebrian, H. Yamauchi, and E.K. Silbergeld, Variability in human metabolism of arsenic, Environ. Res. 92 (2003) 85-91.

[221] B.K. Mandal, Y. Ogra, K. Anzai, and K.T. Suzuki, Speciation of arsenic in biological samples, Toxicol. Appl. Pharmacol. 198 (2004) 307-318.

[222] O.L. Valenzuela, V.H. Borja-Aburto, G.G. Garcia-Vargas, M.B. Cruz-Gonzalez, E.A. Garcia-Montalvo, E.S. Calderon-Aranda, and L.M. Del Razo, Urinary Trivalent Methylated Arsenic Species in a Population Chronically Exposed to Inorganic Arsenic, Environ. Health Persp. 113 (2005) 250-254.

[223] A. Raab, S.H. Wright, M. Jaspars, A.A. Meharg, and J. Feldmann, Pentavalent arsenic can bind to biomolecules, Angew. Chem. Int. Ed. 46 (2007) 2594-2597.

[224] L. Yehiayan, S. Stice, G. Liu, S. Matulis, L.H. Boise, and Y. Cai, Dimethylarsinothioyl Glutathione as a Metabolite in Human Multiple Myeloma Cell Lines upon Exposure to Darinaparsin, Chemical Research in Toxicology. 27 (2014) 754-764.

[225] S. Stice, G. Liu, S. Matulis, L.H. Boise, and Y. Cai, Determination of multiple human arsenic metabolites employing high performance liquid chromatography inductively coupled plasma mass spectrometry, J. Chromatogr. B. 1009 (2016) 55-65.

[226] N. Hua, R. Kanwal, L. X Chris, and D.J. Thomas, Formation of methylated oxyarsenicals and thioarsenicals in wild-type and arsenic (+3 oxidation state) methyltransferase knockout mice exposed to arsenate, Anal. Bioanal. Chem. 405 (2013) 1885-1891.

[227] B. Chen, X. Lu, S. Shen, L.L. Arnold, S.M. Cohen, and X.C. Le, Arsenic Speciation in the Blood of Arsenite-Treated F344 Rats, Chem. Res. Toxicol. 26 (2013) 952-962.

[228] H. Naranmandura, N. Suzuki, K. Iwata, S. Hirano, and T. Suzuki, Arsenic Metabolism and Thioarsenicals in Hamsters and Rats, Chem. Res. Toxicol. 20 (2007) 616-624.

[229] R. Raml, A. Rumpler, W. Goessler, M. Vahter, L. Li, T. Ochi, and K.A. Francesconi, Thio-dimethylarsinate is a common metabolite in urine samples from arsenic-exposed women in Bangladesh, Toxicol. Appl. Pharmacol. 222 (2007) 374-380.

[230] T. Van de Wiele, C.M. Gallawa, K.M. Kubachka, J.T. Creed, N. Basta, E.A. Dayton, S. Whitacre, G. Du Laing, and K. Bradham, Arsenic metabolism by human gut microbiota upon in vitro digestion of contaminated soils, Environ. Health Persp. 118 (2010) 1004-1009.

[231] R. Raml, W. Goessler, P. Traar, T. Ochi, and K.A. Francesconi, Novel Thioarsenic Metabolites in Human Urine after Ingestion of an Arsenosugar, 2‘,3‘-Dihydroxypropyl 5-Deoxy-5-dimethylarsinoyl-β-d-riboside, Chem. Res. Toxicol. 18 (2005) 1444-1450.

[232] R. Raml, W. Goessler, and K.A. Francesconi, Improved chromatographic separation of thio-arsenic compounds by reversed-phase high performance liquid chromatography-inductively coupled plasma mass spectrometry, J. Chromatogr. A. 1128 (2006) 164-170.

[233] K.T. Suzuki, B.K. Mandal, A. Katagiri, Y. Sakuma, A. Kawakami, Y. Ogra, K. Yamaguchi, Y. Sei, K. Yamanaka, K. Anzai, M. Ohmichi, H. Takayama, and N. Aimi, Dimethylthioarsenicals as Arsenic Metabolites and Their Chemical Preparations, Chem. Res. Toxicol. 17 (2004) 914-921.

[234] H. Naranmandura and K.T. Suzuki, Formation of dimethylthioarsenicals in red blood cells, Toxicol. Appl. Pharmacol. 227 (2008) 390-399.

[235] H. Naranmandura, N. Suzuki, and K.T. Suzuki, Trivalent arsenicals are bound to proteins during reductive methylation, Chem. Res. Toxicol. 19 (2006) 1010-1018.

[236] G. Yang, X. Xu, W. Wang, L. Xu, G. Chen, and F. Fu, A new interface used to couple capillary electrophoresis with an inductively coupled plasma mass spectrometry for speciation analysis, Electrophoresis. 29 (2008) 2862-2868.

[237] G.-D. Yang, J.-P. Zheng, H.-X. Huang, G.-M. Qi, J.-H. Xu, and F.-F. Fu, Speciation Analysis of Arsenic in Seafood with Capillary Electrophoresis-UV Detection, Chin. J. Anal. Chem. 37 (2009) 532-536.

[238] G. Yang, J. Zheng, L. Chen, Q. Lin, Y. Zhao, Y. Wu, and F. Fu, Speciation analysis and characterisation of arsenic in lavers collected from coastal waters of Fujian, south-eastern China, Food Chem. 132 (2012) 1480-1485.

[239] L. Yehiayan, M. Pattabiraman, K. Kavallieratos, X. Wang, L.H. Boise, and Y. Cai, Speciation, formation, stability and analytical challenges of human arsenic metabolites, Journal of Analytical Atomic Spectrometry. 24 (2009) 1397-1405.

[240] E.B. Hanlon, R. Manoharan, T.W. Koo, K.E. Shafer, J.T. Motz, M. Fitzmaurice, J.R. Kramer, I. Itzkan, R.R. Dasari, and M.S. Feld, Prospects for in vivo Raman spectroscopy, Phys. Med. Biol. 45 (2000) R1-R59.

[241] J. Gailer, Arsenic–selenium and mercury–selenium bonds in biology, Coord. Chem. Rev. 251 (2007) 234-254.

[242] X. Qian, X.H. Peng, D.O. Ansari, Q. Yin-Goen, G.Z. Chen, D.M. Shin, L. Yang, A.N. Young, M.D. Wang, and S. Nie, In vivo tumor targeting and spectroscopic detection with surface-enhanced Raman nanoparticle tags, Nat. Biotechnol. 26 (2008) 83-90.

[243] G. Trachta, B. Schwarze, B. Sägmüller, G. Brehm, and S. Schneider, Combination of high-performance liquid chromatography and SERS detection applied to the analysis of drugs in human blood and urine, J. Mol. Struct. 693 (2004) 175-185.

[244] J. Lin, R. Chen, S. Feng, J. Pan, Y. Li, G. Chen, M. Cheng, Z. Huang, Y. Yu, and H. Zeng, A novel blood plasma analysis technique combining membrane electrophoresis with silver nanoparticle-based SERS spectroscopy for potential applications in noninvasive cancer detection, Nanomed. Nanotechnol. Biol. Med. 7 (2011) 655-663.

[245] S. Feng, R. Chen, J. Lin, J. Pan, G. Chen, Y. Li, M. Cheng, Z. Huang, J. Chen, and H. Zeng, Nasopharyngeal cancer detection based on blood plasma surface-enhanced Raman spectroscopy and multivariate analysis, Biosens. Bioelectron. 25 (2010) 2414-2419.

[246] A. Rogstad, High-temperature laser Raman spectroscopic study on mixtures of arsenic and sulphur vapours, J. Mol. Struct. 14 (1972) 421-426.

[247] W. Mikenda, H. Steidl, and A. Preisinger, Raman spectra of Na3AsS4·8(D, H)2O and Na3SbS4·9(D, H)2O and OD(H)…S bonds in salt hydrates, J. Raman Spectrosc. 12 (1982) 217-221.

[248] E.E. Zvereva, A.R. Shagidullin, and S.A. Katsyuba, Ab initio and DFT predictions of infrared intensities and Raman activities, J. Phys. Chem. A. 115 (2011) 63-69.

[249] G.R. Helz, J.A. Tossell, J.M. Charnock, R.A.D. Pattrick, D.J. Vaughan, and C.D. Garner, Oligomerization in As (III) sulfide solutions: Theoretical constraints and spectroscopic evidence, Geochim. Cosmochim. Acta. 59 (1995) 4591-4604.

[250] M.C. Teixeira, V.S.T. Ciminelli, M.S.S. Dantas, S.F. Diniz, and H.A. Duarte, Raman spectroscopy and DFT calculations of As(III) complexation with a cysteine-rich biomaterial, J. Colloid. Interf. Sci. 315 (2007) 128-134.

[251] J.A. Tossell and M.D. Zimmermann, Calculation of the structures, stabilities, and vibrational spectra of arsenites, thioarsenites and thioarsenates in aqueous solution, Geochim. Cosmochim. Acta. 72 (2008) 5232-5242.

[252] M. Fricke, M. Zeller, W. Cullen, M. Witkowski, and J. Creed, Dimethylthioarsinic anhydride: a standard for arsenic speciation, Anal. Chim. Acta. 583 (2007) 78-83.

[253] M.W. Fricke, M. Zeller, H. Sun, V.W.-M. Lai, W.R. Cullen, J.A. Shoemaker, M.R. Witkowski, and J.T. Creed, Chromatographic separation and identification of products from the reaction of dimethylarsinic acid with hydrogen sulfide, Chem. Res. Toxicol. 18 (2005) 1821-1829.

[254] N. Garnier, G.G.J. Redstone, M.S. Dahabieh, J.N. Nichol, S.V. del Rincon, Y. Gu, D.S. Bohle, Y. Sun, D.S. Conklin, K.K. Mann, and W.H. Miller, The Novel Arsenical Darinaparsin is Transported by Cystine Importing Systems, Mol. Pharmacol. (2014) 576-585.

[255] X. Xu and D.G. Truhlar, Accuracy of effective core potentials and basis sets for density functional calculations, including relativistic effects, as illustrated by calculations on arsenic compounds, J. Chem. Theory Comput. 7 (2011) 2766-2779.

[256] F. Weigend and R. Ahlrichs, Balanced basis sets of split valence, triple zeta valence and quadruple zeta valence quality for H to Rn: design and assessment of accuracy, Phys. Chem. Chem. Phys. 7 (2005) 3297-3305.

[257] P.B. Armentrout and I. Kretzschmar, Experimental and Theoretical Studies of the Reaction of Rh+ with CS2 in the Gas Phase: Thermochemistry of RhS+ and RhCS+, J. Phys. Chem. A. 113 (2009) 10955-10965.

[258] G. Schaftenaar and J.H. Noordik, Molden: a pre-and post-processing program for molecular and electronic structures, J. Comput.Aid. Mol. Des. 14 (2000) 123-134.

[259] T. Lu and F. Chen, Multiwfn: a multifunctional wavefunction analyzer, J. Comput. Chem. 33 (2012) 580-592.

[260] A.P. Scott and L. Radom, Harmonic vibrational frequencies: an evaluation of Hartree-Fock, Møller-Plesset, quadratic configuration interaction, density functional theory, and semiempirical scale factors, J. Phys. Chem. 100 (1996) 16502-16513.

[261] R.F. Hout, B.A. Levi, and W.J. Hehre, Effect of electron correlation on theoretical vibrational frequencies, J. Comput. Chem. 3 (1982) 234-250.

[262] J.A. Pople, H.B. Schlegel, R. Krishnan, D.J. Defrees, J.S. Binkley, M.J. Frisch, R.A. Whiteside, R.F. Hout, and W.J. Hehre, Molecular orbital studies of vibrational frequencies, Int. J. Quantum Chem. 20 (1981) 269-278.

[263] H.-V. Gründler, H.-D. Schumann, and E. Steger, Raman and infrared spectroscopic investigation of alkyl derivatives of arsenic acid, J. Mol. Struct. 21 (1974) 149-157.

[264] I. Silaghidumitrescu, L. Silaghidumitrescu, And I. Haiduc, Normal Coordinate Analysis Of The Vibrational-Spectrum Of Dimethyldithioarsinato Anion,(CH3)2AsS2-, Rev Roum. Chim. 27 (1982) 911-916.

[265] L.S. Dumitrescu, I. Haiduc, and J. Weiss, Preparation and properties of some organotin dimethyl- and diphenyl-dithioarsinates. The crystal structure of (CH3)2Sn[S2As(CH3)2]2, J. Organomet. Chem. 263 (1984) 159-165.

[266] I. Haiduc and L. Silaghi-Dumitrescu, Organotin and tin(IV) derivatives of dimethyldithioarsinic acid, Journal of Organometallic Chemistry. 225 (1982) 225-232.

[267] J. De Gelder, K. De Gussem, P. Vandenabeele, and L. Moens, Reference database of Raman spectra of biological molecules, J. Raman Spectrosc. 38 (2007) 1133-1147.

[268] K.B. Wiberg, Basis set effects on calculated geometries: 6-311++ G** vs. aug-cc-pVDZ, J. Comput. Chem. 25 (2004) 1342-1346.

[269] P. Sinha, S.E. Boesch, A. Changming Gu, R.A. Wheeler, and A.K. Wilson, Harmonic Vibrational Frequencies: Scaling Factors for HF, B3LYP, and MP2

Methods in Combination with Correlation Consistent Basis Sets, J. Phys. Chem. A. 108 (2004) 9213-9217.

[270] G.E. Walrafen, Raman Spectral Studies of Aqueous Solutions of Selenic Acid, J. Chem. Phys. 39 (1963) 1479-1492.

[271] M. Falk and P.A. Giguère, INFRARED SPECTRA AND STRUCTURE OF SELENIOUS ACID, Can. J. Chem. 36 (1958) 1680-1685.

[272] M.W. Wong, Vibrational frequency prediction using density functional theory, Chem. Phys. Lett. 256 (1996) 391-399.

[273] R.A. Zingaro, K.J. Irgolic, D.H. O'Brien, and L.J. Edmonson, Rearrangement of tetramethyldiarsine disulfide, J. Am. Chem. Soc. 93 (1971) 5677-5681.

[274] W.R. Cullen, G.B. Deacon, and J.H.S. Green, VIBRATIONAL SPECTRA OF SOME ALKYLARSONIUM COMPOUNDS, Can. J. Chem. 43 (1965) 3193-3200.

[275] A Relation between Bond Force Constants, Bond Orders, Bond Lengths, and the Electronegativities of the Bonded Atoms, J. Chem. Phys. 14 (1946) 305-320.

[276] I. Haiduc and L. Silaghi-Dumitrescu, Organotin and tin (IV) derivatives of dimethyldithioarsinic acid, J. Organomet. Chem. 225 (1982) 225-232.

[277] A. Casey, N. Ham, D. Mackey, and R. Martin, Synthesis and infrared spectra of some dithiocacodylate complexes, Aust. J. Chem. 23 (1970) 1117-1123.

[278] V. Tkachev, V. Perov, and Y.F. Gatilov, Crystal and molecular structure of dipropylphenylarsine sulfide (C 3 H 7) 2 (C 6 H 5) AsS, J Struct. Chem. 25 (1984) 144-146.

[279] R.A. Zingaro, R.E. McGlothin, and R.M. Hedges, Infra-red absorption spectra of eleven arsine sulphides from 15 to 30 [small micro]. The as-S stretching frequency, T. Faraday Soc. 59 (1963) 798-805.

VITA

MINGWEI YANG

2005-2009	B.S., Chemistry Fuzhou University Fujian, China
2009-2012	M.S., Environmental Chemistry Excellent Master Thesis Award Fuzhou University Fujian, China
2012 -2017	Doctoral Candidate, Chemistry Florida International University Miami, Florida
	Teaching Assistant Florida International University Miami, Florida

PUBLICATIONS AND PRESENTATIONS

Yang, M. W.; Wang, Z. W.; Fang, L.; Zheng, J. P.; Xu, L. J.; Fu, F. F., Simultaneous and ultra-sensitive quantification of multiple peptides by using europium chelate labeling and capillary electrophoresis-inductively coupled plasma mass spectrometry. J. Anal. Atom. Spectrom. 2012, 27 (6), 946-951.

Yang, M. W..; Wu, W.; Ruan, Y.; Huang, L.; Wu, Z.; Cai, Y.; Fu, F., Ultra-sensitive quantification of lysozyme based on element chelate labeling and capillary electrophoresis–inductively coupled plasma mass spectrometry. Anal. Chim. Acta 2014, 812, 12-17.

Jiang, W.; Cai, Q.; Xu, W.; Yang, M. W.; Cai, Y.; Dionysiou, D. D.; O'Shea, K. E., Cr(VI) adsorption and reduction by humic acid coated on magnetite. Environ. Sci. Technol. 2014, 48 (14), 8078-85.

Yang, M. W.; Matulis, S.; Boise, L. H.; McGoron, A. J.; Cai, Y., Potential application of SERS for arsenic speciation in biological matrices, Anal. Bioanal. Chem., accepted as forefront article on May 26, 2017

Yang, M. W.; Sun, Y. Z.; Zhang, X. B.; McCord, B.; McGoron, A. J.; Mebel, A.; Cai, Y., Raman spectra of thiolated arsenicals with biological importance, under preparation

Yang, M. W.; Fan, C. J.; Sylvers, K.; McGoron, A. J.; Liu, G. L.; Cai, Y., Employing coffee ring effect on silver nanofilm for arsenic speciation study, under preparation

91st Florida Annual Meeting and Exposition, 5/2015, Tampa, FL (poster)

2017 Florida International University Graduate Student Appreciation Week, 3/2017, Miami, FL (poster)